Požarna analiza AB stupova: proračun realnog (varijabilnog) aksijalnog opterećenja modeliranjem većeg dijela konstrukcija sustava

Tadić, Ivan

Master's thesis / Diplomski rad

2022

Degree Grantor / Ustanova koja je dodijelila akademski / stručni stupanj:
University of Split, Faculty of Civil Engineering, Architecture and Geodesy / Sveučilište u Splitu, Fakultet građevinarstva, arhitekture i geodezije

Permanent link / Trajna poveznica: https://urn.nsk.hr/urn:nbn:hr:123:624024

Rights / Prava: In copyright/Zaštićeno autorskim pravom.

Download date / Datum preuzimanja: **2024-12-27**

Repository / Repozitorij:

SVEUČILIŠTE U SPLITU

FAKULTET GRAĐEVINARSTVA ARHITEKTURE I GEODEZIJE

DIPLOMSKI RAD

Ivan Tadić

Split, 2022.

SVEUČILIŠTE U SPLITU

FAKULTET GRAĐEVINARSTVA ARHITEKTURE I GEODEZIJE

Ivan Tadić

Požarna analiza AB stupova: Proračun realnog (varijabilnog) aksijalnog opterećenja modeliranjem većeg dijela konstrukcijskog sustava

Diplomski rad

Split, 2022.

Zahvala:

Veliku zahvalnost dugujem svom mentoru prof.dr.sc. Alenu Harapinu, a prije svega komentorima doc.dr.sc. Peteru Češarek i doc. dr.sc. Jerneji Česarek Kolšek, koji su me prihvatili i uvijek imali strpljenja i vremena za moja pitanja tijekom izrade ovog rada.

Također, želim se zahvaliti svojoj rodbini, kolegama i prijateljima, koji su mi bili velika podrška tijekom cijelog studiranja.

Najveću zahvalnost upućujem svojim roditeljima, bratu i nevjesti, na neizmjernom strpljenu, moralnoj podršci i razumijevanju, koji su uvijek bili tu uz mene. Hvala vam na svemu!

Požarna analiza AB stupova: Proračun realnog (varijabilnog) aksijalnog opterećenja modeliranjem većeg dijela konstrukcijskog sustava

Sažetak:

Prema sadašnjoj verziji Eurokodova, analiza požara AB konstrukcija može se izvesti na nekoliko različitih načina koji mogu imati različite razine preciznosti i točnosti. Jedna od najprimjenjivanijih i najjednostavnijih načina su tzv. metode analize zasebnih elemenata. Metode analize zasebnih elemenata obično se odnose na metode kod kojih se razmatra samo njezin pojedinačni konstruktivni element, npr. AB stup. U ovom radu prikazan je utjecaj krutosti većeg dijela konstrukcije na varijabilno aksijalno opterećenje stupova u realnim konstrukcijama.

Ključne riječi:

Požarna analiza, Eurokod, AB stup, pojednostavljena analiza elemenata, egzaktna analiza teorije trećeg reda, varijabilno aksijalno opterećenje, spriječena toplinska ekspanzija,...

Fire analysis of RC columns: Accounting for realistic (variable) axial load by modelling a larger part of the structural system

Abstract:

According to the present version of Eurocodes, fire analysis of RC columns can be performed with several models of different levels of accuracy. One of the the and most often applied methods are called member-analysis procedures. The latter usually refer to methods where, instead of a larger part of the structural system, only the observed RC column is calculated as an isolated structural element. This is only possible if the axial force in the column is considered constant during fire. The thesis discusses validity of such approximation and modelling possibilities for its omittance.

Keywords:

Fire analysis, Eurocode, RC column, simplified member analysis, exact third-order theory analysis, variable axial force, hindered thermal expansion,...

SVEUČILIŠTE U SPLITU
FAKULTET GRAĐEVINARSTVA, ARHITEKTURE I GEODEZIJE

STUDIJ: **DIPLOMSKI SVEUČILIŠNI STUDIJ GRAĐEVINARSTVA**

KANDIDAT: **Ivan Tadić**

MATIČNI BROJ (JMBAG): **0083221356**

KATEDRA: **Katedra za betonske konstrukcije i mostove**

PREDMET: **Betonske konstrukcije II**

ZADATAK ZA DIPLOMSKI RAD

Tema:
Požarna analiza AB stupova: Proračun realnog (varijabilnog) aksijalnog opterećenja modeliranjem većeg dijela konstrukcijskog sustava

Opis zadatka:

    Zadatak ovog diplomskog rada je požarna analiza armirano betonskih stupova s gledišta proračuna stvarnog aksijalnog opterećenja, obzirom na utjecaj krutosti većeg dijela konstrukcijskog sustava u požarnom scenariju. Temperaturnim i mehaničkim analizama pojedinačnih elemenata ploča i greda dobivamo realan odaziv okolnih elemenata konstrukcije iz kojih se proračunaju faktori redukcije krutosti istih i promatra se utjecaj na aksijalno opterećenje AB stupova okvirnih konstrukcija.

U Splitu, veljača 2022.

Voditelj Diplomskog rada:

Prof.dr.sc. Alen Harapin

Komentori diplomskog rada:

Doc.dr.sc. Peter Češarek
Doc.dr.sc. Jerneja Češarek Kolšek

Predsjednik Povjerenstva za završne i diplomske ispite:
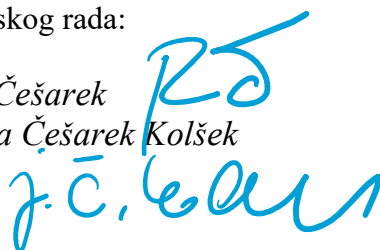
Izv. prof. dr. sc. Ivo Andrić

Table of contents

Introduction

The following discussion is summarised from the work of Kolšek and Česarek [1]. According to the present version of Eurocodes, fire analysis of RC structures can be performed in several different ways which can have different levels of precision and accuracy. One of the most applied and the most simple ways, undoubtedly, are the so-called member-analysis methods. Member-analysis methods usually refer to methods where, instead of the structure as a whole (or at least a larger part of it), we only consider its individual (isolated) structural element, e.g. RC column. This is only possible if two essential assumptions are made:

- internal forces in the element will not change during fire and
- there will be no changes in kinematic boundary conditions at the ends of the element.

In the case of an RC column, the first of the aforementioned assumptions seems particularly problematic. Namely, during a fire, the column will tend to elongate due to the influence of high temperatures and these elongations will be hindered by the rest of the structure (note that thermal expansion coefficient is not negligible for concrete, especially at high temperatures). Furthermore, it seems reasonable to expect, that these obstructed elongations would cause an increase in the axial force of the column at least in the initial stages of the fire. It can also be expected that, in some cases, this increased axial force would cause the column to collapse prematurely compared to what a simplified member-analysis would predict.

Considering everything written above, instead of analysing an isolated RC column, thus, modelling the column as part of a larger portion of the RC structural system would seem more appropriate for structural fire engineering. However, many problems currently exist connected to this idea as explained in what follows below. For the sake of simplicity, the following explanation and this entire master's thesis will be dedicated only to the most typical type of RC structures, i.e. to structures with RC columns and RC walls representing the vertical structural elements and with plain RC slabs resting on RC beams playing a role of horizontal structural members.

For a fire analysis of a larger RC structural system, only the most complex type of structural fire calculation method is usually applicable, i.e. a geometrically and materially non-linear (or often called *third-order theory*) method. In such analysis, all governing equations of the problem are in each time period satisfied on the current (deformed) shape of the structure and the material response is captured in an exact manner (i.e considering high-temperature specificities of the material, such as thermal reductions of material strength, thermal expansion, high-temperature creep, etc.). There are some commercial softwares currently on the market which can support applications of analyses of such degree of complexity (e.g. Abaqus [2], Ansys [12], Safir [13]...). For everyday engineering practices, where time-efficiency is often the top priority, their use is sometimes recognized as too complex and time-consuming. To date, thus, strenuous research efforts are being dedicated worldwide to make these analyses simpler without significantly compromising their accuracy.

An important part that contributes to the complexity of the third-order fire analyses of RC structures, as discussed above, is the complexity of the selected material models for concrete. A good example is the often applied so-called *concrete damage-plasticity model* as integrated e.g. in Abaqus [2]. Unfortunately, although very precise, this model is complex and often leads to numerical instabilities and poor convergency thereby to substantial prolongations of computing times of the overall analysis.

1

On top of that, the model is dependent on many material parameters (e.g. dilation angle) which are not generally known nor found easily in the available literature (even for the ambient let alone for elevated temperatures). To avoid these problems, a simplified *reduced-stiffness material model for reinforced concrete* has been proposed recently in [1] and currently awaits further validations.

In addition to simplifying material models for concrete, researchers are also seeking other possibilities for reducing the computational dependency of third-order fire analyses of larger RC structures. One of these, for example, is including only those portions of the structure into the model that, during the assumed fire, actually affects the structural element of our interest (e.g. the specific RC column) and for which influence on this element cannot be accounted for in any of the possible indirect manners. By the term 'indirect manners' it is referred to modelling manoeuvres such as, e.g.:

- prescribing appropriate boundary conditions at the ends of a specific portion of the structure around the element of our interest (i.e. around particular RC column) instead of modelling the entire structure,

- modelling the slab above the observed RC column only within the area of the slab's so-called *effective widths* instead of modelling the whole slab,

- etc.

In relation to the above, this master's thesis will try to contribute to answering two important questions:

- To what degree can the axial force in a specific RC column change during a specific fire?

- What part of the RC structure from an analyzed building needs to be modelled explicitly if we are only interested in the fire response of an individual RC column of this building?

In the thesis, these questions will be addressed by performing fire analyses of the structure of a selected real RC building (Chapter 3). All the analyses will be performed with third-order theory models computed in the Abaqus FEMA environment [2]. The proposal of [1] for the reduced stiffness material model for reinforced concrete will be implemented in these models. According to [1], this material model is to be validated more extensively in the future and some starting contributions to this validation will also be provided in this thesis (Chapter 2). The conclusion of the thesis will be presented in Chapter 4.

Chapter 1. Theoretical background

1.1.   Fire analyses of RC structures according to EN 1992-1-2

Section 1.1. of this thesis is dedicated to the theoretical foundations of fire analysis of reinforced concrete (RC) structures as per Eurocode EN 1992-1-2 [3]. The text of this section is taken mainly from sources [4] and [5].

EN 1992-1-2 [3] generally requires that the design resistance of the structure at a specific time t of the assumed fire and at the prescribed load combination for fire design situation $R_{fi,d,t}$ is greater than the design value of internal forces in the structure at this time and this load combination $E_{fi,d,t}$:

$$R_{fi,d,t} \geq E_{fi,d,t} \tag{1}$$

Note that according to EN 1990 [6], Section 6.4.3.3, the fire design situation is a part of the so called ultimate limit state (ULS) situations, more precisely of the group of accidental design situations. The general form of the corresponding load combination is as follows:

$$\sum_{j \geq 1} G_{k,j} + A_d + (\psi_{1,1} \text{ or } \psi_{2,1}) * Q_{k,1} + \sum_{i \geq 1} \psi_{2,i} + Q_{k,i} \tag{2}$$

In this combination $G_{k,j}$ denotes a permanent action on the structure, $Q_{k,1}$ is the predominant variable action, and $Q_{k,i}$ are other variable actions. Moreover, A_d, are accidental actions, i.e. in this thesis representing the effects of elevated temperatures due to the fire. These can be of a direct or indirect nature. Direct actions A_d are influences of high temperature on essential material properties (reduction of the strength of concrete and reinforcing steel, thermal expansion etc.). However, indirect actions A_d are influences of high temperatures that not only depend on the material but also on the characteristics of the structure. A good example of an indirect action A_d is an increase in the axial force of an RC column in the initial stages of the fire due to its tendency for fire-induced thermal elongations which are being hindered by the rest of the structure (e.g. by an RC plate on top of the column). Moreover, $\psi_{1,1}$ and $\psi_{2,1}$ are load combination factors where the application of one or the other is usually prescribed by a national annex to EN 1991-1-2 [7] depending on the type of the accident.

As written above, the values on both sides of inequality (1) generally change over time, so it is necessary to define the ultimate time t by which this condition should still be met in the assumed fire. Typically, the ultimate time will be prescribed in the scope of a document presenting the results of a study of the building's fire safety. This will be prepared by the fire engineer responsible for the specific building and will be a mandatory part of the construction permit project documentation. In the study, these data will be given in the form of the symbol 'R' (referring to the term 'resistance') and the following number, e.g. R30, R60 or R120 etc., where the number will apply to the above-mentioned ultimate time in minutes. In addition, definition of the fire curve, i.e. fire scenario, to which this ultimate time should apply, will be given in the study as well.

1.1.1. Direct fire actions A_d

The term direct action of fire, usually refers to the change of the mechanical properties of the material (material strength and the corresponding strain at peak stress, ultimate strain,...) due to high temperatures. According to EN 1992-1-2 [3], the design value of a material's mechanical property at a specific temperature $X_{d,fi,\theta}$ can be calculated using the following equation:

$$X_{d,fi,\theta} = k_\theta \frac{X_k}{\gamma_{M,fi}}$$ (3)

Where k_θ is the temperature-dependent reduction factor, X_k is the characteristic value of the mechanical property at room temperature of 20°C and $\gamma_{M,fi}$ is the material safety factor. The latter, is equal to 1 according to Eurocode instructions. Moreover, for concrete, coefficient k_θ depends on the nature of aggregates of the concrete mixture (calcareous or siliceous aggregate), and, for reinforcing steel, k_θ depends on whether cold-formed or hot-rolled steel is in question. Values of k_θ for the two materials in accordance with EN 1992-1-2 [3] are shown in the tables below.

Concrete temperature	Siliceous aggregates			Calcareous aggregates		
θ [°C]	$f_{c,\theta} / f_{ck}$	$\varepsilon_{c1,\theta}$	$\varepsilon_{cu1,\theta}$	$f_{c,\theta} / f_{ck}$	$\varepsilon_{c1,\theta}$	$\varepsilon_{cu1,\theta}$
20	1.00	0.0025	0.0200	1.00	0.0025	0.0200
100	1.00	0.0040	0.0225	1.00	0.0040	0.0225
200	0.95	0.0055	0.0250	0.97	0.0055	0.0250
300	0.85	0.0070	0.0275	0.91	0.0070	0.0275
400	0.75	0.0100	0.0300	0.85	0.0100	0.0300
500	0.60	0.0150	0.0325	0.74	0.0150	0.0325
600	0.45	0.0250	0.0350	0.60	0.0250	0.0350
700	0.30	0.0250	0.0375	0.43	0.0250	0.0375
800	0.15	0.0250	0.0400	0.27	0.0250	0.0400
900	0.08	0.0250	0.0425	0.15	0.0250	0.0425
1000	0.04	0.0250	0.0450	0.06	0.0250	0.0450
1100	0.01	0.0250	0.0475	0.02	0.0250	0.0475
1200	0.00	-	-	0.00	-	-

Table 1: Mechanical characteristics of concrete with siliceous and calcareous aggregates at high temperatures (i.e. compressive strength compared to its initial value at ambient temperature, strain at peak stress, and ultimate strain at failure). The table is taken from EN 1992-1-2 [3].

Steel temperature	$f_{sy,\theta} / f_{yk}$		$f_{sp,\theta} / f_{yk}$		$E_{s,\theta} / E_s$	
θ [°C]	hot rolled	cold worked	hot rolled	cold worked	hot rolled	cold worked
20	1.00	1.00	1.00	1.00	1.00	1.00
100	1.00	1.00	1.00	0.96	1.00	1.00
200	1.00	1.00	0.81	0.92	0.90	0.87
300	1.00	1.00	0.61	0.81	0.80	0.72
400	1.00	0.94	0.42	0.63	0.70	0.56
500	0.78	0.67	0.36	0.44	0.60	0.40
600	0.47	0.40	0.18	0.26	0.31	0.24
700	0.23	0.12	0.07	0.08	0.13	0.08
800	0.11	0.11	0.05	0.06	0.09	0.06
900	0.06	0.08	0.04	0.05	0.07	0.05
1000	0.04	0.05	0.02	0.03	0.04	0.03
1100	0.02	0.03	0.01	0.02	0.02	0.02
1200	0.00	0.00	0.00	0.00	0.00	0.00

Table 2: Mechanical characteristics of reinforcing steel at high temperatures compared to their initial values at ambient temperature, i.e. maximum stress level (strength of steel), proportional limit, and elastic modulus. The table is taken from EN 1992-1-2 [3].

Likewise, the term direct action of the fire can also refer to thermal expansion to which the material is prone due to the influence of high temperatures. Relative expansion coefficient in EN 1992-1-2 [3] designated as $\Delta l/l$, is for concrete defined as (Fig. 1):

- Siliceous aggregates:

$$\varepsilon_C(\theta) = -1.8 * 10^{-4} + 9 * 10^{-6}\theta + 2.3 * 10^{-1}\ \theta^3 \qquad \text{for } 20°C \leq \theta \leq 700°C \qquad (4)$$
$$\varepsilon_C(\theta) = 14 * 10^{-3} \qquad \text{for } 700°C < \theta \leq 1200°C \qquad (5)$$

- Calcareous aggregates:

$$\varepsilon_C(\theta) = -1.2 * 10^{-4} + 6 * 10^{-6}\theta + 1.4 * 10^{-11}\theta^3 \qquad \text{for } 20°C \leq \theta \leq 805°C \qquad (6)$$
$$\varepsilon_C(\theta) = 12 * 10^{-3} \qquad \text{for } 805°C < \theta \leq 1200°C \qquad (7)$$

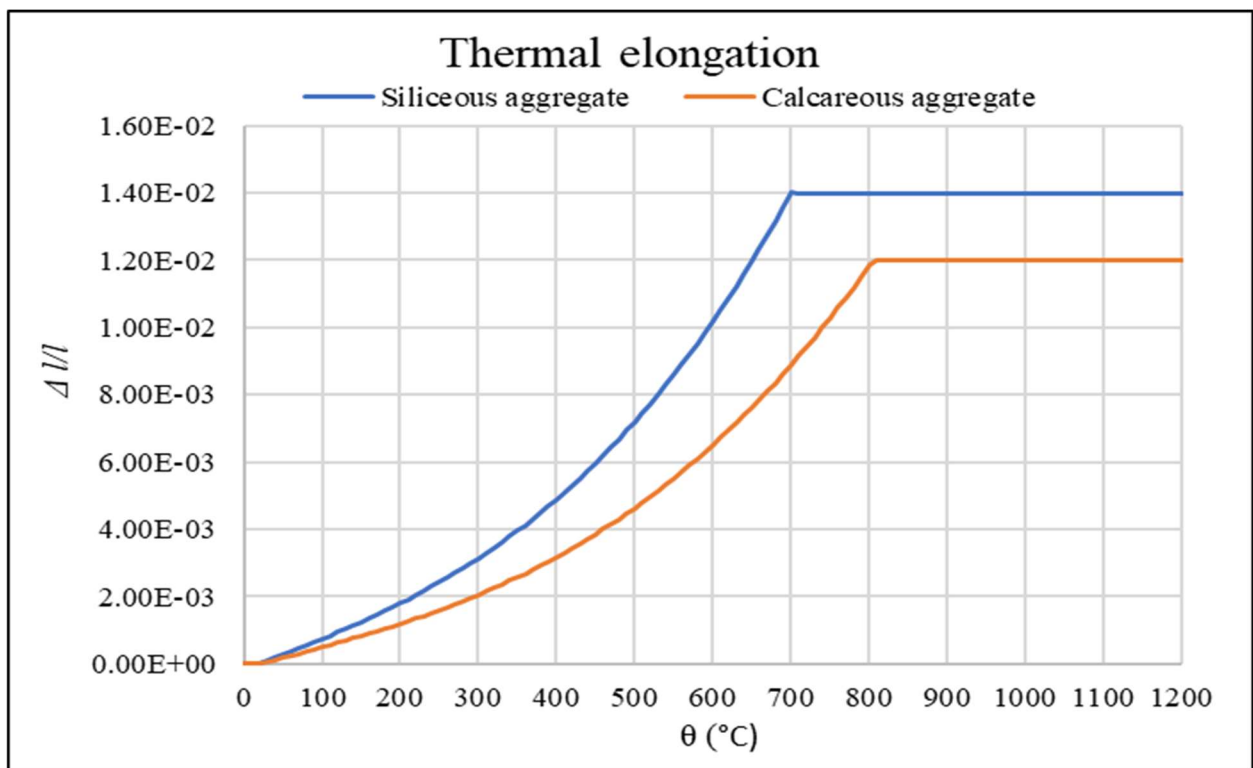Where θ is the concrete temperature (°C).

Figure 1. Total thermal elongation of concrete. Figure is taken from EN 1992-1-2 [3].

Moreover, the relative expansion coefficient for reinforcing steel is defined as follows (Fig. 2):
$$\varepsilon_S(\theta) = -2.416 * 10^{-4} + 1.2 * 10^{-5}\theta + 0.4 * 10^{-8}\theta^2 \qquad \text{for } 20°C \leq \theta \leq 750°C \qquad (8)$$
$$\varepsilon_S(\theta) = 11 * 10^{-3} \qquad \text{for } 750°C < \theta \leq 860°C \qquad (9)$$
$$\varepsilon_S(\theta) = -6.2 * 10^{-3} + 2 * 10^{-5}\theta \qquad \text{for } 860°C < \theta \leq 1200°C \qquad (10)$$

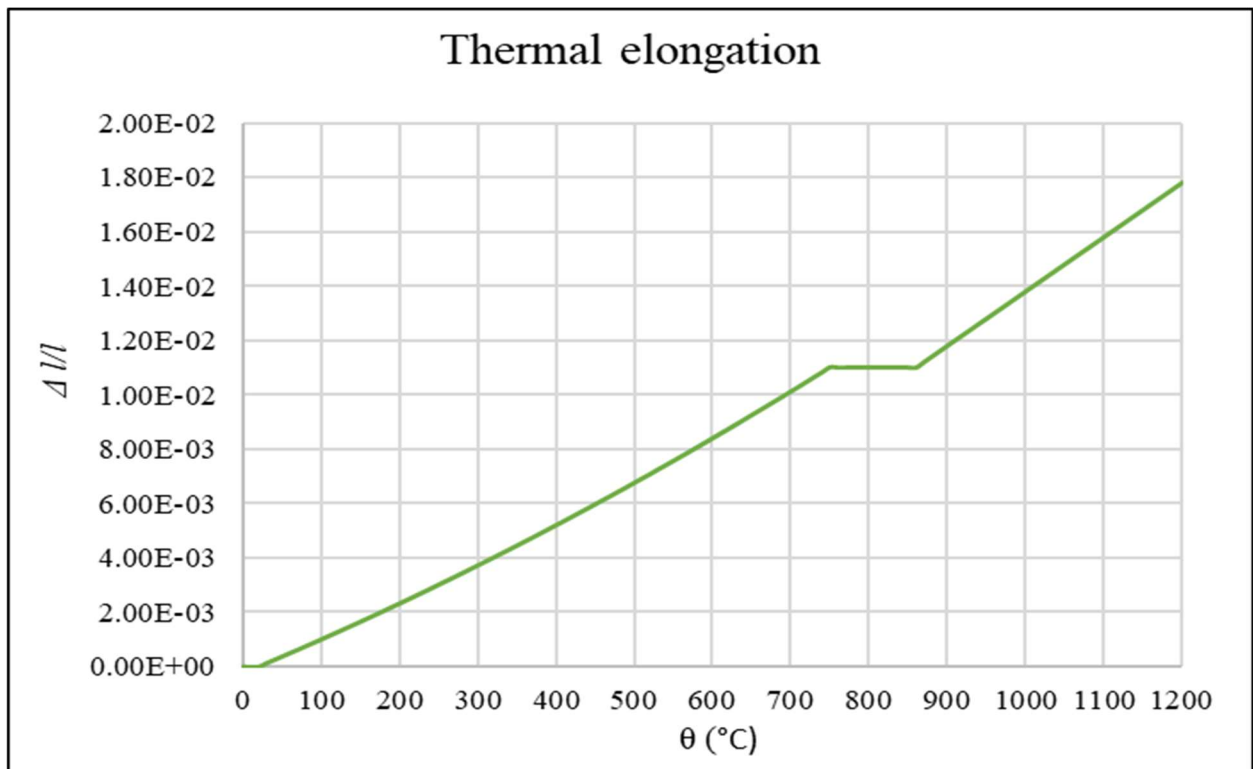Where θ is the steel temperature (°C).

Figure 2. Total thermal elongation of reinforcing steel. Figure is taken from EN 1992-1-2 [3].

1.1.2. Indirect fire actions A_d

Indirect actions of a fire are creep of concrete and creep of reinforcing steel, hindered temperature deformations and spalling of concrete. They depend on the material as well as on the structure's characteristics.

Creep is permanent material deformation that increases with time under constant stress. The phenomenon is more pronounced at higher temperatures. According to EN 1992-1-2 [3], it can be assumed that the influence of high-temperature creep in a structural fire analysis is already covered indirectly within the values of the reduction coefficients k_θ, presented in section 2.1.2 above, if only the rate of heating of the material is within limits between 2 K/min – 50 K/min. In the opposite case, creep should be accounted for separately and accordingly.

Within the overall structural system, thermal elongations of individual structural elements are often hindered in one way or another, which causes additional stress. This phenomenon is called *hindered temperature deformations*.

In what follows, another indirect fire action on a concrete structure will be discussed, i.e. *concrete spalling*. Concrete is a composite of aggregate, cement stone and gel pores filled with chemically bound water. The remaining part is represented by capillary pores in which there is free water and air. When the temperature of the material rises, water vaporizes first in concrete (causing an increase in the internal pressure and moisture concentration gradient), which evokes the flow of free water, water vapor and dry air through the pores. This way, heat passes through the interior of the concrete not only by conduction but also by convection. In addition, at around 200°C, dehydration (release of chemically bound water) occurs, which causes an accelerated deterioration of the material's mechanical properties.

6

When flowing through the pores of the element, free water and gases travel partially towards the heated edge of the structural element and partially towards the colder interior of the element, where water vapor condenses. Especially in concrete with low permeability or high humidity (concrete structures of underground garages, tunnels, etc.), the condensation may lead toward a formattion of a clogged zone. The result is an increase in pore pressures in front of the zone and an increase in the degree of damage to the material in this region (opening and propagation of concrete cracks).

Over time, this can lead to sudden detachment of the outer layers of the concrete element, which is called explosive spalling. The latter can result in a significantly increased exposure of the reinforcement to high temperatures and, thus, in a reduction of fire resistance of the structural element. In extreme cases, the result of explosive spalling can even be a complete break in the contact between concrete and its steel reinforcement and the element's collapse.
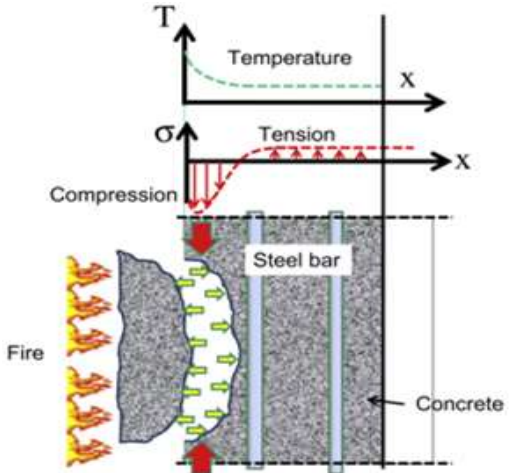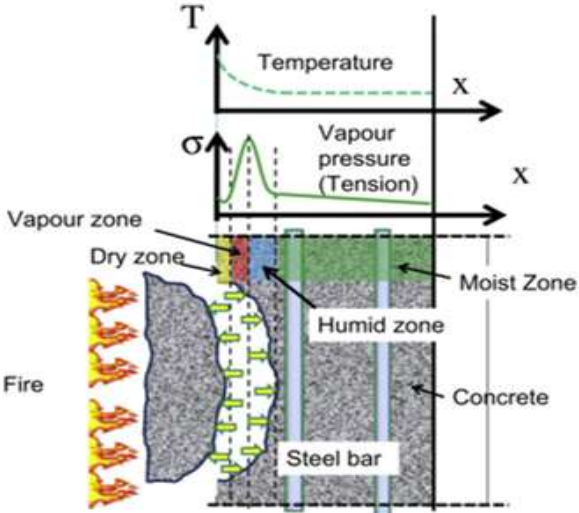

Figure 3: Fire-exposed RC column. *Left* (top and bottom): diagram of the mechanisms of explosive spalling of concrete (figure taken from source [8]), *right*: photo of damage to a column after a fire test (figure taken from source [9])

1.2. *Meeting the criterion $R_{fi,d,t} \geq E_{fi,d,t}$ (the procedure)*

The process of checking the criterion $R_{fi,d,t} \geq E_{fi,d,t}$ in this thesis will be divided into three essential phases:
- Determining a suitable fire scenario (fire curves)
- thermal analysis of the structure
- mechanical analysis of the structure

According to Eurocode, each phase can be performed in several different ways (more simple or more complex).

1.2.1. *Fire scenario*

In the most general form, a fire scenario is a function of temperatures of the surroundings of the analysed structure which depends on the time and space (i.e. on the exact location within the affected fire compartment). With the term 'surroundings temperature' we here refer to:

- The temperature of the surrounding gas, which is important for convective transfer of heat to and from the analysed structure

- Temperature of the surrounding solid obstructions that exchange heat with the structure

During a *fully developed fire [1]*, which usually interests us the most from the point of view of fire resistance of the structure, this function can usually be simplified to a less complicated (space-independent) function, i.e. fire curve (Fig. 4). With this simplification, it is assumed that at a particular time *t* the temperature of the surroundings of the structure or its specific part will be uniform in space (the same at each particular location).

While searching for an applicable fire curve, a fire engineer has a choice between the so-called nominal curves, which usually describe the heating but not the cooling phase of the fire, or parametric curves (known as natural fire curves). The formerly mentioned curves are determined by straightforward analytical expressions taken, e.g., from EN 1991-1-2 [7], and selection between them is made exclusively considering the general type of the fire (i.e. cellulosic fire, external fire or hydrocarbon fire, Fig. 4). The latter mentioned curves, however, are in most cases calculated by a more or less advanced numerical procedure (for example in computer programmes such as Ozone [10], FDS [11],…). On top of the general type of fire, these curves also take into account several other distinguishing features of the building affecting the dynamics of the fire (e.g. the size of fire compartments, the amount and location of flammable materials, the size of the openings of the building's facade such as windows and doors, which provide access to oxygen during a fire and increase burning rate, etc.).

As explained later in this thesis, the so called hydrocarbon nominal fire curve will be taken for purposes of analyses in this thesis. In the case of applying the nominal fire curve from EN 1991-1-2 [7], this is chosen exclusively considering the general type of the fire (i.e. cellulosic fire, external fire, or hydrocarbon fire) and not taking into consideration any other building specifics.

---

[1] The fire may be declared as fully developed when reaching a period of burning where the maximum heat is released and flames fill the entire fire compartment (all suitable surfaces ignite). The fire compartment represents a region inside the building in question, which is separated from neighboring regions by fire-resistant surfaces (e.g. fire resistant walls). In case of a fire, these surfaces will prevent the fire from spreading to neighboring compartments for a designed period of time.

For example, the so-called standard fire curve represents the time development of temperatures within the affected fire compartment in a typical cellulosic fire. Commonly these can be found in standard office and/or residential buildings. Moreover, the external fire curve is applied for the fire analyses of structural elements found on the outer side of buildings (e.g. baldachin girders etc.) which are usually exposed to flames from façade fires. In the case of such fire heating from the flame, it is continually reduced by the cool external air; to some degree lower temperatures are commonly applied with this external curve compared to an internal curve of a building fire. Furthermore, the hydrocarbon curve is applied while analyzing structural elements exposed to a hydrocarbon fire (e.g. to fire of an oil tank truck in a road tunnel, a fire in an industrial facility etc.).

Supplementary to nominal fire curves, parametric fire curves may also be used to take into account several other factors of the building and fire (e.g. the size of fire compartments, the amount and location of flammable materials, the size of openings of the building's envelope such as windows and doors, which provide access to oxygen during a fire and increase burning rate, etc). This gives the parametric curves an important upper hand over the nominal curves while considerably ameliorating their precision.
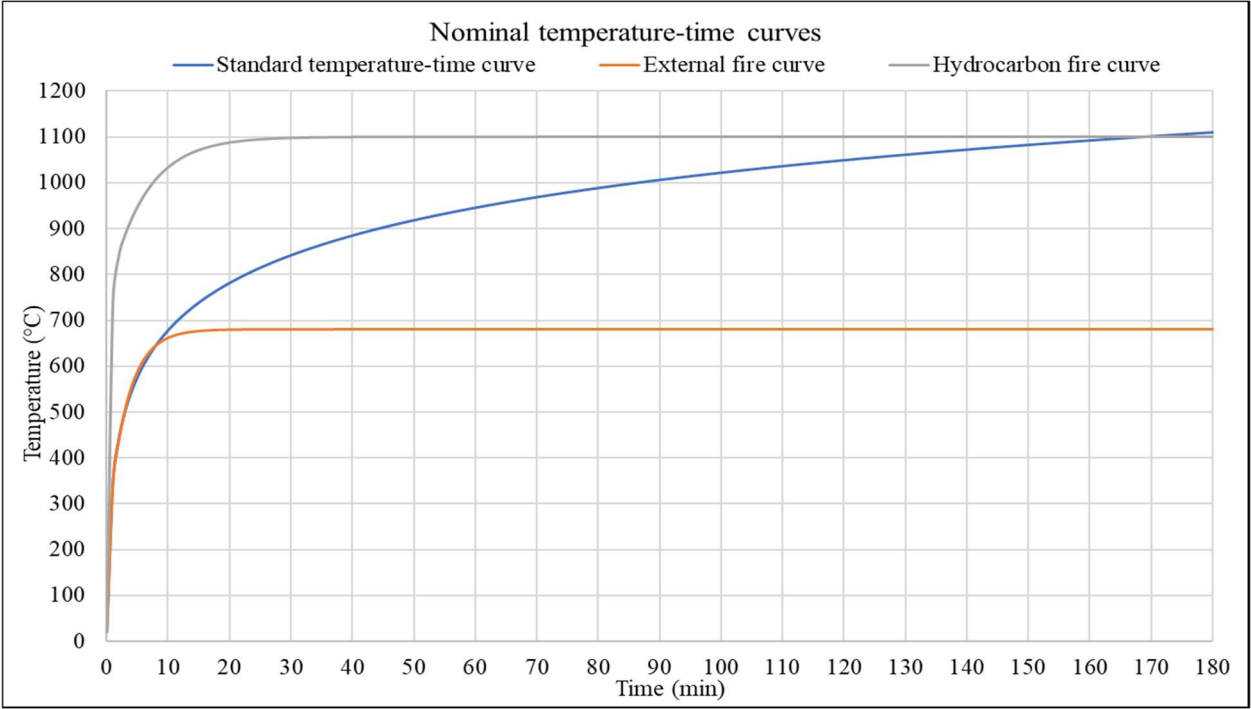

Figure 4: Nominal fire curves according to EN 1991-1-2 [7].

1.2.2. Thermal analysis

In this thesis, thermal analysis of reinforced-concrete (RC) structures will be founded on acknowledged principles, postulations and equations of the theory of non-stationary heat transfer through solid bodies This theory is based on the well-known standard Fourier partial differential equation:

$$V: \quad \frac{\partial}{\partial x_i}\left(\lambda_{ij}\frac{\partial T}{\partial x_j}\right) + Q - \rho c \frac{\partial T}{\partial t} = 0 \; ; (i,j = 1,2,3) \tag{11}$$

Where:

T represents the temperature of an individual point of the solid [°C]

λ_{ij} is a component of the thermal conductivity tensor of the material of the solid $[W/mK]$

Q is specific volume heat flux $[W/m^3]$

ρ is the density of the material $[kg/m^3]$

c is the specific heat of the material $[J/kgK]$

According to EN 1992-1-3 [3] thermal conductivity of concrete varies with the material temperature (Fig. 5) and is at each temperature somewhere between the following limits:

- Upper bound limit:

$$\lambda_c = 2 - 0{,}2451\left(\frac{T}{100}\right) + 0{,}0107\left(\frac{T}{100}\right)^2 \quad [W/mK] \tag{12}$$

- Lower bound limit:

$$\lambda_c = 1{,}36 - 0{,}136\left(\frac{T}{100}\right) + 0{,}0057\left(\frac{T}{100}\right)^2 \quad [W/mK] \tag{13}$$

In addition, specific heat depends on temperature as well as it also depends on the moisture content in concrete (Fig. 6):

- For moisture content of 0% by weight of concrete:

$$c_p(\theta) = 900 \qquad\qquad [J/kgK] \qquad\qquad \text{for } 20°C \leq \theta \leq 100°C \tag{14}$$
$$c_p(\theta) = 900 + (T - 100) \quad [J/kgK] \qquad\qquad \text{for } 100°C < \theta \leq 200°C \tag{15}$$
$$c_p(\theta) = 1000 + \frac{T-200}{2} \quad [J/kgK] \qquad\qquad \text{for } 200°C < \theta \leq 400°C \tag{16}$$
$$c_p(\theta) = 1100 \qquad\qquad [J/kgK] \qquad\qquad \text{for } 400°C \leq \theta \leq 1200°C \tag{17}$$

- For moisture content of 1.5% by weight of concrete:
  Identical equations apply for 0% moisture content with one vital dissimilarity. I.e. at 100 °C the specific heat suddenly rises to 1470 (J/kgK) and remains at this value, on the interval [100°C - 115°C]. Finally, it is linearly declining to a value of 1000 (J/kgK) at temperatures between [115°C - 200°C].

- For moisture content of 3.5% by weight of concrete:
  The same general rules apply for the case of 1.5% moisture content, except that at 100°C specific heat is increased to a value of 2020 (J/kgK).
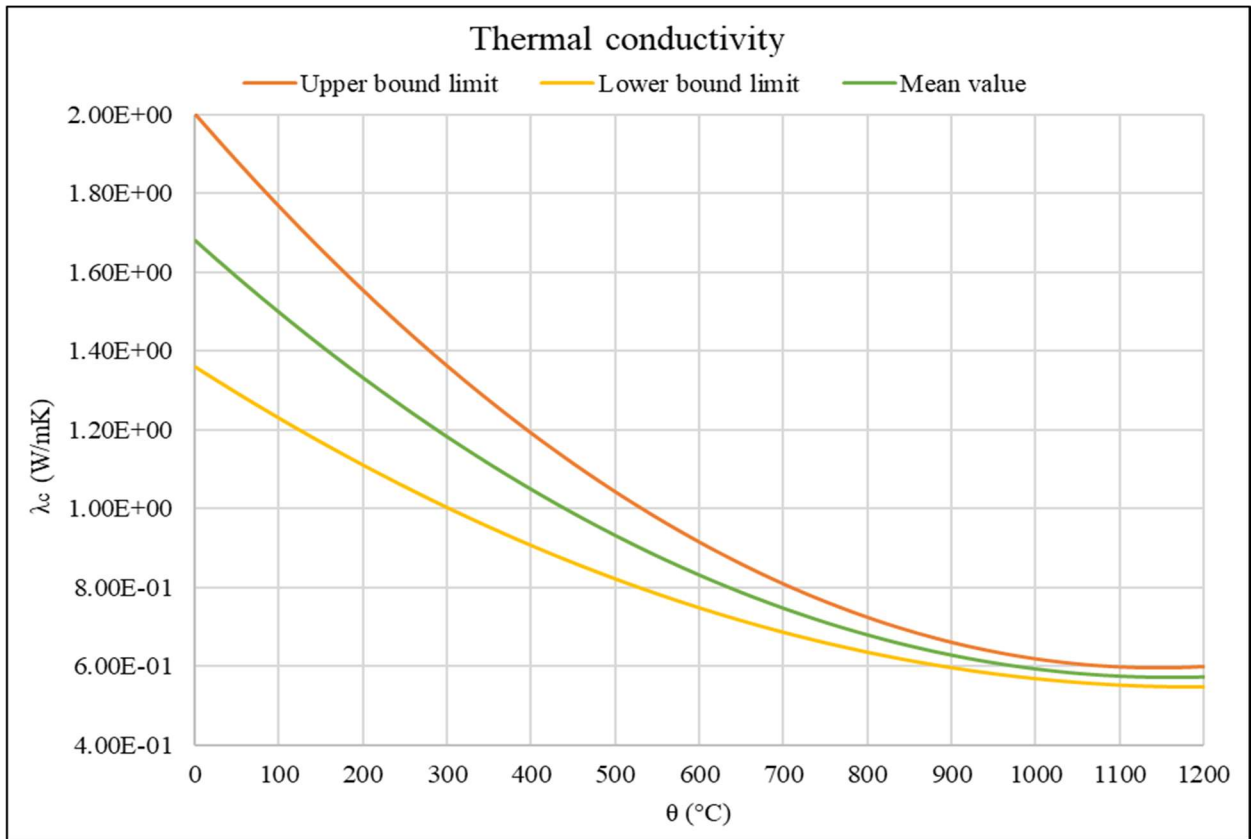
Figure 5: Thermal conductivity of concrete λ_c $[W/mK]$ as a function of temperature as defined in EN 1992-1-2 [3].
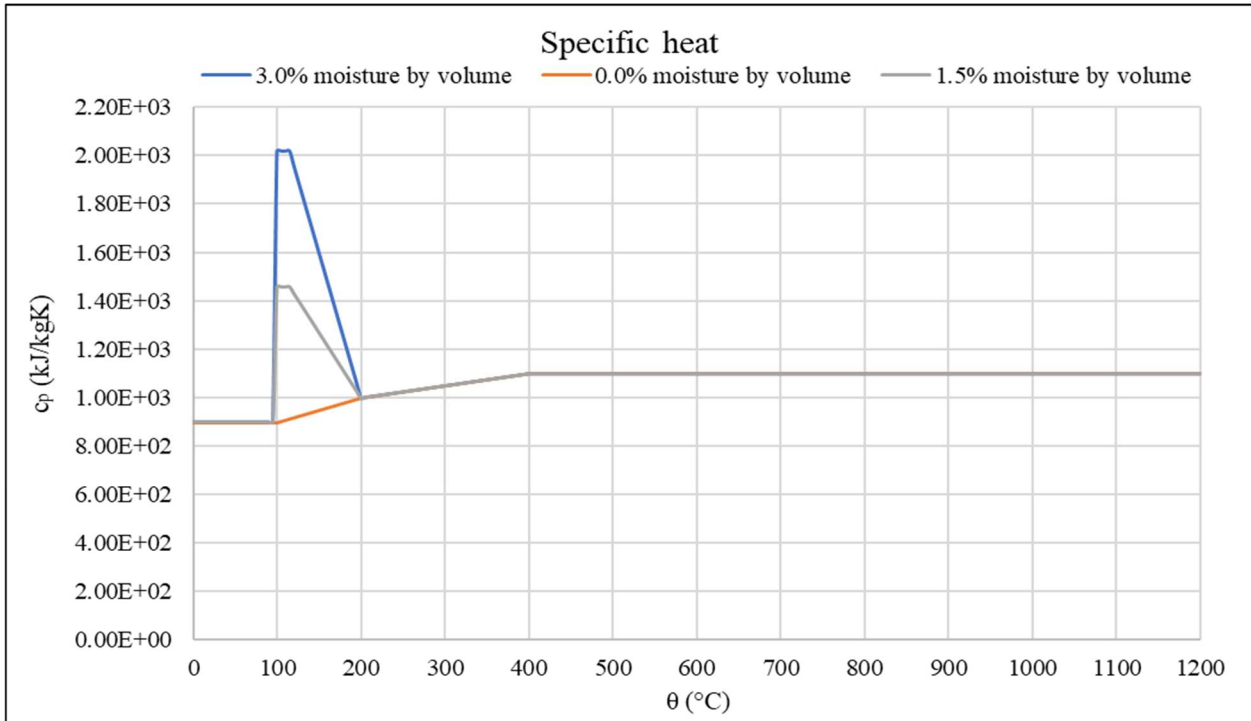
Figure 6: Specific heat c_p $[kJ/kgK]$ as a function of temperature as defined in EN 1992-1-2 [3].

Although density of concrete also varies with temperature, but these variations usually do not have a greater impact on the results of the thermal analysis. In this thesis thus, a constant value of 2500 kg/m^3 will be declared as the density of concrete.

For obtaining the correct solution of the standard Fourier equation, i.e. Eq. 10 suitable boundary conditions defining the heat flow at the surface of the solid need to be set as well:

$$S_d: \lambda_{ij} \frac{\partial T}{\partial x_i} n_i = q_s = q_{s,c} + q_{s,r} \tag{18}$$

Where:

S_d is the surface of the solid body

n_i is the ith component of the unit vector of the normal to this surface

q_s is specific surface heat flux $[W/m^2]$ where this is defined as the sum of two fluxes, i.e. convective and radiative:

$$q_s = q_{s,c} + q_{s,r} \tag{19}$$

Convective flux:

$$q_{s,c} = \alpha_c (\theta_g + \theta_m) \tag{20}$$

Radiative flux:

$$q_{s,r} = \varepsilon_m \sigma \left[\left(\theta_g + 273 \right)^4 - (\theta_m + 273)^4 \right] \tag{21}$$

In Eq. (19) and Eq. (20):

α_c is convective heat transfer coefficient $[W/m^2 K]$; according to EN 1992-1-2 [3] this is dependent on the side of the structure (fire-exposed or unexposed) and the selected fire curve. For *fire-exposed surfaces*: 25 $W/m^2 K$ should be taken in case of standard or external fire, 50 $W/m^2 K$ in case of hydrocarbon fire and 35 $W/m^2 K$ should be applied in case of a natural fire. For *fire-unexposed surfaces*: 4 $W/m^2 K$ should be taken in every case or, the effects of heat transfer by radiation are to be accounted for indirectly with the same coefficient; this value should be increased to 9 $W/m^2 K$.

θ_g is the temperature of the surroundings of the solid body $[°C]$,

θ is the surface temperature of the solid body $[°C]$,

ε_m is the surface emissivity of the solid body $[–]$ which; can be taken as 0.7 for concrete structures according to instructions of EN 1992-1-2 [3]

σ is the Stefan–Boltzmann constant: $5.6704 \cdot 10^{-8} W/m^2 K^4$.

In addition, appropriate initial conditions (initial temperatures of the structure) need to be defined as well for solving the Fourier equation:

$$V: \theta(t = 0) = \theta_0 \tag{22}$$

Where:

V is the volume of the solid and

θ_0 is its initial temperature $[°C]$.

Essentially, the Fourier equation with the corresponding boundary and initial conditions as described above cannot be solved using analytical calculation methods, but numerical methods will be necessary (such as FEM, differential method, etc.). The solution will, thus, be typically obtained in dedicated software, such as ABAQUS [2], ANSYS [12], SAFIR [13] and others.

1.2.3. Structural response analysis

Only based on the structure's calculated temperature field canwe finally start examining the criterion $R_{fi,d,t} \geq E_{fi,d,t}$. For this purpose, Eurocode generally allows several different computational design methods. However, only the most accurate of them, which are based on the equations of the geometrically and materially nonlinear third-order theory of solid body mechanics at high temperatures, will generally be suitable for the cases of larger structural systems.

Unfortunately, this mentioned theory exceeds the usual framework of the master's study program of Structural engineering at the Faculty of Civil engineering, Architecture and Geodesy in Split, and it goes beyond this master's thesis framework. Thus, we refrain from its detailed description here. Instead, we only mention that the governing equations of this theory, are in fact a more complex version of the equilibrium, kinematic and constitutive equations of the corresponding first-order theory, which applies if the conditions of small displacements and rotations is presented, e.g. in the textbook [14].
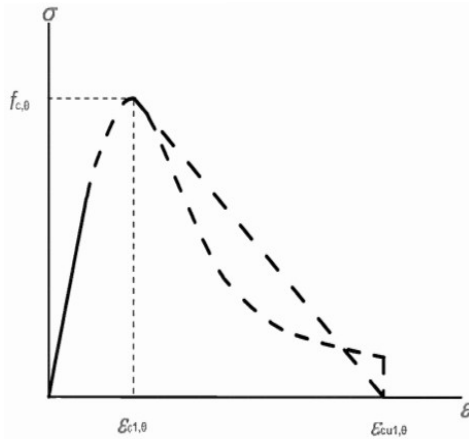
For the most accurate fire analysis of structures where large deformations and displacements of the structure occur, it is necessary to convert these equations in accordance with third-order theory approaches (exact kinematics). This means that it is necessary to write down the equilibrium conditions for the deformed state of the body instead of the undeformed one, as well as express the specific changes in lengths, changes of angles and changes in elementary plates with the components of the large deformation tensor.

Transformation of the basic equations of the problem (kinematic, constitutive and equilibrium) from the first-order to the third-order theory of solid body mechanics as mentioned above generally leads to a system of nonlinear equations that can only be solved numerically, e.g. using FEM in appropriate software, such as ABAQUS [2], ANSYS [12], SAFIR [13] and others.

While a detailed understanding of the equilibrium and kinematic equations of the theory is usually not necessary for the successful execution of structural fire analyses in these computer programs, a basic understanding for the constitutive equations is often a necessity (often suitable for our definition of the initial material input data will depend on it). Thus, these equations will be discussed in more detail further on.

Constitutive equations

Constitutive (i.e. material equations) define the relationship between stresses and strains of a material. Determination of this relationship usually begins in a laboratory with material's uniaxial tension/compression test. The relationship between *uniaxial stress* and *uniaxial strain* is determined as follows: $\sigma = f(\varepsilon)$. For concrete and reinforcing steel at high temperatures, a proposal for such a relationship is provided in EN 1992-1-2 [3] (Fig. 7 and Fig. 8 below):

Range	Stress $\sigma(\theta)$
$\varepsilon \leq \varepsilon_{c1,\theta}$	$\dfrac{3\varepsilon f_{c,\theta}}{\varepsilon_{c1,\theta}\left(2 + \left(\dfrac{\varepsilon}{\varepsilon_{c1,\theta}}\right)^3\right)}$
$\varepsilon_{c1(\theta)} < \varepsilon \leq \varepsilon_{cu1,\theta}$	For numerical purposes a descending branch should be adopted. Linear or non-linear models are permitted.

Figure 7: Stress-strain relationships of concrete under compression at elevated temperatures according to EN 1992-1-2 [3].
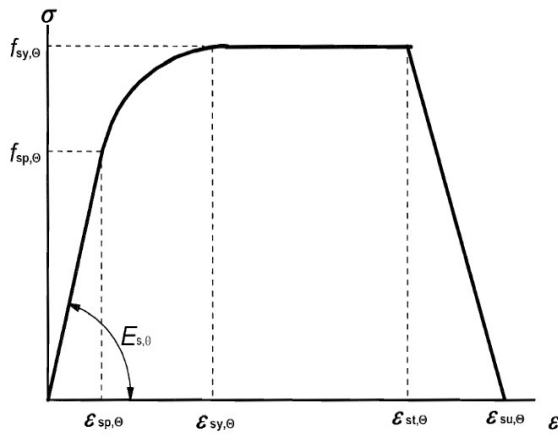
Range	Stress $\sigma(\theta)$	Tangent modulus
$\varepsilon_{sp,\theta}$	$\varepsilon E_{s,\theta}$	$E_{s,\theta}$
$\varepsilon_{sp,\theta} \leq \varepsilon \leq \varepsilon_{sy,\theta}$	$f_{sp,\theta} - c + (b/a)[a^2 - (\varepsilon_{sy,\theta} - \varepsilon)^2]^{0,5}$	$\dfrac{b(\varepsilon_{sy,\theta} - \varepsilon)}{a\left[a^2 - \left(\varepsilon - \varepsilon_{sy,\theta}\right)^2\right]^{0,5}}$
$\varepsilon_{sy,\theta} \leq \varepsilon \leq \varepsilon_{st,\theta}$	$f_{sy,\theta}$	0
$\varepsilon_{st,\theta} \leq \varepsilon \leq \varepsilon_{su,\theta}$	$f_{sy,\theta}[1 - (\varepsilon - \varepsilon_{st,\theta})/(\varepsilon_{su,\theta} - \varepsilon_{st,\theta})]$	-
$\varepsilon = \varepsilon_{su,\theta}$	0,00	-
Parameter *)	$\varepsilon_{sp,\theta} = f_{sp,\theta} / E_{s,\theta}$ $\quad \varepsilon_{sy,\theta} = 0,02 \quad \varepsilon_{st,\theta} = 0,15 \quad \varepsilon_{su,\theta} = 0,20$ Class A reinforcement: $\quad \varepsilon_{st,\theta} = 0,05 \quad \varepsilon_{su,\theta} = 0,10$	
Functions	$a^2 = (\varepsilon_{sy,\theta} - \varepsilon_{sp,\theta})(\varepsilon_{sy,\theta} - \varepsilon_{sp,\theta} + c/E_{s,\theta})$ $b^2 = c(\varepsilon_{sy,\theta} - \varepsilon_{sp,\theta})E_{s,\theta} + c^2$ $c = \dfrac{(f_{sy,\theta} - f_{sp,\theta})^2}{(\varepsilon_{sy,\theta} - \varepsilon_{sp,\theta})E_{s,\theta} - 2(f_{sy,\theta} - f_{sp,\theta})}$	

Figure 8: Stress-strain relationships of reinforcing steel at elevated temperatures according to EN 1992-1-2 [3].

In order to be able to use the relationship between the uniaxial material stress and strain $\sigma = f(\varepsilon)$ (also for cases of spatial stress-strain) conditions, the term comparative or equivalent stress σ_e is introduced in the literature. For *homogeneous*[2] and *isotropic*[3] materials that behave the same in compression and tension (in RC structures such as material, is steel reinforcement), the so-called Von Mises equivalent stress σ_e^M is often defined as follows:

---

[2] Homogeneous bodies are bodies that have the same structure, quality, and mechanical properties at every point direction within the area they occupy in space.
[3] Isotropy is the property of a substance to behave the same in all directions.

14

$$\sigma_e^M = \sqrt{\frac{1}{2} \left[(\sigma_{11} - \sigma_{22})^2 + (\sigma_{22} - \sigma_{33})^2 + (\sigma_{33} - \sigma_{11})^2 \right]} \qquad (23)$$

Where, σ_{11}, σ_{22} and σ_{33} are the components of the diagonalised stress tensor in the considered material point of the solid body.

The Von Mises equivalent stress defined in this way can also be used for modelling material such as concrete, so far as the sign of material stress is the same throughout the entire structure, e.g. the material is loaded only in compression as is typical with RC columns. A bigger problem arises when parts of concrete are also stressed in tension. In this case (because the response of concrete in compression is not the same as the response in tension) it will be necessary to choose a more complex form of equivalent stress function. This increase in complexity of the material definition will reflect on the global level of the computational analysis (often, even substantial prolongation of the analysis computing time will be observed). In addition, another problem will be that more complex forms of equivalent stress will typically depend on a larger number of various material parameters, for which the correct data will sometimes be hard to obtain in the available literature – the latter holding even for normal (room) temperatures, let alone at elevated temperatures.

To avoid the problems described above, which are imperatively related to the use of more complex material models for concrete in third-order theory fire analyses of RC structures, the authors Kolšek and Češarek [1] recently proposed the use of the so-called *reduced flexural stiffness material model for reinforced concrete.*

The following idea was proposed, that concrete, together with its steel reinforcement, was to be modelled as a homogeneous, isotropic material behaving bilinear in tension and compression as shown in the figure below. Note that in the first (i.e. elastic) part of the suggested curves, the inclination of each curve was considered to correspond to the elastic modulus of pure concrete.

This was said to be reduced in the same manner as in EN 1992-1-2 [3] proposed for high-temperature reductions of concrete compressive strength, i.e. $E_{C,\theta} = k_\theta E_{C,20°C}$ (k_θ taken from Table 1, as shown previously in the thesis). In addition, it was also considered to correspond to the actual cracking of concrete in tension which was accounted for indirectly by reducing the element's flexural stiffness $E_{RC,\theta} I_{RC} = k_{RC,EI} E_{C,\theta} I_{RC}$. The idea originates from the basic principles of modelling cracked RC members at ambient temperature conditions that are often adopted in simplified procedures of building codes and standards (e.g. [15]).
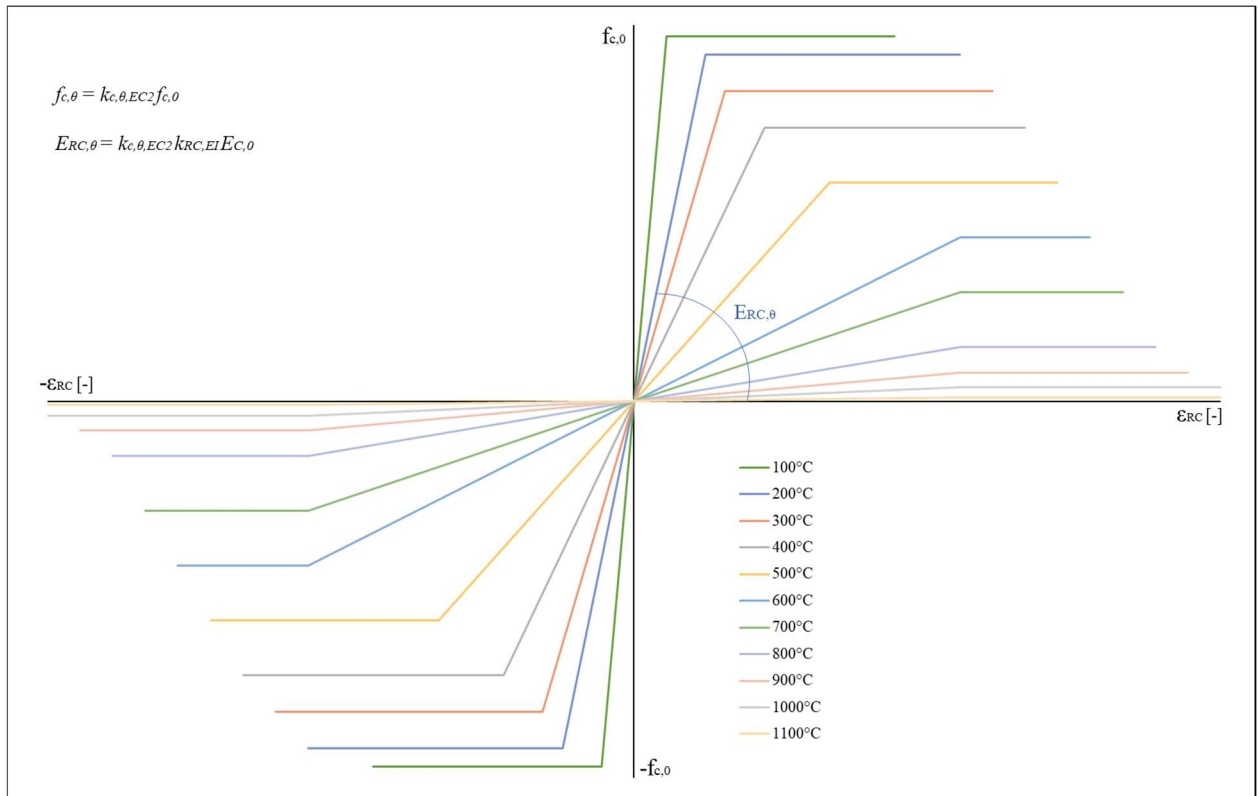
Figure 9: A material model of reinforced concrete at elevated temperatures according to [1].

Thermal strains

In addition to mechanical strains (i.e. due to the mechanical loading on the structure), which are connected to stresses through the relationship $\sigma_e = f(\varepsilon_e)$, thermal strains should also be mentioned explicitly discussing a structural fire analysis. The following equation defines the tensor of the latter:

$$\varepsilon_{th} = \alpha_T \Delta T \, \mathbf{I} \tag{24}$$

Where:

I is the unit tensor

α_T is the temperature-dependent relative expansion coefficient, denoted as $\Delta l / l$ in EN 1992-1-2 [3] (see section 1.1.1. of this thesis for the definition of the latter)

Chapter 2: Exploring the validity the of simplified material model for reinforced concrete

In this chapter of the master's thesis we try to contribute to the validation of the so-called *reduced flexural stiffness material model for reinforced concrete*, proposed by Kolšek and Česarek [1]. The model was described in more detail in chapter 1.2.3. Validation of the model is carried out with the help of computer reproductions of fire response of several RC plates and beams, which were experimentally tested by Bailey and Toh [16] and Monther B.M. Dwaikat [19], respectively.

2.1. Fire experiments of Bailey and Toh [16]

The research of Bailey and Toh [16], was conducted to test the membrane action of concrete/reinforced concrete plates subjected to ambient and elevated temperatures. Their development includes the refinement and improvement of assumed membrane stress and yield-line load in RC plates. The design method they suggested was tested on a sample of 44 tests of horizontally unrestrained plates with an aspect ratio of 1.0 or 1.55, respectively. The plates were reinforced with mild steel or stainless-steel welded mesh with different grades, ductility, sizes and bar spacing. All of the mentioned tests have shown the presence of membrane action of the plates, with the ambient test supporting a greater load than the theoretical yield-line load, and the elevated temperature tests reaching a higher temperature at failure compared to those calculated with the yield-line theory. Comparison between the developed simple design approach and test results showed good correlation both at ambient and elevated temperatures.

As we are generally interested in the behaviour of concrete (made with siliceous aggregate) reinforced with mild steel at elevated temperatures, in this thesis, only the appurtenant tests carried out at an elevated temperatures were analysed. The experimental programme at elevated temperatures, consists of 10 RC plates, with the same geometry, reinforcement and support conditions, adopted in the ambient tests. Details of the geometry, mechanical characteristics of the material and applied loads are shown in the table below (Tab. 3).

Test	Dimensions $L \times l \times H$ (mm)	Wires in long span			Wires in short span			Wire spacing (mm)	f_{cu} (MPa)	P (kN/m^2)	P_{test} (kN/m^2)	P_{test}/P	T_{mesh} (°C)	Δ_T	T_{pred} based on Δ_T (°C)	T_{pred}/T_{mesh}
		$\emptyset$ (mm)	f_y/f_u (MPa)	Ductility (%)	$\emptyset$ (mm)	f_y/f_u (MPa)	Ductility (%)									
MF1	$1700 \times 1100 \times 19.7$	2.43	695/727	2.86	2.41	722/742	3.46	50.8	43.2	9.52	5.280	0.55	764.9	54.38	641	0.84
MF2	$1100 \times 1100 \times 23.1$	2.41	684/736	3.19	2.43	780/795	1.07	50.8	43.3	19.00	5.519	0.29	747.1	37.33	679	0.91
MF3	$1700 \times 1100 \times 19.0$	1.54	336/404	18.76	1.54	349/420	12.57	25.4	39.1	4.07	3.655	0.90	727	41.74	543	0.75
MF4	$1100 \times 1100 \times 19.8$	1.54	336/404	18.76	1.54	349/420	12.57	25.4	39	6.36	5.429	0.85	700.1	30.74	537	0.77
MF5	$1700 \times 1100 \times 20.1$	1.51	402/463	12.84	1.52	467/498	6.53	12.7	37.1	13.47	5.280	0.39	721.9	43.88	647	0.90
MF6	$1100 \times 1100 \times 19.5$	1.51	402/463	12.84	1.52	467/498	6.53	12.7	38.5	14.35	7.900	0.55	782.4	32.73	620	0.79
MF7	$1700 \times 1100 \times 18.8$	0.85	405/444	5.40	0.83	470/486	3.65	12.7	43.8	3.36	4.460	1.33	556.5	44.95	439	0.79
MF8	$1100 \times 1100 \times 20.9$	0.85	405/444	5.40	0.83	470/486	3.65	12.7	43.5	5.65	4.646	0.82	653.9	32.13	545	0.83
MF9	$1700 \times 1100 \times 21.6$	0.71	371/382	3.40	0.68	449/455	1.44	6.35	47.1	5.23	3.697	0.71	652.1	41.82	568	0.87
MF10	$1100 \times 1100 \times 21.0$	0.71	371/382	3.40	0.68	449/455	1.44	6.35	40.4	7.18	5.494	0.77	686.0	31.07	555	0.81

Table 3: Details of slab tests with mild steel at elevated temperatures. The table is taken from Bailey and Toh [16].

The tests were conducted for 4 hours and subjected to elevated temperatures. All tests were carried out under a transient heating state, with a predefined working load (P_{test}) uniformly applied on the top surface of the plate by using dead weights. It was observed that the mild steel slabs, in general collapsed more suddenly, whereas the collapse of the stainless-steel slabs was more subtle, which is thought to be due to the difference in the ductility of the reinforcement meshes.

All of the tests failed in a similar manner (Fig. 10 right) showing the classic membrane action behaviour of horizontally unrestrained slabs. Setup of the test and a general mode of failure is shown below.
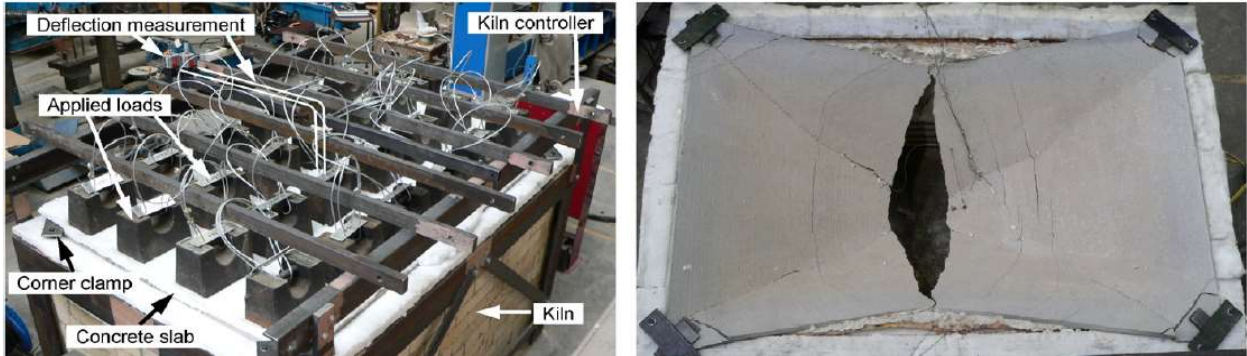

Figure 10: Setup of the elevated temperature tests (*left*) and general failure mode of tested slabs (*right*). Figures were taken from [16].

An electric kiln, located beneath the slabs, provided a heating rate of 300 ℃/*h*, up to a maximum temperature of 1000 ℃, which was maintained for the test duration. The temperature inside the kiln, the bottom and top surfaces of the slab, and the temperature of reinforcement at three locations at the centre of the slab, were recorded during each test using thermal gauges (thermocouples). Along with temperatures, vertical deflections of the plates were measured at their geometric center using LVDT devices.
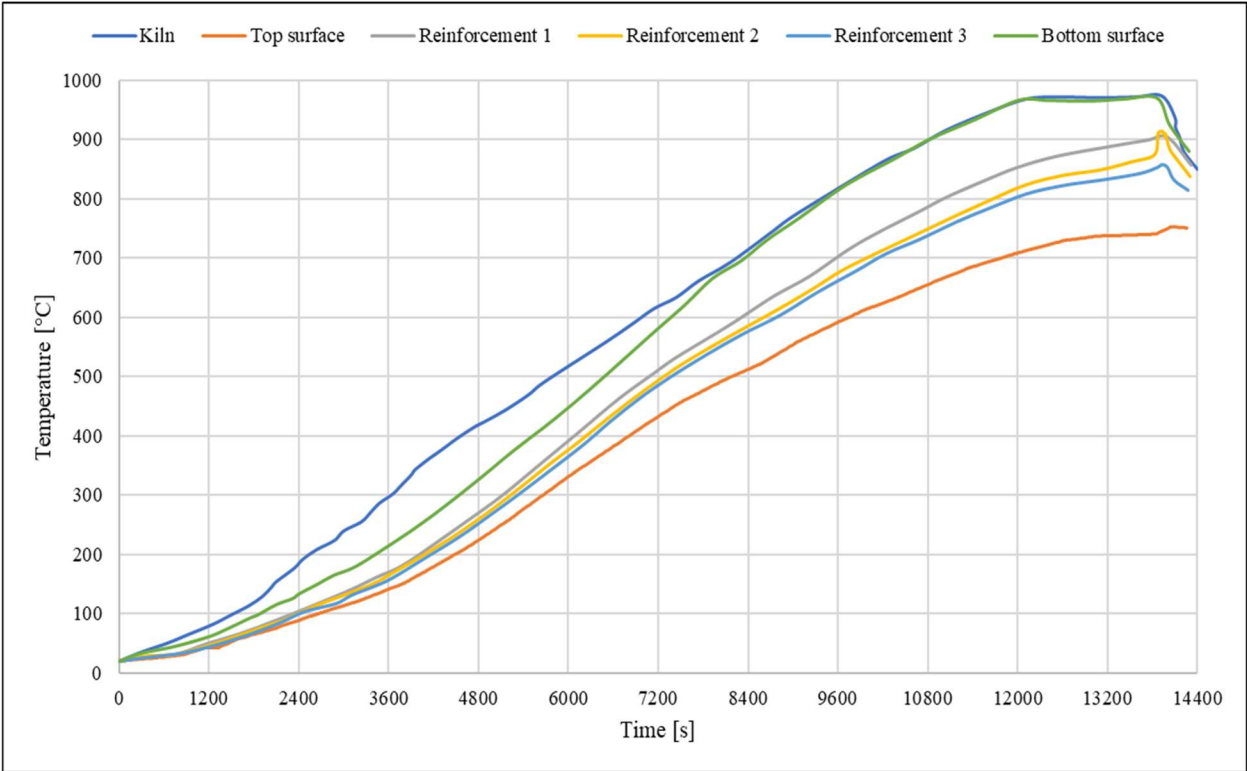

Figure 11: Values of temperatures during the test on various locations of the plate SF1. Figure was taken from [16].

2.2. Computer simulations for plates

The models for thermal and mechanical analysis of each plate were set up in ABAQUS [2]. For the models, a mesh convergence test was made, where the thermal and mechanical analysis results were compared to the experimental values. The test consisted of three different finite element variants, two with linear elements (one with three elements per thickness of the plate, and the other with six elements per thickness) and one with quadratic elements with three elements per thickness of plates. A comparison of the temperature values for each model result is shown below.
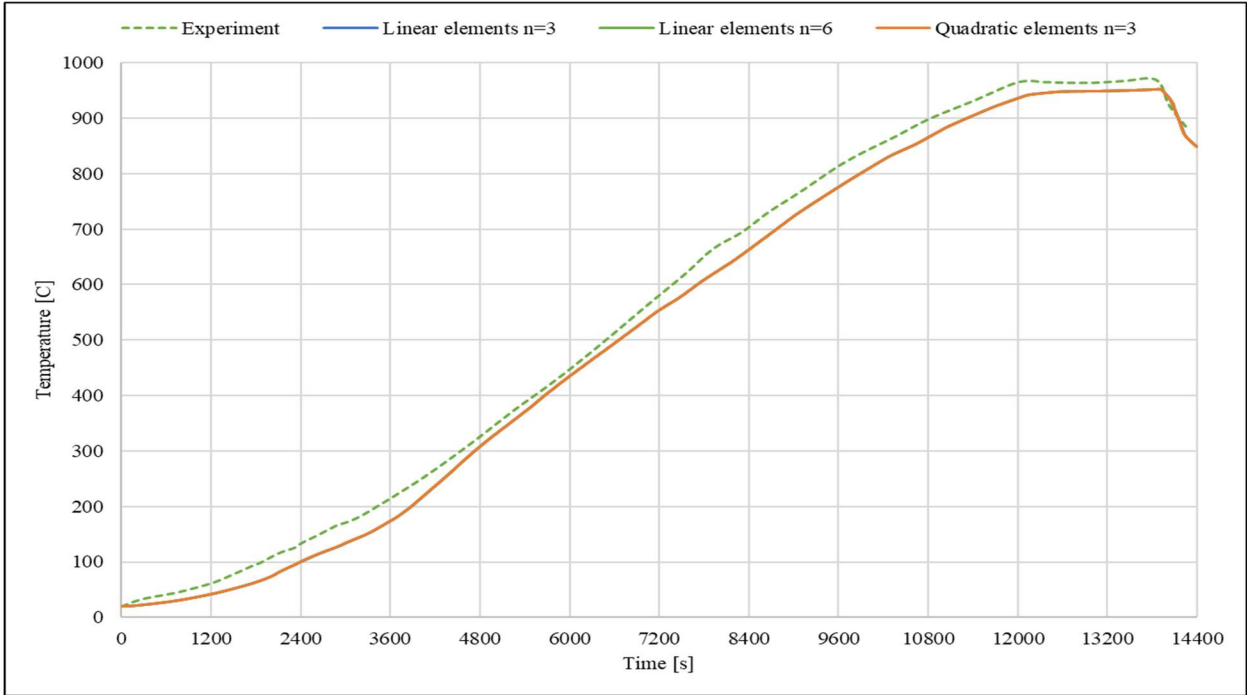

Figure 12: Comparison of temperature values on the bottom surface of the plate.
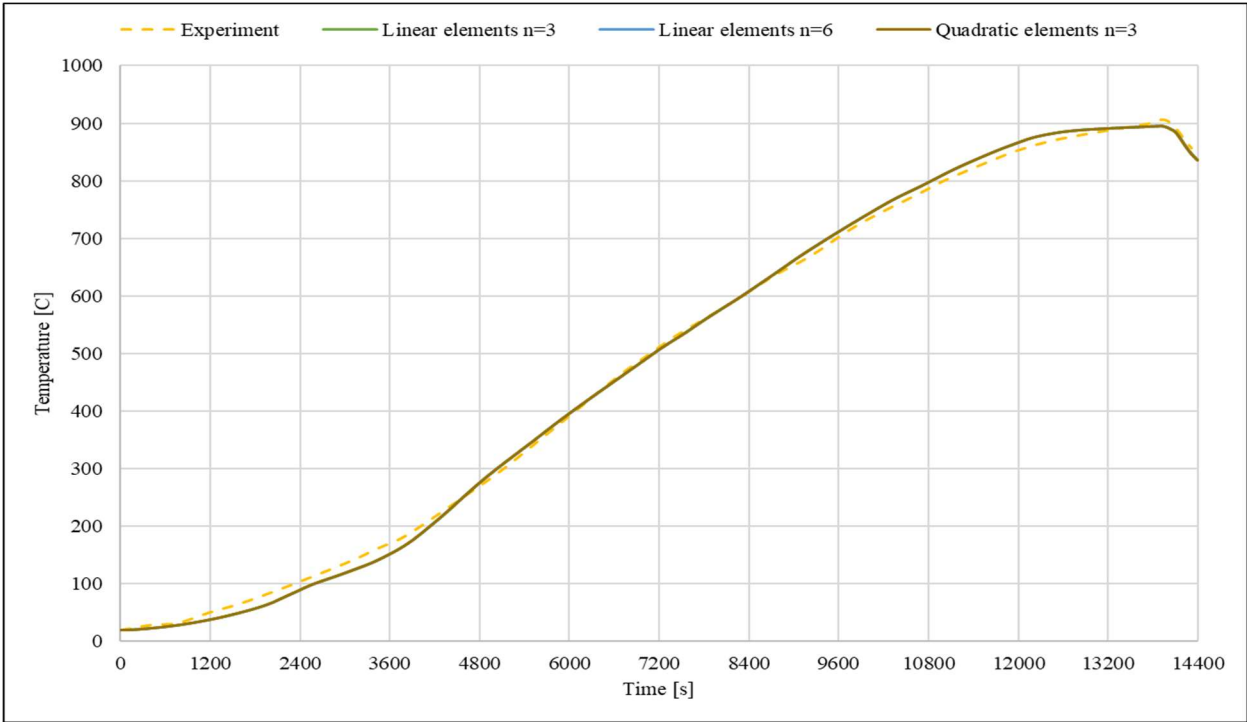
Figure 13: Comparison of temperature values on the reinforcement of the plate.

19
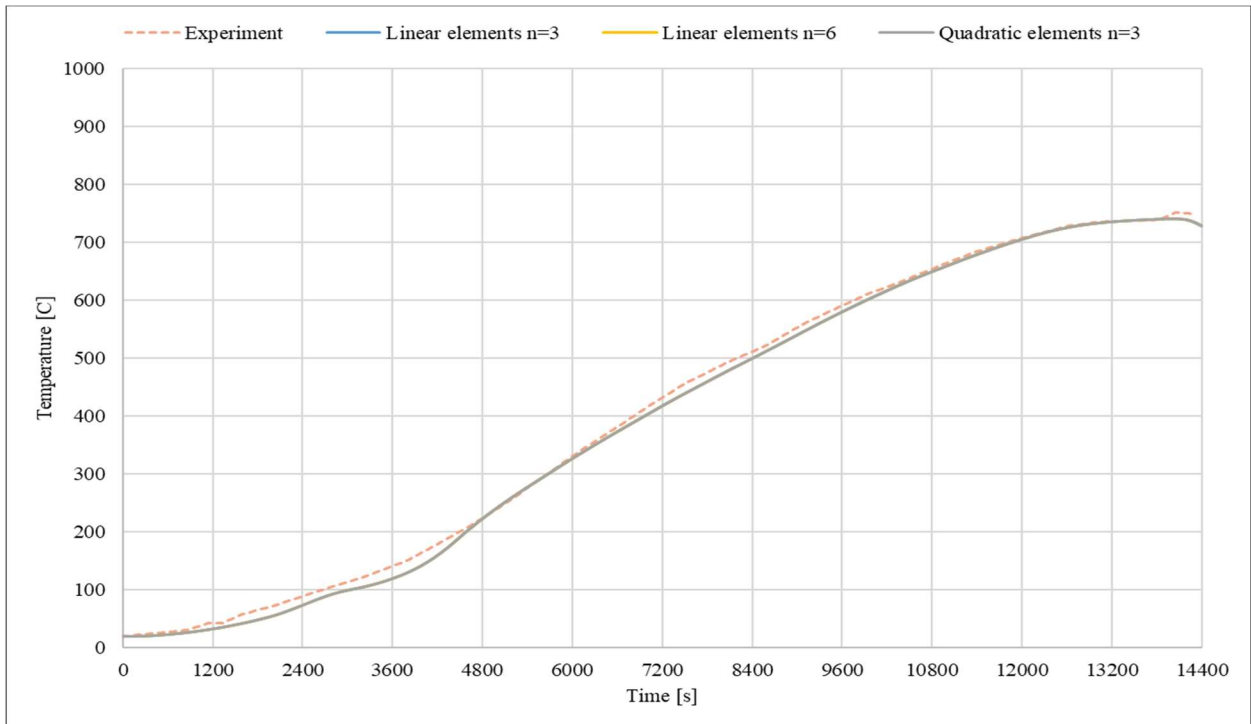
Figure 14: Comparison of temperature values on the top surface of the plate.

All of the previously mentioned variants have shown a very similar, and acceptable correlation of results with the experimental values. Furthermore, the variant with linear elements and six elements per thickness was used to carry out both the thermal and mechanical analysis for plates. The reason being, that even though the results of each variant were similar, the variant with linear elements and six elements per thickness was the most similar to the experimental value.

2.2.1. Thermal analysis of the plates

The thermal analysis model was prepared according to the geometry of the tested plate MF1 (see Table 3). Mesh of the model, consists of $91,476$ linear heat transfer finite elements with reduced integration (C3D8R) and approximate size of $l/w/h = 12/12/4\ mm$ (it was chosen this way so the aspect ratio would not be greater than ~3). The bottom surface (in between the simply supported edges) of the model was subjected to a transient heating regime according to the kiln temperature curve of the experiment (Fig. 11). In contrast, the rest of the model was assigned to be as ambient temperature.
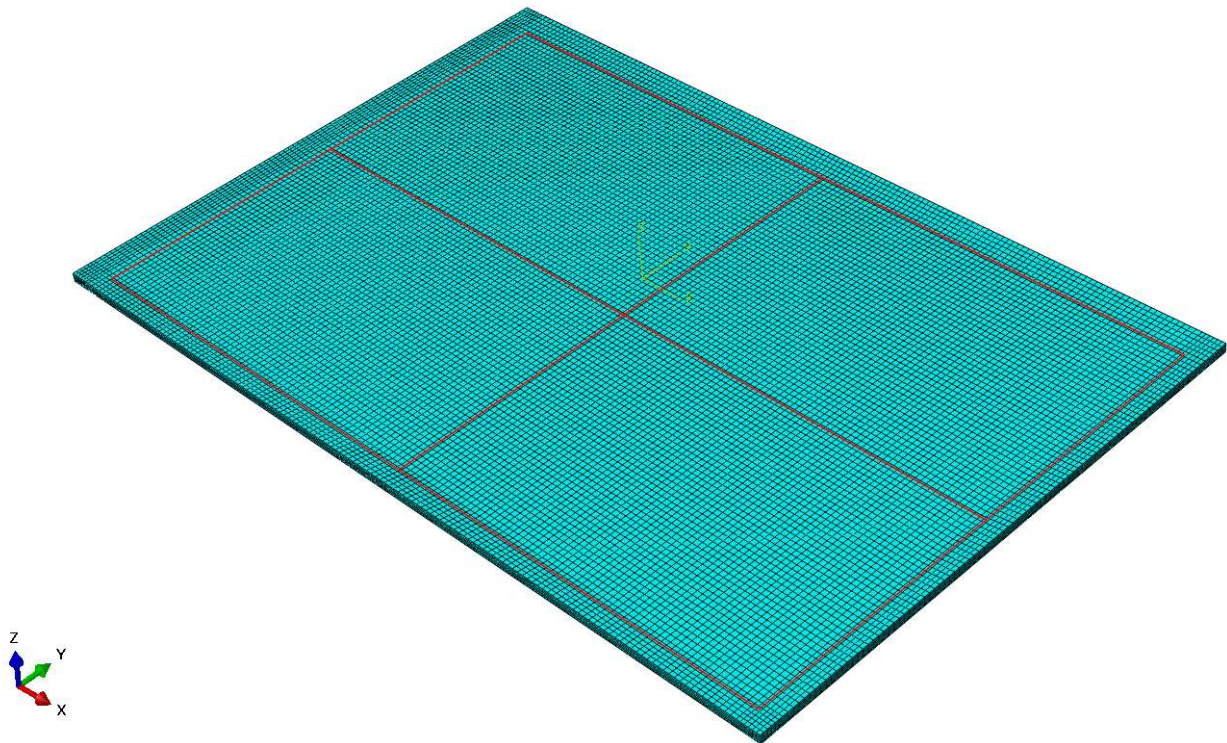
Figure 15: Display of the meshed model with the highlighted heated bottom surface.

Thermal characteristics of the material were calculated according to EN 1992-1-2 [3] (see Tab. 5). Furthermore, data for ambient heating, convection and surface radiation, was also used as per the recommendations of EN 1992-1-2 [3] and is listed below (Tab. 4).

	Ambient	Convection	Surface radiation
Film coefficient	9.00	25.00	-
Sink temperature	20.00	1.00	1.00
Sink amplitude	-	Fire curve	Fire curve
Emissivity	-	-	0.70

Table 4: Ambient, convection and radiation properties assigned to the model.

According to EN 1992-1-3 [3] thermal conductivity of concrete varies with the material temperature (Fig. 5). For the purpose of the model, a mean value of the lower and upper limit has been chosen as the representative value (see Section 1.2.2. and Fig. 5).

As is the case for thermal conductivity, specific heat, also depends on temperature. In addition, specific heat also depends on the moisture content in concrete (Fig. 6). For these models a value of 3% moisture content was chosen as a representative value for the calculation of specific heat.

Penultimate, alongside thermal conductivity and specific heat of concrete, the thermal expansion coefficient, also depends on concrete's temperature. Thermal expansion was calculated from the thermal elongation of concrete, as per the instructions in EN 1992-1-2 [3].

Ultimately, the last material property needed for the thermal analysis, is the density of concrete, which also varies with the temperature of concrete. However, the change od density is negligable and the effect does not influence the results much. A constant value of $2500\ kg/m^3$, was choosen as the representative value, which is the usual value for common reinforced concrete found in civil high-rise structures.

Temperature	Thermal conductivity	Specific heat	Thermal elongation	Thermal expansion	Density
			Siliceous aggregate		
T [°C]	λc [W/mK]	$c_P\ (\theta)$ [J/kg K]	α_{CL} [-]	α_{CV} [-]	γ [kg/m3]
0	1.68	900.00	1.84E-07	9.06E-06	2500.00
20	1.64	900.00	1.84E-07	9.06E-06	2500.00
30	1.62	900.00	9.06E-05	9.06E-06	2500.00
40	1.61	900.00	1.81E-04	9.07E-06	2500.00
50	1.59	900.00	2.73E-04	9.10E-06	2500.00
60	1.57	900.00	3.65E-04	9.12E-06	2500.00
70	1.55	900.00	4.58E-04	9.16E-06	2500.00
80	1.53	900.00	5.52E-04	9.20E-06	2500.00
90	1.52	900.00	6.47E-04	9.24E-06	2500.00
100	1.50	2020.00	7.43E-04	9.29E-06	2500.00
110	1.48	2020.00	8.41E-04	9.34E-06	2500.00
120	1.46	1960.00	9.40E-04	9.40E-06	2500.00
130	1.45	1840.00	1.04E-03	9.46E-06	2500.00
140	1.43	1720.00	1.14E-03	9.53E-06	2500.00
150	1.41	1600.00	1.25E-03	9.60E-06	2500.00
160	1.40	1480.00	1.35E-03	9.67E-06	2500.00
170	1.38	1360.00	1.46E-03	9.75E-06	2500.00
180	1.36	1240.00	1.57E-03	9.84E-06	2500.00
190	1.35	1120.00	1.69E-03	9.93E-06	2500.00
200	1.33	1000.00	1.80E-03	1.00E-05	2500.00
210	1.32	1005.00	1.92E-03	1.01E-05	2500.00
220	1.30	1010.00	2.04E-03	1.02E-05	2500.00
230	1.29	1015.00	2.17E-03	1.03E-05	2500.00
240	1.27	1020.00	2.30E-03	1.04E-05	2500.00
250	1.25	1025.00	2.43E-03	1.06E-05	2500.00
260	1.24	1030.00	2.56E-03	1.07E-05	2500.00
270	1.23	1035.00	2.70E-03	1.08E-05	2500.00
280	1.21	1040.00	2.84E-03	1.09E-05	2500.00
290	1.20	1045.00	2.99E-03	1.11E-05	2500.00
300	1.18	1050.00	3.14E-03	1.12E-05	2500.00
310	1.17	1055.00	3.30E-03	1.14E-05	2500.00
320	1.15	1060.00	3.45E-03	1.15E-05	2500.00

330	1.14	1065.00	3.62E-03	1.17E-05	2500.00
340	1.13	1070.00	3.78E-03	1.18E-05	2500.00
350	1.11	1075.00	3.96E-03	1.20E-05	2500.00
360	1.10	1080.00	4.13E-03	1.22E-05	2500.00
370	1.09	1085.00	4.32E-03	1.23E-05	2500.00
380	1.07	1090.00	4.50E-03	1.25E-05	2500.00
390	1.06	1095.00	4.69E-03	1.27E-05	2500.00
400	1.05	1100.00	4.89E-03	1.29E-05	2500.00
410	1.04	1100.00	5.10E-03	1.31E-05	2500.00
420	1.02	1100.00	5.30E-03	1.33E-05	2500.00
430	1.01	1100.00	5.52E-03	1.35E-05	2500.00
440	1.00	1100.00	5.74E-03	1.37E-05	2500.00
450	0.99	1100.00	5.97E-03	1.39E-05	2500.00
460	0.98	1100.00	6.20E-03	1.41E-05	2500.00
470	0.97	1100.00	6.44E-03	1.43E-05	2500.00
480	0.95	1100.00	6.68E-03	1.45E-05	2500.00
490	0.94	1100.00	6.94E-03	1.48E-05	2500.00
500	0.93	1100.00	7.20E-03	1.50E-05	2500.00
510	0.92	1100.00	7.46E-03	1.52E-05	2500.00
520	0.91	1100.00	7.73E-03	1.55E-05	2500.00
530	0.90	1100.00	8.01E-03	1.57E-05	2500.00
540	0.89	1100.00	8.30E-03	1.60E-05	2500.00
550	0.88	1100.00	8.60E-03	1.62E-05	2500.00
560	0.87	1100.00	8.90E-03	1.65E-05	2500.00
570	0.86	1100.00	9.21E-03	1.67E-05	2500.00
580	0.85	1100.00	9.53E-03	1.70E-05	2500.00
590	0.84	1100.00	9.85E-03	1.73E-05	2500.00
600	0.83	1100.00	1.02E-02	1.76E-05	2500.00
610	0.82	1100.00	1.05E-02	1.78E-05	2500.00
620	0.81	1100.00	1.09E-02	1.81E-05	2500.00
630	0.81	1100.00	1.12E-02	1.84E-05	2500.00
640	0.80	1100.00	1.16E-02	1.87E-05	2500.00
650	0.79	1100.00	1.20E-02	1.90E-05	2500.00
660	0.78	1100.00	1.24E-02	1.93E-05	2500.00
670	0.77	1100.00	1.28E-02	1.96E-05	2500.00
680	0.76	1100.00	1.32E-02	2.00E-05	2500.00
690	0.76	1100.00	1.36E-02	2.03E-05	2500.00
700	0.75	1100.00	1.40E-02	2.06E-05	2500.00
710	0.74	1100.00	1.40E-02	2.03E-05	2500.00
720	0.73	1100.00	1.40E-02	2.00E-05	2500.00
730	0.73	1100.00	1.40E-02	1.97E-05	2500.00
740	0.72	1100.00	1.40E-02	1.94E-05	2500.00
750	0.71	1100.00	1.40E-02	1.92E-05	2500.00
760	0.71	1100.00	1.40E-02	1.89E-05	2500.00
770	0.70	1100.00	1.40E-02	1.87E-05	2500.00
780	0.69	1100.00	1.40E-02	1.84E-05	2500.00
790	0.69	1100.00	1.40E-02	1.82E-05	2500.00
800	0.68	1100.00	1.40E-02	1.79E-05	2500.00
810	0.67	1100.00	1.40E-02	1.77E-05	2500.00
820	0.67	1100.00	1.40E-02	1.75E-05	2500.00
830	0.66	1100.00	1.40E-02	1.73E-05	2500.00
840	0.66	1100.00	1.40E-02	1.71E-05	2500.00
850	0.65	1100.00	1.40E-02	1.69E-05	2500.00

860	0.65	1100.00	1.40E-02	1.67E-05	2500.00
870	0.64	1100.00	1.40E-02	1.65E-05	2500.00
880	0.64	1100.00	1.40E-02	1.63E-05	2500.00
890	0.63	1100.00	1.40E-02	1.61E-05	2500.00
900	0.63	1100.00	1.40E-02	1.59E-05	2500.00
910	0.63	1100.00	1.40E-02	1.57E-05	2500.00
920	0.62	1100.00	1.40E-02	1.56E-05	2500.00
930	0.62	1100.00	1.40E-02	1.54E-05	2500.00
940	0.61	1100.00	1.40E-02	1.52E-05	2500.00
950	0.61	1100.00	1.40E-02	1.51E-05	2500.00
960	0.61	1100.00	1.40E-02	1.49E-05	2500.00
970	0.60	1100.00	1.40E-02	1.47E-05	2500.00
980	0.60	1100.00	1.40E-02	1.46E-05	2500.00
990	0.60	1100.00	1.40E-02	1.44E-05	2500.00
1000	0.59	1100.00	1.40E-02	1.43E-05	2500.00
1010	0.59	1100.00	1.40E-02	1.41E-05	2500.00
1020	0.59	1100.00	1.40E-02	1.40E-05	2500.00
1030	0.59	1100.00	1.40E-02	1.39E-05	2500.00
1040	0.59	1100.00	1.40E-02	1.37E-05	2500.00
1050	0.58	1100.00	1.40E-02	1.36E-05	2500.00
1060	0.58	1100.00	1.40E-02	1.35E-05	2500.00
1070	0.58	1100.00	1.40E-02	1.33E-05	2500.00
1080	0.58	1100.00	1.40E-02	1.32E-05	2500.00
1090	0.58	1100.00	1.40E-02	1.31E-05	2500.00
1100	0.58	1100.00	1.40E-02	1.30E-05	2500.00
1110	0.58	1100.00	1.40E-02	1.28E-05	2500.00
1120	0.57	1100.00	1.40E-02	1.27E-05	2500.00
1130	0.57	1100.00	1.40E-02	1.26E-05	2500.00
1140	0.57	1100.00	1.40E-02	1.25E-05	2500.00
1150	0.57	1100.00	1.40E-02	1.24E-05	2500.00
1160	0.57	1100.00	1.40E-02	1.23E-05	2500.00
1170	0.57	1100.00	1.40E-02	1.22E-05	2500.00
1180	0.57	1100.00	1.40E-02	1.21E-05	2500.00
1190	0.57	1100.00	1.40E-02	1.20E-05	2500.00
1200	0.57	1100.00	1.40E-02	1.19E-05	2500.00

Table 5: Calculated material properties assigned to the thermal analysis model.

The analysis was carried out for a time period of 14,400 seconds with the standard calculation protocol. The results of the analysis is shown below, alongside with the comparison of experimentally measured values and the results obtained through the thermal analysis model.
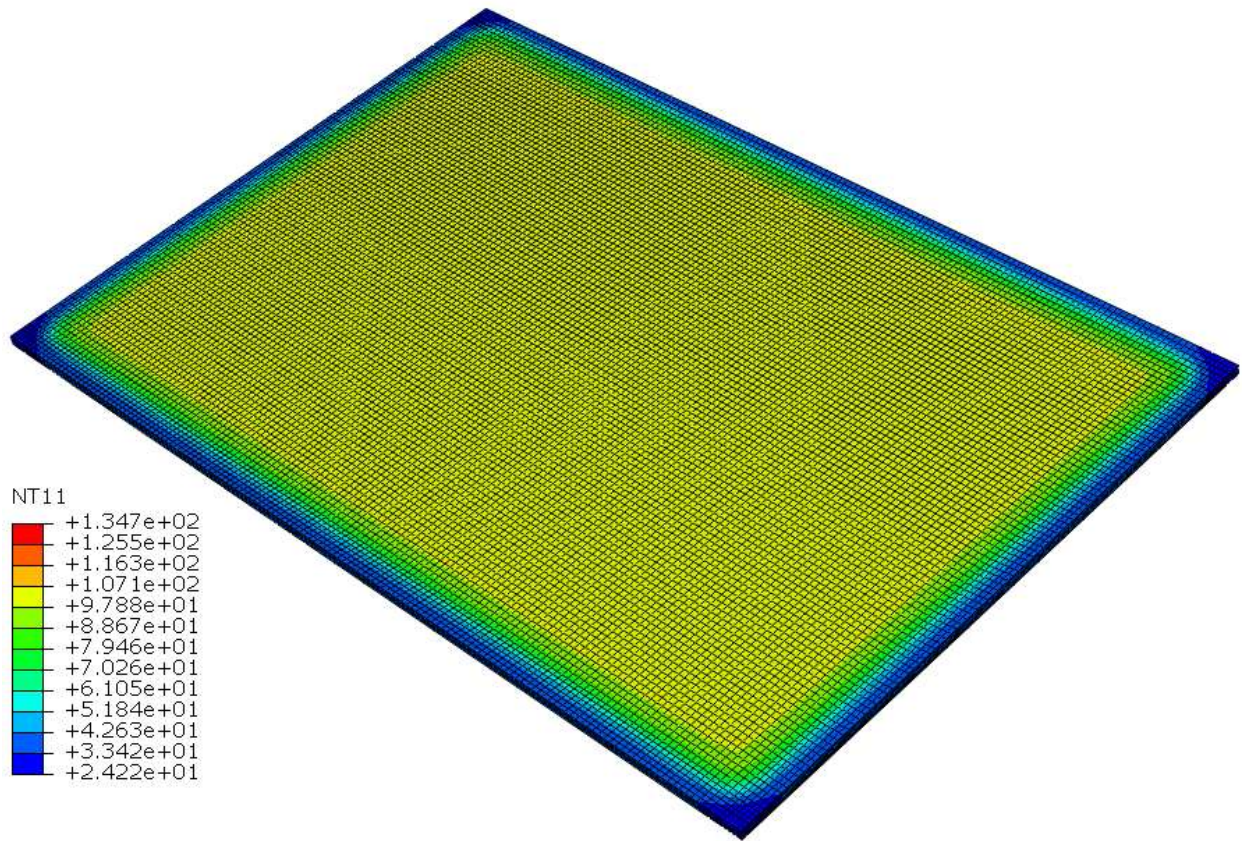
NT11
+1.347e+02
+1.255e+02
+1.163e+02
+1.071e+02
+9.788e+01
+8.867e+01
+7.946e+01
+7.026e+01
+6.105e+01
+5.184e+01
+4.263e+01
+3.342e+01
+2.422e+01

Figure 16: Results of the thermal analysis model at 3,000 seconds.

NT11
+8.162e+02
+7.605e+02
+7.048e+02
+6.491e+02
+5.934e+02
+5.377e+02
+4.821e+02
+4.264e+02
+3.707e+02
+3.150e+02
+2.593e+02
+2.036e+02
+1.479e+02

Figure 17: Results of the thermal analysis model at 10,000 seconds.

25
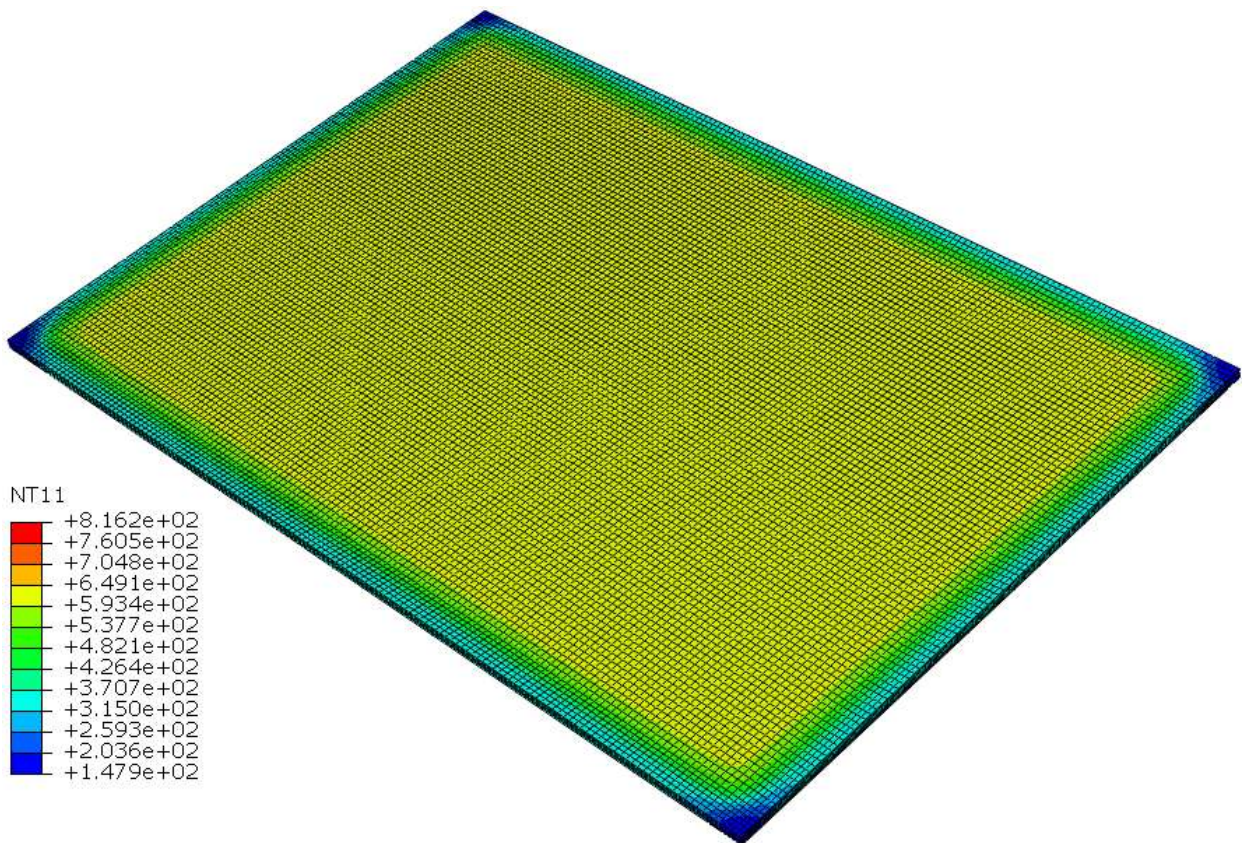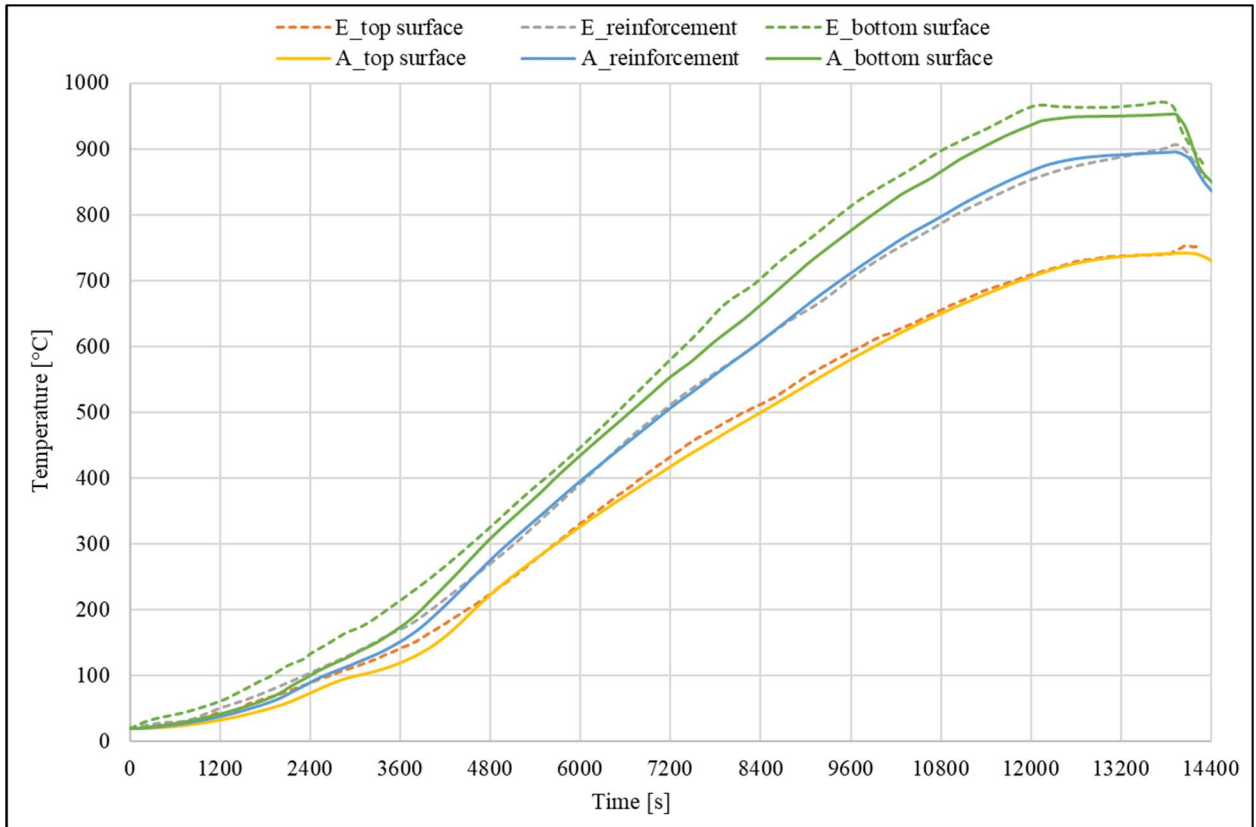
Figure 18: Comparison of measured experimental values of temperatures in different locations of the plate (*'E'*) and the numerical results obtained with the model in Abaqus (*'A'*).

As it is shown in the figure above, the results obtained through the thermal analysis model, have a satisfactory correlation with the experimentally measured values. The results for reinforcement and the top surface of the concrete plate, have a good correspond with the experimental ones, while the results for the bottom surface (i.e. the surface that is exposed to the heating) are slightly less corresponding with the experimental results. This is presumed to be the case, because of numerical errors due to the nature of the analysis. However, it can also be due to human error while obtaining the results.

2.2.2. Structural analysis of the plates

The mechanical analysis model was prepared in accordance with the thermal analysis model. Mesh of the model consists of 91,476 linear 3D stress finite elements with reduced integration (C3D8R) and hourglass control. The mesh is compatible with the thermal analysis models mesh.

For the first step of the analysis, boundary conditions were assigned to the model. The plate is simply supported alongside the internal edge of the heated surface with restricted vertical displacement ($U_3 = 0$), while other translations and rotations are free. Furthermore, to replicate the experiment setup, where the corners of the plates are clamped, was achieved by restraining vertical displacement on a $5x5cm$ square on the top surface of the corner of the plate. Assigning the boundary conditions in this way resulted in a realistic deformation behaviour of the.
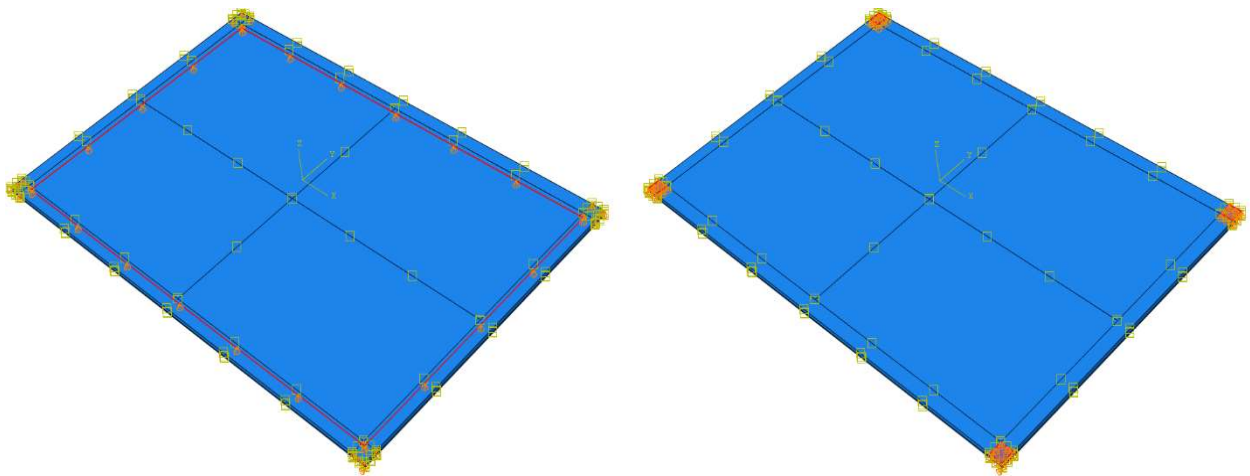

Figure 19: Boundary conditions assigned to the model. Simply supported edges with vertical deflections restrained (*left*) and clamped corners (*right*).

As is the case for the thermal analysis, for the mechanical analysis at elevated temperatures all material properties were calculated according to EN 1992-1-2 [3] and the experimental values. However, there are slight deviations from the norms for the replication of experimental results and simulating realistic behaviour of the plates. More precisely, additional reduction coefficients were needed for the material's elastic Young modulus and yield strength.

Yield strenght	Elastic modulus	Yield strain	Poisson ratio
f_{ck}	E_c	ε	ν
[MPa]	[GPa]	[-]	[-]
43.2	33.78	0.0025	0.2

Table 6: Concrete characteristics of the tested plate at ambient temperature.

Firstly, yield strength and elastic modulus at elevated temperatures were adjusted according to steel's elastic modulus reduction factor from EN 1992-1-2 [3] (see Tab. 2).

Secondly, for simulating the cracking of concrete and the decline of stiffness (EI) of the cross-section under mechanical loading, the values have been further reduced according to the formula from ACI 318-08 [18] (section 10.10.4.1) for flexural members. The formula was adjusted as an elastic modulus reduction factor instead of a reduction of the moment of inertia, because there is no possibility for the reduction of the moment of inertia through the numerical model. A reduction of the elastic modulus can be used instead. The adjusted formula is shown below:

$$k_{RC,EI} = (0.10 + 25\rho)(1.20 + 0.20\frac{b_w}{d}) \qquad (25)$$

or

$$k_{RC,EI} = 0.35 \qquad \text{for beams}$$
$$k_{RC,EI} = 0.25 \qquad \text{for plates and slabs}$$

Where:

ρ is the ratio of the area of longitudal reinforcement and concrete cross-section area
b_w is the width of the members web
d is the static height of the cross-section

For the analysed plate, the additional stiffness reduction was calculated at a value of 0.178 and applied as a constant reduction for all temperatures.

Thirdly, for simulating the creep of reinforcement at elevated temperatures and the increase of deflection, caused by the decrease of stiffness, an additional reduction factor was applied from a temperature value of 500°C onward, at a value of 0.20 i.e. an 80% reduction.

Temperature	Reduction factor
θ	k_{add}
[°C]	[-]
20	1.00
100	1.00
200	1.00
300	1.00
400	1.00
500	0.20
600	0.20
700	0.20
800	0.20
900	0.20
1000	0.20
1100	0.20
1200	0.20

Table 7: Additional reduction factor for simulating reinforcement creep and deformation increase.

Finally, the superposition of all reduction factors was made to replicate the experiments as closely as possible. The final values of concrete material properties used for the mechanical analysis model, were calculated following the reductions previously listed.

Temperature	Yield strenght	Elastic modulus	Yield strain	Poisson ration
θ	$f_{c,\theta}$	$E_{c,\theta}$	ε_θ	ν
[°C]	[N/m2]	[N/m2]	[-]	[-]
0	7.78E+06	3.11E+09	0.0025	0.20
20	7.78E+06	3.11E+09	0.0025	0.20
100	7.78E+06	1.94E+09	0.0040	0.20
200	7.39E+06	1.34E+09	0.0055	0.20
300	6.61E+06	9.44E+08	0.0070	0.20
400	5.83E+06	5.83E+08	0.0100	0.20
500	4.67E+06	3.11E+08	0.0150	0.20
600	2.80E+06	1.12E+08	0.0250	0.20
700	1.87E+06	7.46E+07	0.0250	0.20
800	9.33E+05	3.73E+07	0.0250	0.20
900	4.98E+05	1.99E+07	0.0250	0.20
1000	2.49E+05	9.95E+06	0.0250	0.20
1100	6.22E+04	2.49E+06	0.0250	0.20
1200	1.00E+00	1.00E+00	0.0000	0.20

Table 8: Values of mechanical properties of concrete at elevated temperatures used for the mechanical analysis.

The analysis was carried out for a period of 14,400 seconds with the standard calculation protocol and included material and geometric non-linearity (third-order theory). The analysis results are shown below, alongside the comparison of experimentally measured values and the results obtained through the mechanical analysis model.
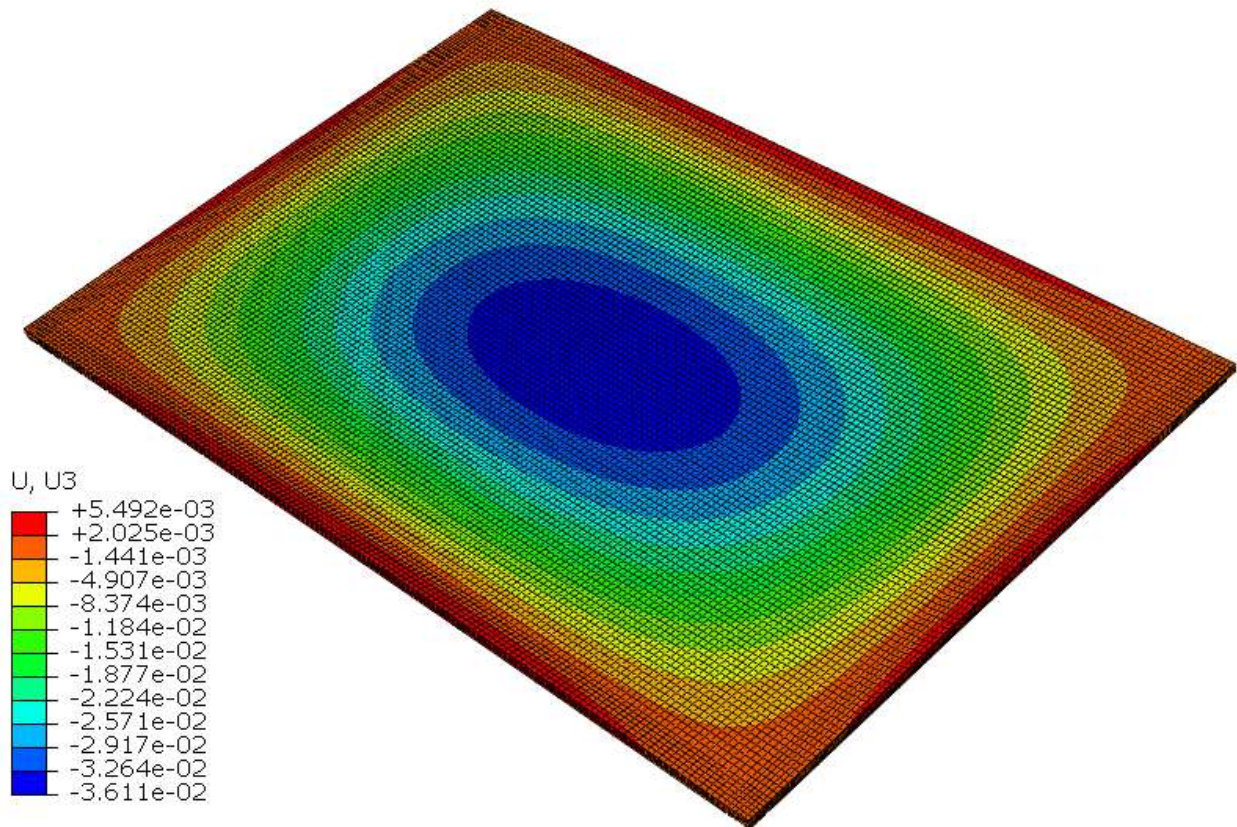
Figure 20: Results of vertical displacements for mechanical analysis model at 3,000 seconds.
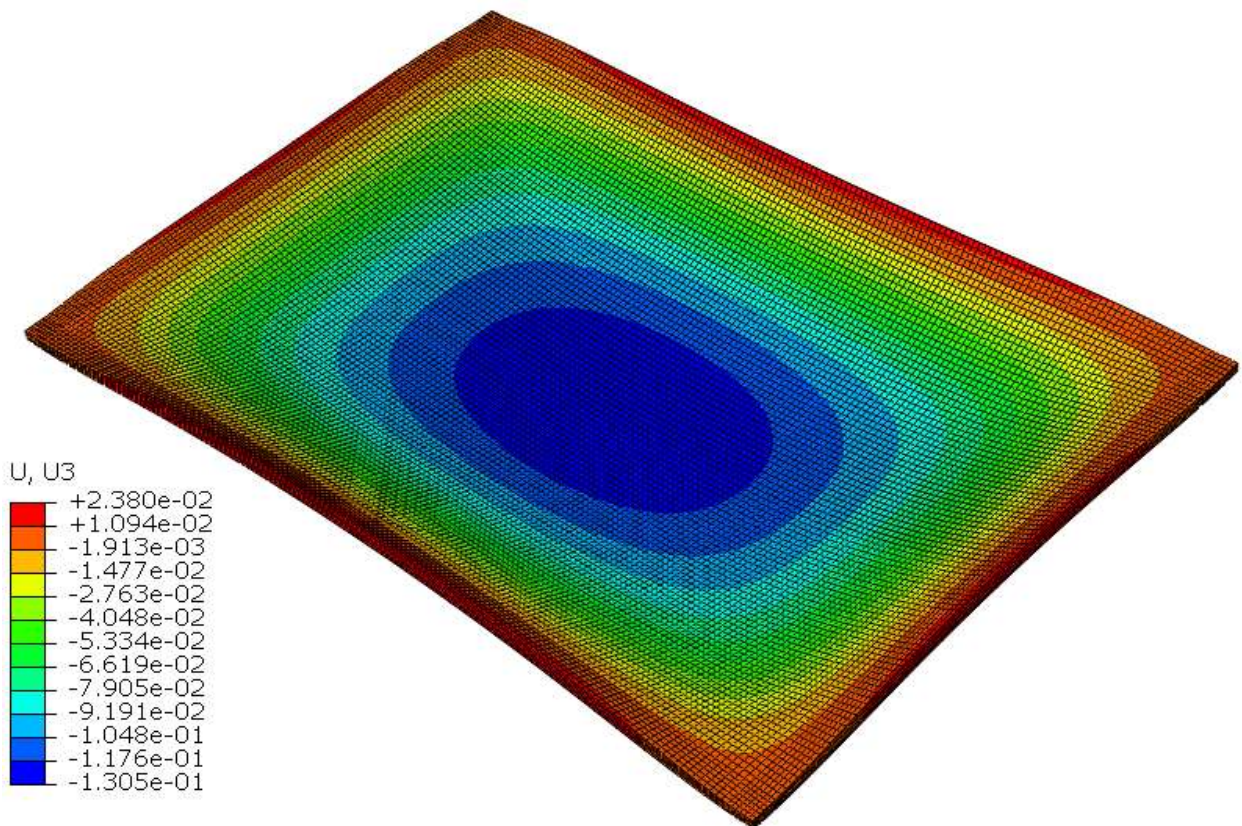

Figure 21: Results of vertical displacements for mechanical analysis model at 10,000 seconds.
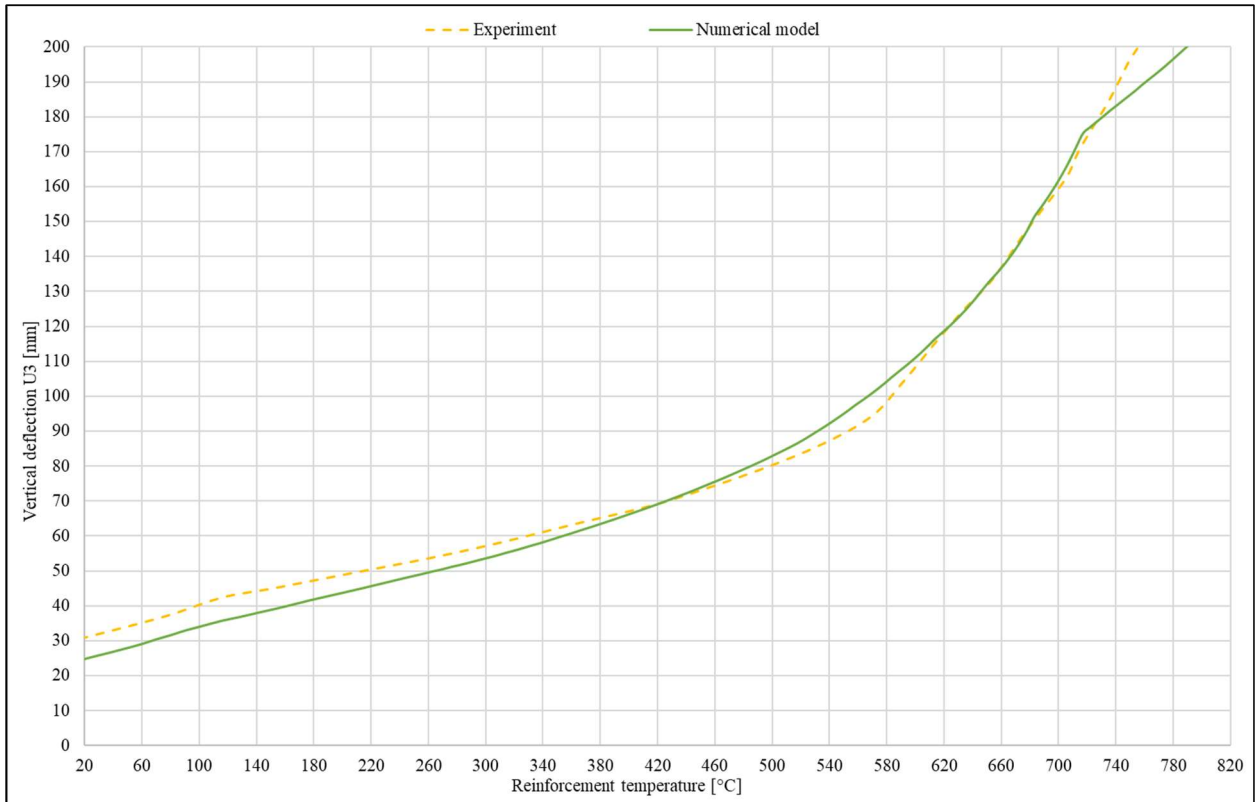
Figure 22: Comparison of measured experimental values of vertical deflections on the geometric center of the plate and the numerical results obtained with the model in Abaqus.

As is shown in the figure above, the results obtained through the mechanical analysis model, have a satisfactory correlation with the experimentally measured values. While there is a slight divergence, the difference is not significant, with a maximal difference of approximately 15% of the experimental value (values near ambient temperatures). There are a few possibilities of why this is the case, such as limited information about the experimental measurements (information given on loading of plates does not include if the part of the plate was loaded until static equilibrium and afterwards subjected to heating, or simultaneously loaded by both, as well as not mentioning the timing of the placement of LVDT devices is not mentioned), inaccurate assigning of boundary conditions in the numerical model (slight deviations in temperature values, obtained experimentally and replicated numericaly, see Fig. 18) or human error in processing the data.

2.3. Fire experiments of Monther B.M. Dwaikat [19]

In general, most experimental studies are under 'standard' conditions that do not cover important factors such as the fire scenario, fire induced spalling, and axial restraint, which will influence the fire response of RC beams. For these reasons, Monther B.M. Dwaikat [19] carried out experiments on NSC (normal strength concrete), and HSC (high strength concrete) beams under realistic fire, loading, and axial restraint conditions.

The experimental program consisted of conducting fire resistance tests on six RC beams designated Bl to B6. Four of these beams, B3, B4, B5 and B6, were made of HSC. The other two beams, Bl and B2, were made with NSC. All beams were $3,960mm$ long and of the rectangular cross-section of $b/h = 406/254mm$. These beams were designed as per ACI318 [18].

This thesis, is generally interested in the behaviour of NSC beams under typical design fire scenarios. Thus only the appurtenant tests of beams B1 and B2 carried out at elevated temperatures were analysed. The beams were designed with $3\emptyset 19\ mm$ bars as the tensile reinforcement and $2\emptyset 13\ mm$ bars as compressive reinforcement. The shear reinforcement consisted of $\emptyset 6mm$ stirrups spaced at $150mm$ over the length of the beam. Details of the geometry, mechanical characteristics of materials and applied loads are described in the following paragraphs.
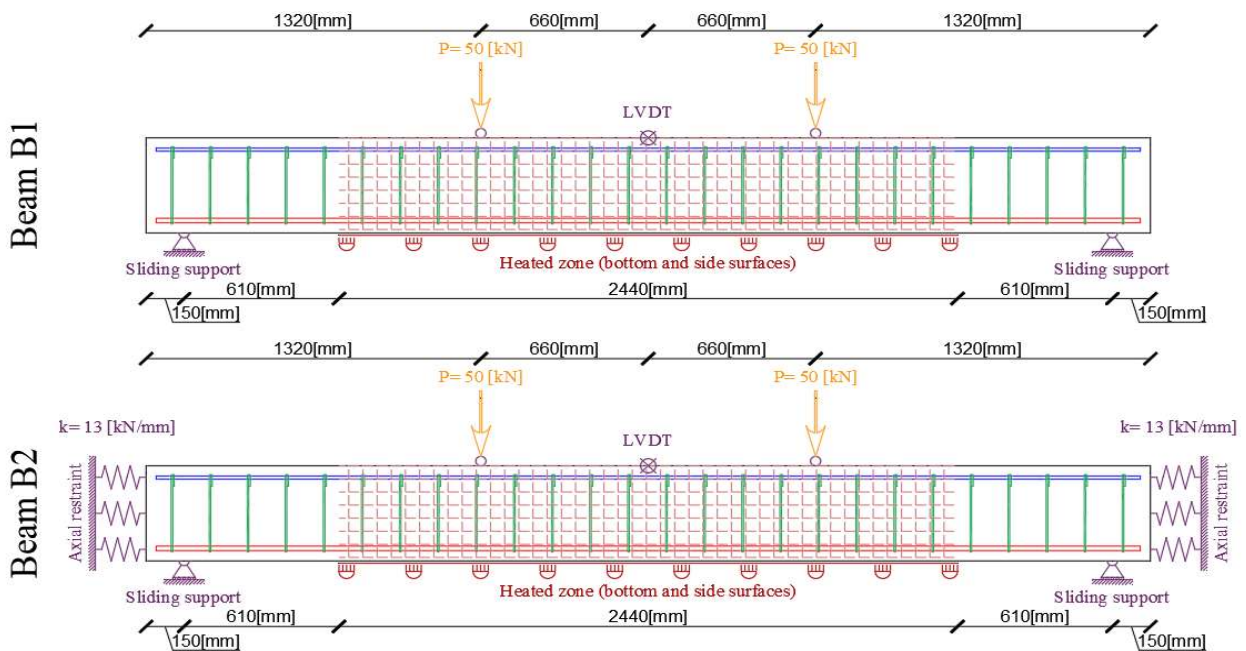

Figure 23: Representation of the test setup of beams B1 and B2.

Material tests on concrete and reinforcing steel specimens were carried out to obtain strength properties of the materials used in the beam fabrication. Concrete cylinders were made from the concrete mixture batch used to prepare the two NSC beams, the cylinders were tested to obtain the compressive strength at 28 days and on the day of the corresponding fire test. The commpressive strength, tested on the day of the experiments, was measured to be $58.2\ MPa$.

Tensile tests were performed on $\emptyset 19mm$ steel bars similar to those used as tensile reinforcement in the concrete beams. The yield strength, ultimate strength, and ultimate strain were found to be about $450\ MPa$, $705\ MPa$ and 0.17, respectively.
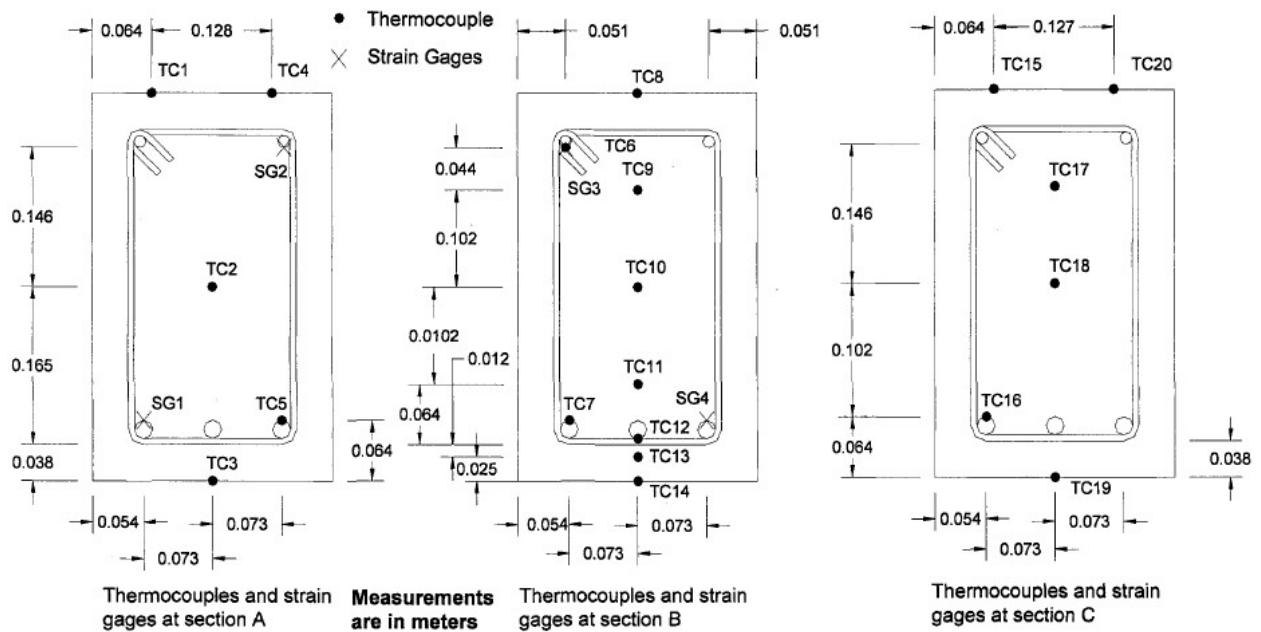
Figure 24: Cross-section of tested beams with marked locations of measurement devices. Figure is taken from [19].

The furnace used for the experiments, consists of a steel framework supported by four steel columns and with a fire chamber that is $2.44m$ wide, $3.05m$ long, and $1.68m$ high. The maximum heat power the furnace can produce is $2.5MW$. Natural gas burners within the furnace provide thermal energy. Thermocouples, distributed throughout the test chamber monitor the furnace temperature during a fire test. During the fire test, these furnace temperatures were used to adjust fuel supply manually, and maintain a temperature profile consistent with a pre-determined standard or realistic fire scenario. Beam B1 was exposed to the standard fire curve ASTM E119, while beam B2 was exposed to the fire scenario curve SF.

The fire resistance tests were conducted by placing two RC beams in the furnace and exposing them to a targeted fire scenario. The beams were exposed to fire from three sides (bottom and two sides). The top surface of the beam was insulated with a $50mm$ layer of insulation (ceramic fiberfrax material) to prevent heat penetration from the top. This is similar to the conditions in practice where the top side of the beam is generally covered with a concrete slab.

Both beams were tested under two point loads, each placed at $1.32m$ from the end of the beams. Each of the two point loads for both beams was $50kN$, which is about 54% of the beam capacity according to ACI 318 [18]. The load was maintained constant throughout the test. The load was applied for approximately 30 minutes before the fire test's start and maintained until a static condition was reached, at which point no further increase in the deflection could be measured.

The measured axial restraint force for beam B2 increased with fire exposure time in the first 100 minutes. This is presumed to be, because of restraining the beam's thermal expansion, which increased with fire exposure. A gradual decrease in the axial restraint force was followed with a plateau in the axial restraint force between 100 and 140 minutes. This can be attributed to the relief valve in the restraint system, which reduces the axial restraint stiffness. This was put in action, to avoid possible damage to the test facility and loading frame.

2.4. Computer simulations for beams

The models for thermal and mechanical analysis of each plate were set up in ABAQUS [2]. For each beam, a thermal and mechanical analysis model were prepared.

2.4.1. Thermal analyses of beams

The thermal analysis model was prepared according to the geometry of the tested beams B1 and B2 (see Fig. 23 and Fig. 24). Mesh of the models consists of 16,000 quadratic heat transfer finite elements with reduced integration (C3D20R) and the approximate size of $l/w/h = 50/50/12\ mm$ (it was chosen this way so the aspect ratio would not be greater than ~3). The bottom and side surfaces of the models were subjected to a transient heating regime according to the design fire curves of the experiments. In contrast, the rest of the model was assigned to be as ambient temperature.
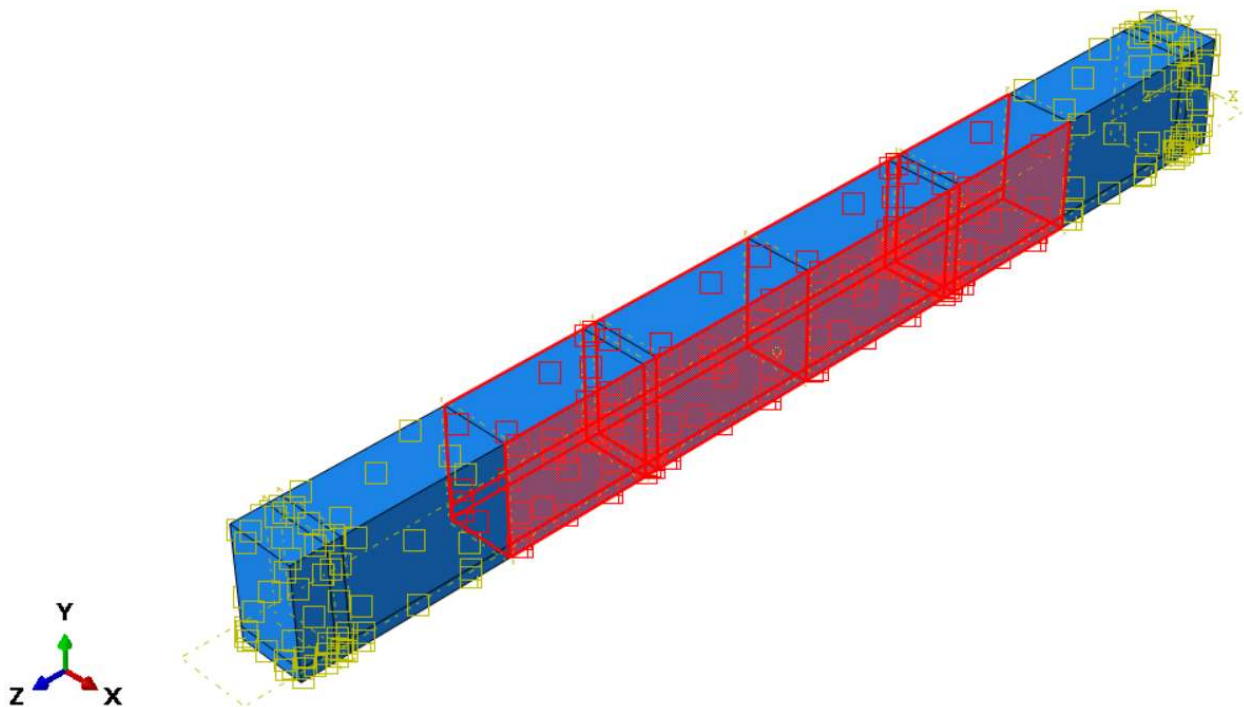

Figure 25: Display of the thermal analyses models B1 and B2 with highlighted heated surfaces.

For the experimental test of beam B1, a standard design fire scenario curve ASTM E119 was applied to the heated surfaces of the beam, while for the case of the test of beam B, a more rapidly developing short duration fire design curve SF was applied. The fire curves are shown in the figure below.
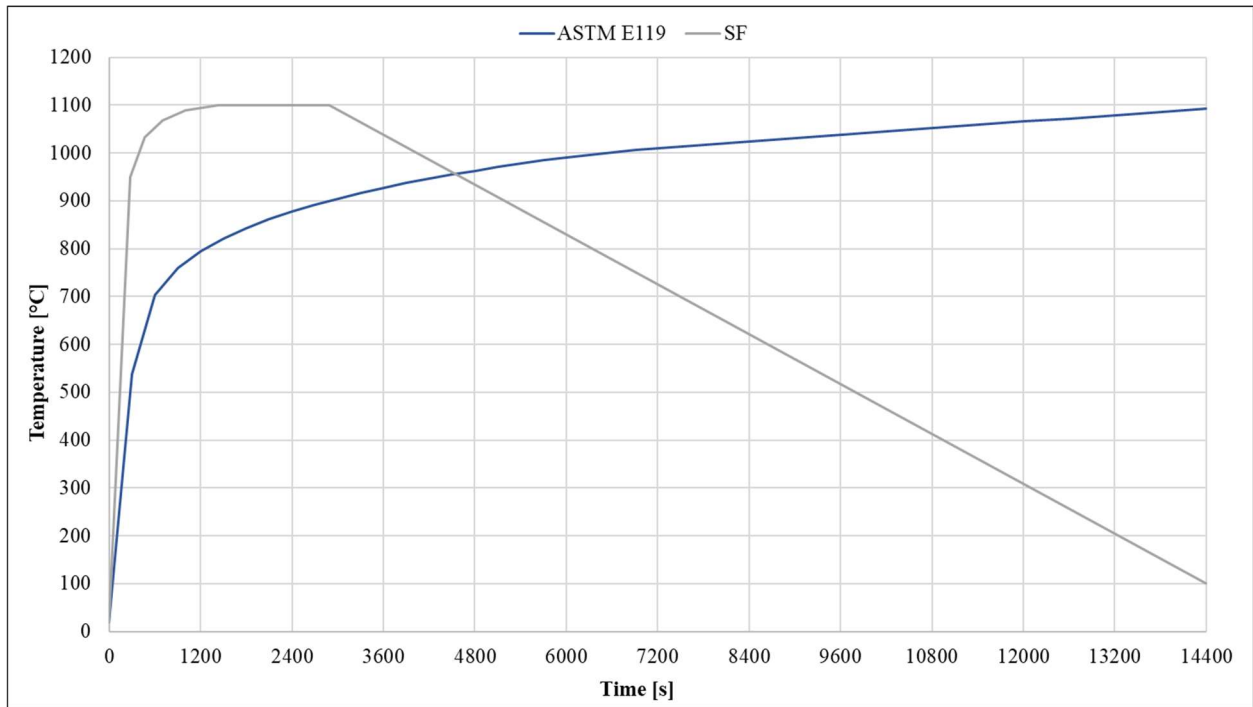
Figure 26: Fire design curves ASTM E119 and SF.

Thermal characteristics of the material were calculated according to EN 1992-1-2 [3] (see Tab. 10). Furthermore, data for ambient heating, convection and surface radiation, was also used as per the recommendations of EN 1992-1-2 [3], and they are listed below (Tab. 9).

	Ambient		Convection		Surface radiation	
	B1	B2	B1	B2	B1	B2
Film coefficient	9.00	9.00	25.00	35.00	-	-
Sink temperature	20.00	20.00	1.00	1.00	1.00	1.00
Sink amplitude	-	-	ASTM E119	SF	ASTM E119	SF
Emissivity	-	-	-	-	0.70	0.90

Table 9: Ambient, convection and radiation properties assigned to the models B1 and B2.

According to EN 1992-1-3 [3], thermal conductivity of concrete varies with the material temperature. For the models, a mean value of the lower and upper limit has been chosen as the representative value (see Section 1.2.2. and Fig. 5). As is the case for thermal conductivity, specific heat, also depends on temperature. In addition, specific heat also depends on the moisture content in concrete (Fig. 6). For these models a value of 3% moisture content was chosen as a representative value for the calculation of specific heat.

Penultimate, alongside thermal conductivity and specific heat of concrete, the thermal expansion coefficient, also depends on concrete's temperature. Thermal expansion was calculated from the thermal elongation of concrete, as per the instructions in EN 1992-1-2 [3].

Ultimately, the last material property needed for the thermal analysis is the density of concrete, which also varies with the temperature of concrete. However, the change of density is negligible and the effect does not influence the results much. A constant value of 2500 kg/m^3, was choosen as the representative value, which is the usuall value for common reinforced concrete found in civil high-rise structures.

Temperature	Thermal conductivity	Specific heat	Thermal elongation	Thermal expansion	Density
			Siliceous aggregate		
T [°C]	λ_c [W/mK]	$c_p(\theta)$ [J/kg K]	α_{CL} [-]	α_{CV} [-]	γ [kg/m3]
0	1.68	900.00	1.84E-07	9.06E-06	2500.00
20	1.64	900.00	1.84E-07	9.06E-06	2500.00
30	1.62	900.00	9.06E-05	9.06E-06	2500.00
40	1.61	900.00	1.81E-04	9.07E-06	2500.00
50	1.59	900.00	2.73E-04	9.10E-06	2500.00
60	1.57	900.00	3.65E-04	9.12E-06	2500.00
70	1.55	900.00	4.58E-04	9.16E-06	2500.00
80	1.53	900.00	5.52E-04	9.20E-06	2500.00
90	1.52	900.00	6.47E-04	9.24E-06	2500.00
100	1.50	2020.00	7.43E-04	9.29E-06	2500.00
110	1.48	2020.00	8.41E-04	9.34E-06	2500.00
120	1.46	1960.00	9.40E-04	9.40E-06	2500.00
130	1.45	1840.00	1.04E-03	9.46E-06	2500.00
140	1.43	1720.00	1.14E-03	9.53E-06	2500.00
150	1.41	1600.00	1.25E-03	9.60E-06	2500.00
160	1.40	1480.00	1.35E-03	9.67E-06	2500.00
170	1.38	1360.00	1.46E-03	9.75E-06	2500.00
180	1.36	1240.00	1.57E-03	9.84E-06	2500.00
190	1.35	1120.00	1.69E-03	9.93E-06	2500.00
200	1.33	1000.00	1.80E-03	1.00E-05	2500.00
210	1.32	1005.00	1.92E-03	1.01E-05	2500.00
220	1.30	1010.00	2.04E-03	1.02E-05	2500.00
230	1.29	1015.00	2.17E-03	1.03E-05	2500.00
240	1.27	1020.00	2.30E-03	1.04E-05	2500.00
250	1.25	1025.00	2.43E-03	1.06E-05	2500.00
260	1.24	1030.00	2.56E-03	1.07E-05	2500.00
270	1.23	1035.00	2.70E-03	1.08E-05	2500.00
280	1.21	1040.00	2.84E-03	1.09E-05	2500.00
290	1.20	1045.00	2.99E-03	1.11E-05	2500.00
300	1.18	1050.00	3.14E-03	1.12E-05	2500.00
310	1.17	1055.00	3.30E-03	1.14E-05	2500.00
320	1.15	1060.00	3.45E-03	1.15E-05	2500.00
330	1.14	1065.00	3.62E-03	1.17E-05	2500.00
340	1.13	1070.00	3.78E-03	1.18E-05	2500.00
350	1.11	1075.00	3.96E-03	1.20E-05	2500.00
360	1.10	1080.00	4.13E-03	1.22E-05	2500.00
370	1.09	1085.00	4.32E-03	1.23E-05	2500.00
380	1.07	1090.00	4.50E-03	1.25E-05	2500.00
390	1.06	1095.00	4.69E-03	1.27E-05	2500.00
400	1.05	1100.00	4.89E-03	1.29E-05	2500.00
410	1.04	1100.00	5.10E-03	1.31E-05	2500.00
420	1.02	1100.00	5.30E-03	1.33E-05	2500.00
430	1.01	1100.00	5.52E-03	1.35E-05	2500.00
440	1.00	1100.00	5.74E-03	1.37E-05	2500.00
450	0.99	1100.00	5.97E-03	1.39E-05	2500.00
460	0.98	1100.00	6.20E-03	1.41E-05	2500.00
470	0.97	1100.00	6.44E-03	1.43E-05	2500.00

480	0.95	1100.00	6.68E-03	1.45E-05	2500.00
490	0.94	1100.00	6.94E-03	1.48E-05	2500.00
500	0.93	1100.00	7.20E-03	1.50E-05	2500.00
510	0.92	1100.00	7.46E-03	1.52E-05	2500.00
520	0.91	1100.00	7.73E-03	1.55E-05	2500.00
530	0.90	1100.00	8.01E-03	1.57E-05	2500.00
540	0.89	1100.00	8.30E-03	1.60E-05	2500.00
550	0.88	1100.00	8.60E-03	1.62E-05	2500.00
560	0.87	1100.00	8.90E-03	1.65E-05	2500.00
570	0.86	1100.00	9.21E-03	1.67E-05	2500.00
580	0.85	1100.00	9.53E-03	1.70E-05	2500.00
590	0.84	1100.00	9.85E-03	1.73E-05	2500.00
600	0.83	1100.00	1.02E-02	1.76E-05	2500.00
610	0.82	1100.00	1.05E-02	1.78E-05	2500.00
620	0.81	1100.00	1.09E-02	1.81E-05	2500.00
630	0.81	1100.00	1.12E-02	1.84E-05	2500.00
640	0.80	1100.00	1.16E-02	1.87E-05	2500.00
650	0.79	1100.00	1.20E-02	1.90E-05	2500.00
660	0.78	1100.00	1.24E-02	1.93E-05	2500.00
670	0.77	1100.00	1.28E-02	1.96E-05	2500.00
680	0.76	1100.00	1.32E-02	2.00E-05	2500.00
690	0.76	1100.00	1.36E-02	2.03E-05	2500.00
700	0.75	1100.00	1.40E-02	2.06E-05	2500.00
710	0.74	1100.00	1.40E-02	2.03E-05	2500.00
720	0.73	1100.00	1.40E-02	2.00E-05	2500.00
730	0.73	1100.00	1.40E-02	1.97E-05	2500.00
740	0.72	1100.00	1.40E-02	1.94E-05	2500.00
750	0.71	1100.00	1.40E-02	1.92E-05	2500.00
760	0.71	1100.00	1.40E-02	1.89E-05	2500.00
770	0.70	1100.00	1.40E-02	1.87E-05	2500.00
780	0.69	1100.00	1.40E-02	1.84E-05	2500.00
790	0.69	1100.00	1.40E-02	1.82E-05	2500.00
800	0.68	1100.00	1.40E-02	1.79E-05	2500.00
810	0.67	1100.00	1.40E-02	1.77E-05	2500.00
820	0.67	1100.00	1.40E-02	1.75E-05	2500.00
830	0.66	1100.00	1.40E-02	1.73E-05	2500.00
840	0.66	1100.00	1.40E-02	1.71E-05	2500.00
850	0.65	1100.00	1.40E-02	1.69E-05	2500.00
860	0.65	1100.00	1.40E-02	1.67E-05	2500.00
870	0.64	1100.00	1.40E-02	1.65E-05	2500.00
880	0.64	1100.00	1.40E-02	1.63E-05	2500.00
890	0.63	1100.00	1.40E-02	1.61E-05	2500.00
900	0.63	1100.00	1.40E-02	1.59E-05	2500.00
910	0.63	1100.00	1.40E-02	1.57E-05	2500.00
920	0.62	1100.00	1.40E-02	1.56E-05	2500.00
930	0.62	1100.00	1.40E-02	1.54E-05	2500.00
940	0.61	1100.00	1.40E-02	1.52E-05	2500.00
950	0.61	1100.00	1.40E-02	1.51E-05	2500.00
960	0.61	1100.00	1.40E-02	1.49E-05	2500.00
970	0.60	1100.00	1.40E-02	1.47E-05	2500.00
980	0.60	1100.00	1.40E-02	1.46E-05	2500.00
990	0.60	1100.00	1.40E-02	1.44E-05	2500.00
1000	0.59	1100.00	1.40E-02	1.43E-05	2500.00

1010	0.59	1100.00	1.40E-02	1.41E-05	2500.00
1020	0.59	1100.00	1.40E-02	1.40E-05	2500.00
1030	0.59	1100.00	1.40E-02	1.39E-05	2500.00
1040	0.59	1100.00	1.40E-02	1.37E-05	2500.00
1050	0.58	1100.00	1.40E-02	1.36E-05	2500.00
1060	0.58	1100.00	1.40E-02	1.35E-05	2500.00
1070	0.58	1100.00	1.40E-02	1.33E-05	2500.00
1080	0.58	1100.00	1.40E-02	1.32E-05	2500.00
1090	0.58	1100.00	1.40E-02	1.31E-05	2500.00
1100	0.58	1100.00	1.40E-02	1.30E-05	2500.00
1110	0.58	1100.00	1.40E-02	1.28E-05	2500.00
1120	0.57	1100.00	1.40E-02	1.27E-05	2500.00
1130	0.57	1100.00	1.40E-02	1.26E-05	2500.00
1140	0.57	1100.00	1.40E-02	1.25E-05	2500.00
1150	0.57	1100.00	1.40E-02	1.24E-05	2500.00
1160	0.57	1100.00	1.40E-02	1.23E-05	2500.00
1170	0.57	1100.00	1.40E-02	1.22E-05	2500.00
1180	0.57	1100.00	1.40E-02	1.21E-05	2500.00
1190	0.57	1100.00	1.40E-02	1.20E-05	2500.00
1200	0.57	1100.00	1.40E-02	1.19E-05	2500.00

Table 10: Calculated material properties assigned to the thermal analysis models.

The analyses were carried out for a time period of 12000 seconds with the standard calculation protocol. The results of the analyses is shown below, alongside the comparison of experimentally measured values and the results obtained through the thermal analysis model.
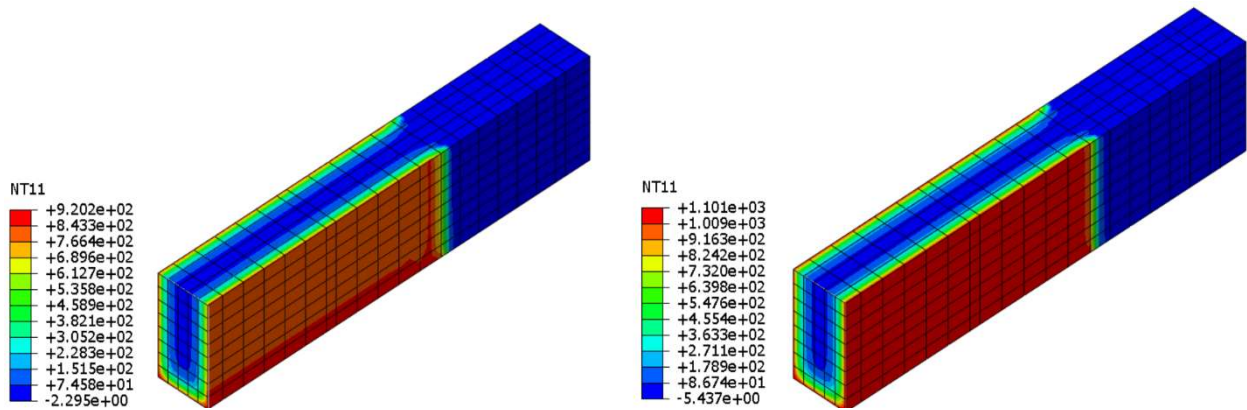
Figure 27: Results of thermal analyses t=3,000 s (at L/2). Beam B1 (left) and beam B2 (right).
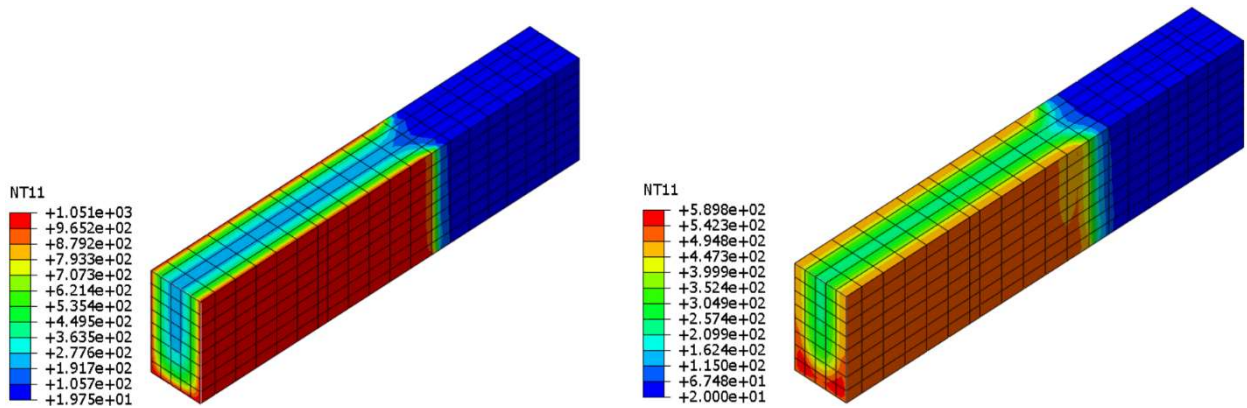
Figure 28: Results of thermal analyses t=10,000 s (at L/2). Beam B1 (left) and beam B2 (right).
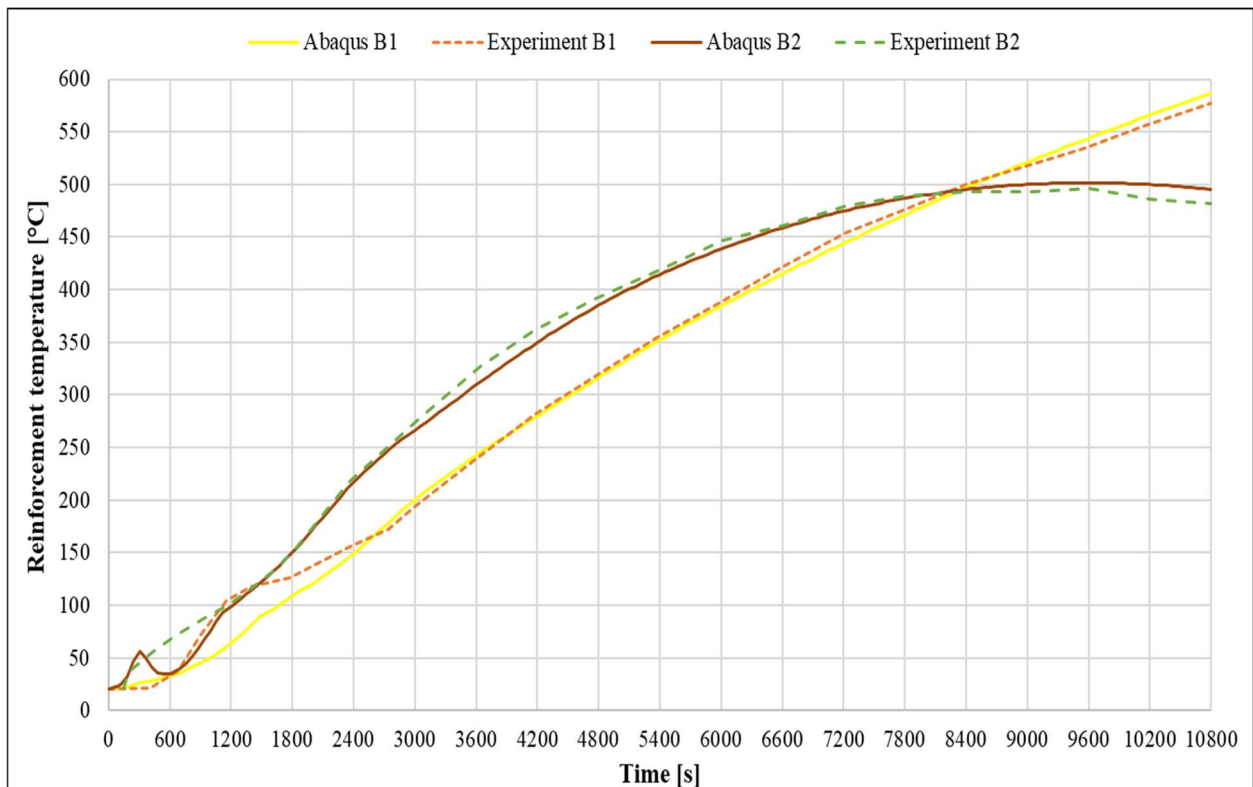
Figure 29: Comparison of the measured experimental values of reinforcement temperatures of the beams and the numerical results obtained with the models in Abaqus.

As it is shown if the figure above, the results obtained through the thermal analyses models, have a satisfactory correlation with the experimentally measured values. Based on the obtained results, we have obtained a valid input of temperatures for the thermal step used in the mechanical models described in the section below.

2.4.2. Structural analyses of the beams

The mechanical analyses models were prepared in accordance with the thermal analyses models. Mesh of the models, consist of 16,000 quadratic 3D stress finite elements with reduced integration (C3D20R) and hourglass control. The mesh is compatible with the thermal analyses model meshes.

Initially, for the first step of the analysis, boundary conditions were assigned to the model. The beam B1 is simply supported, with a hinged support on one end, and a sliding support on the other. The boundary conditions were assigned by constraining nodal values of a $b/h = 50/254mm$ strip to a reference point and assigning the restrained vertical displacement ($U_3 = 0$), while other translations (except the restrained horizontal displacement for the hinged support $U_1 = 0$) and rotations are free. The result of assigning the boundary conditions in this way a realistic deformation behaviour of the beam B1 was achieved.

For beam B2, the boundary conditions were assigned in a similar manner, with the exceptions being the axial restraints on each end of the beam and that both of the simply supported ends of the beam were restrained only for vertical displacement ($U_3 = 0$), which was done in order to achieve realistic values of the axial restraint force. The axial restraints of the beam model, was achieved by constraining the nodal values on each face of the beam, to their corresponding reference point, in which a linear spring was applied with a stiffness of $13kN/mm$. The result of assigning the boundary conditions in this way lead to a realistic deformation behaviour of the beam B2.
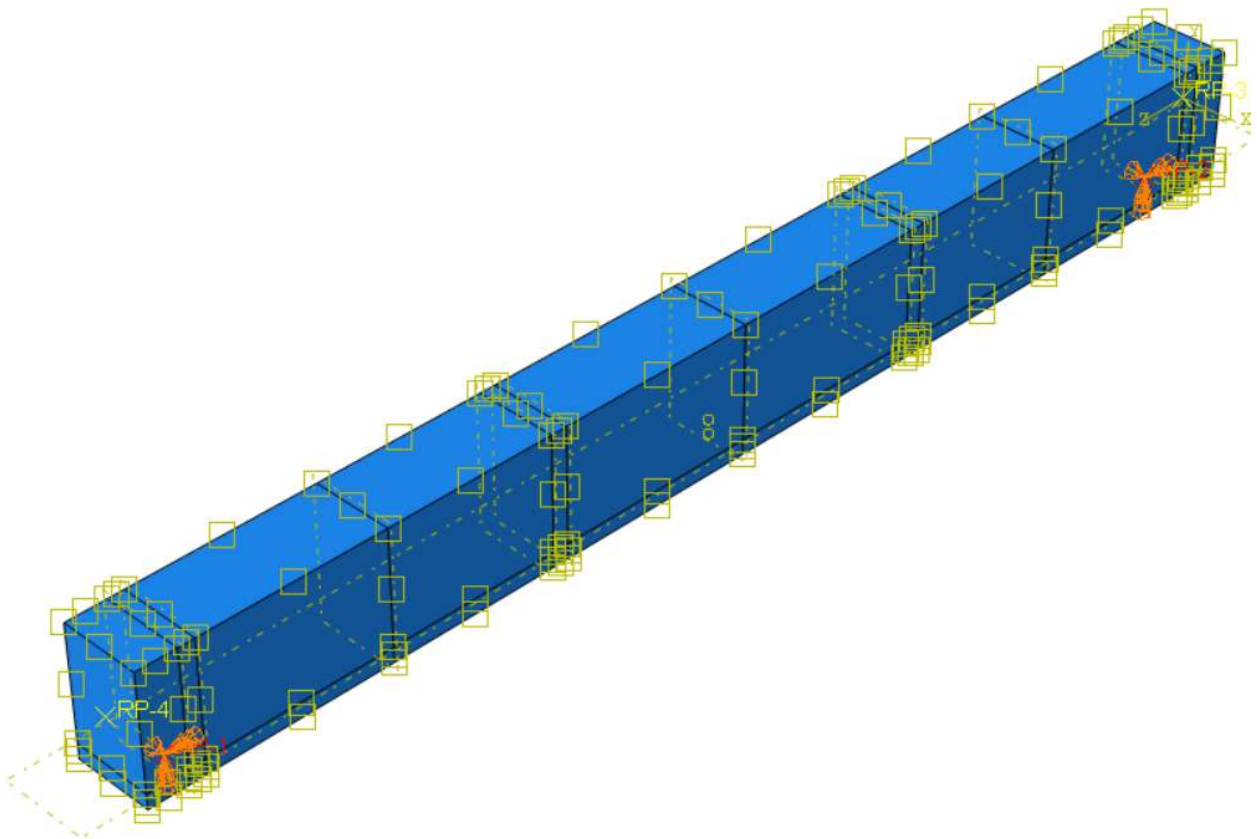
Figure 30: Boundary conditions assigned to the model of simply supported beam B1
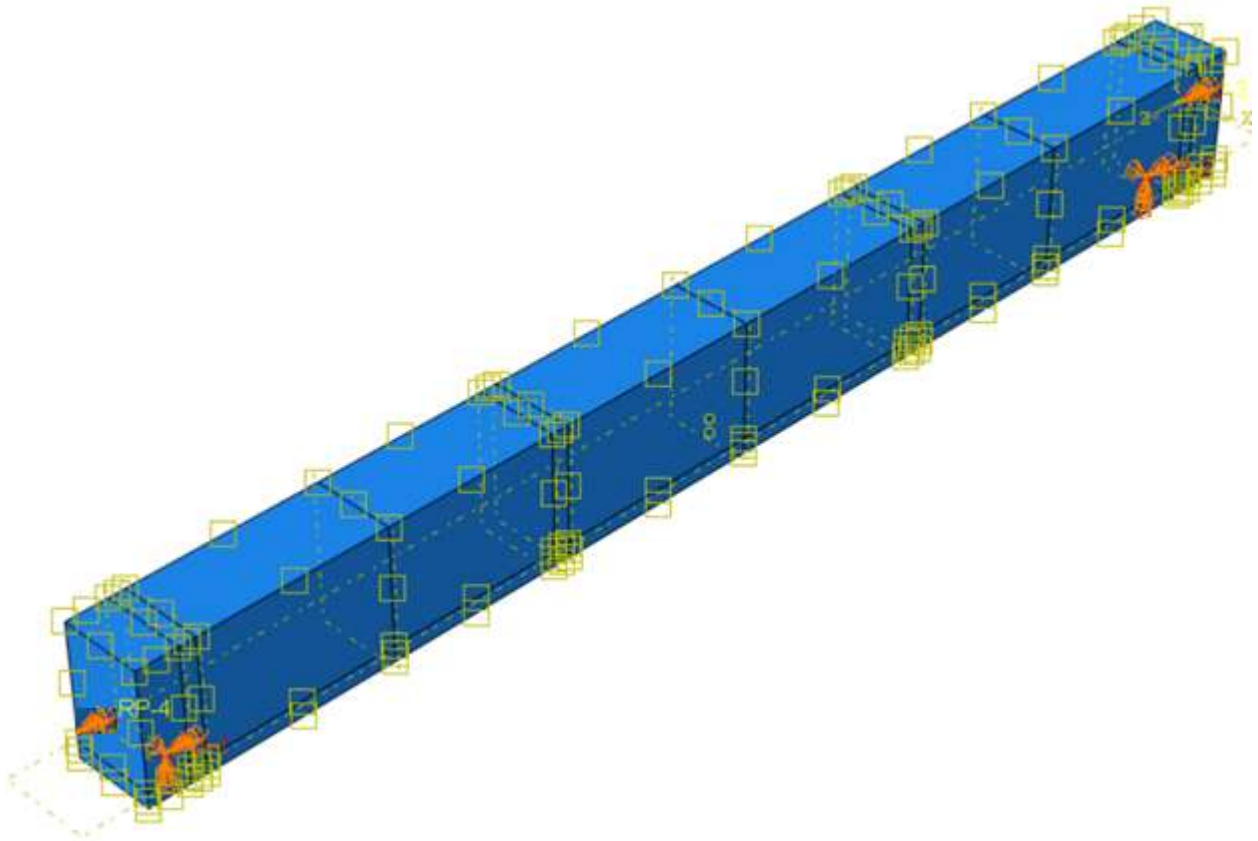
Figure 31: Boundary conditions assigned to the model of simply supported beam B2 with axial restraint springs.

As was the case for the thermal analysis, for the mechanical analysis at elevated temperatures all material properties were claculated according to EN 1992-1-2 [3] and the experimental values that were measured. However, there are slight deviations from the norms. For the replication of experimental results and simulating realistic behaviour of the beams additional reduction coefficients were needed for the materials elastic Young modulus and yield strength.

Yield strenght	Elastic modulus	Yield strain	Poisson ratio
f_{ck}	E_c	ε	ν
[MPa]	[GPa]	[-]	[-]
43.2	33.78	0.0025	0.2

Table 11: Concrete characteristics of tested beams at ambient temperature.

Firstly, the values of the yield strength and elastic modulus, at elevated temperatures, were adjusted accordingto steel's elastic modulus reduction factor from EN 1992-1-2 [3] (see Tab. 2).

Secondly, simmilar to the mechanical properties of plates in section 2.2.2., for simulating the cracking of concrete and decline of stiffness (EI) of the cross-section under mechanical loading, the values have been further reduced according to the formula from ACI 318-08 [18] (section 10.10.4.1) for flexural members. The formula was adjusted as a elastic modulus reduction factor instead of a reduction of the moment of inertia, the reason being that there is no possibility of the reduction of the moment of inertia through the numerical model. A reduction of the elastic modulus has been used instead.

41

For the analysed beams B1 and B2, the additional stiffness reduction was calculated at a value of 0.398, and it was applied as a constant reduction for all temperatures.

Thirdly, same as for the mechanical properties of plates in section 2.2.2., for simulating the creep of reinforcement at elevated temperatures and the increase of deflection, caused by the decrease of stiffness, an additional reduction factor was applied from a temperature value of 500°C onward, at a value of 0.20 i.e. an 80% reduction (see Tab. 7).

Finally, the superposition of all reduction factors was made, to replicate the experiments as closely as possible. The final values of concretes material properties used for the mechanical analyses models, were calculated following the reductions previously listed.

Temperature	Yield strenght	Elastic modulus	Yield strain	Poisson ration
θ	$f_{c,\theta}$	$E_{c,\theta}$	ε_θ	ν
[°C]	[N/m2]	[N/m2]	[-]	[-]
0	2.32E+07	9.27E+09	0.0025	0.20
20	2.32E+07	9.27E+09	0.0025	0.20
100	3.71E+07	9.27E+09	0.0040	0.20
200	4.59E+07	8.35E+09	0.0055	0.20
300	5.19E+07	7.42E+09	0.0070	0.20
400	6.49E+07	6.49E+09	0.0100	0.20
500	1.67E+07	1.11E+09	0.0150	0.20
600	1.44E+07	5.75E+08	0.0250	0.20
700	6.03E+06	2.41E+08	0.0250	0.20
800	4.17E+06	1.67E+08	0.0250	0.20
900	3.25E+06	1.30E+08	0.0250	0.20
1000	1.85E+06	7.42E+07	0.0250	0.20
1100	9.27E+05	3.71E+07	0.0250	0.20
1200	1.00E+00	1.00E+00	0.0000	0.20

Table 12: Values of mechanical properties of concrete at elevated temperatures used for the mechanical analyses.

The analysis was carried out for a period of 12,000 seconds with the standard calculation protocol and included material and geometric non-linearity (third-order theory). The results of the analyses are shown below, alongside the comparison of experimentally measured values and the results obtained through the mechanical analyses models.
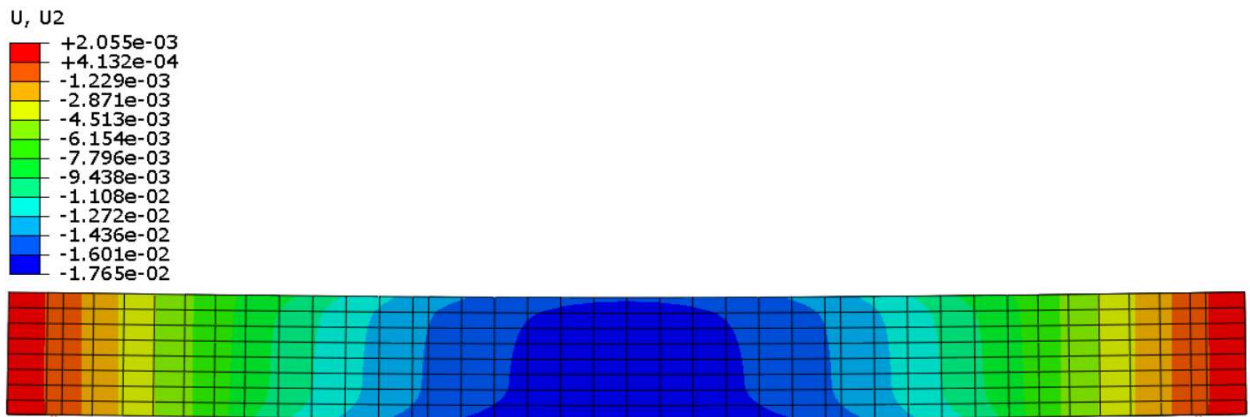
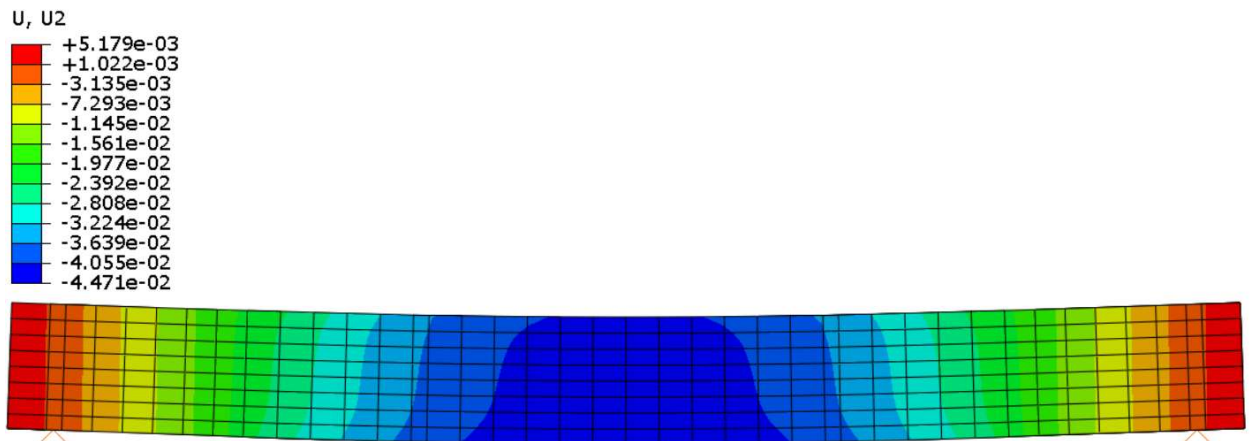Figure 32: Vertical displacements for mechanical analysis of modelled beam B1 at t=3,000 s.

Figure 33: Vertical displacements for mechanical analysis of modelled beam B1 at t=10,000 s.
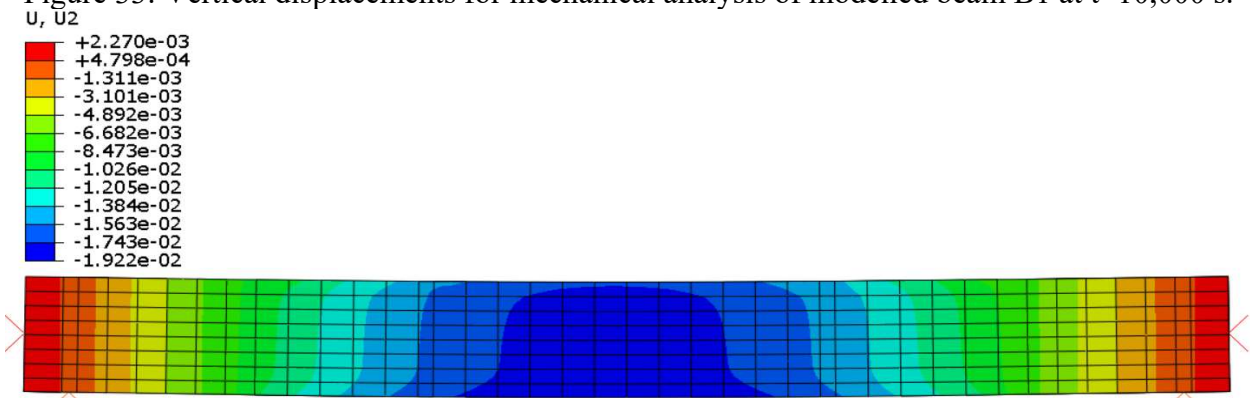

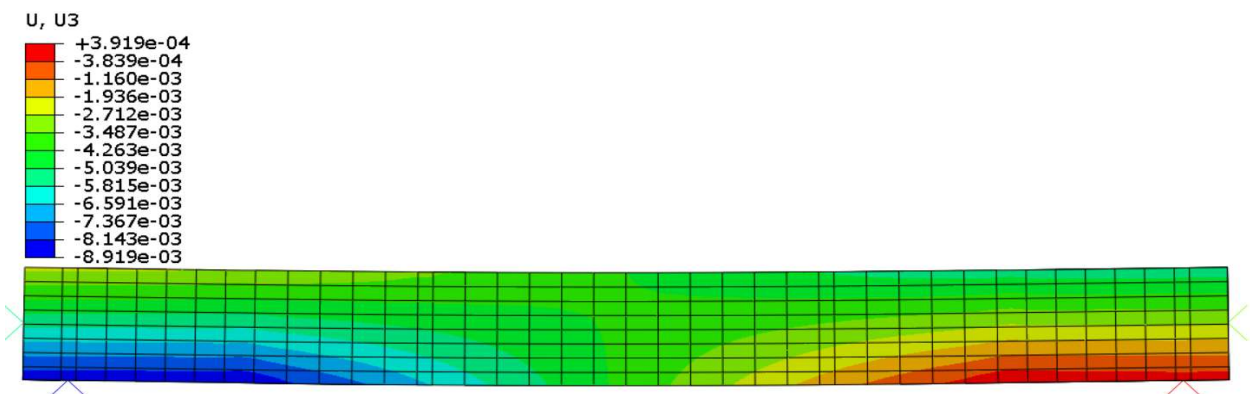Figure 34: Vertical displacements for mechanical analysis of modelled beam B2 at t=3,000 s.

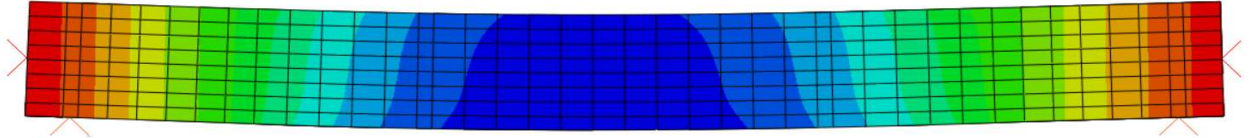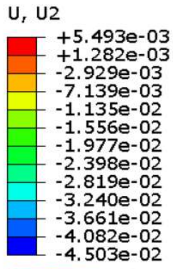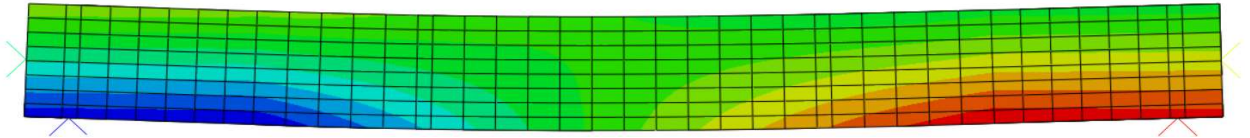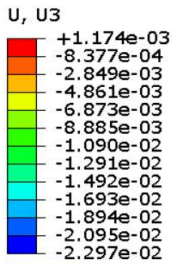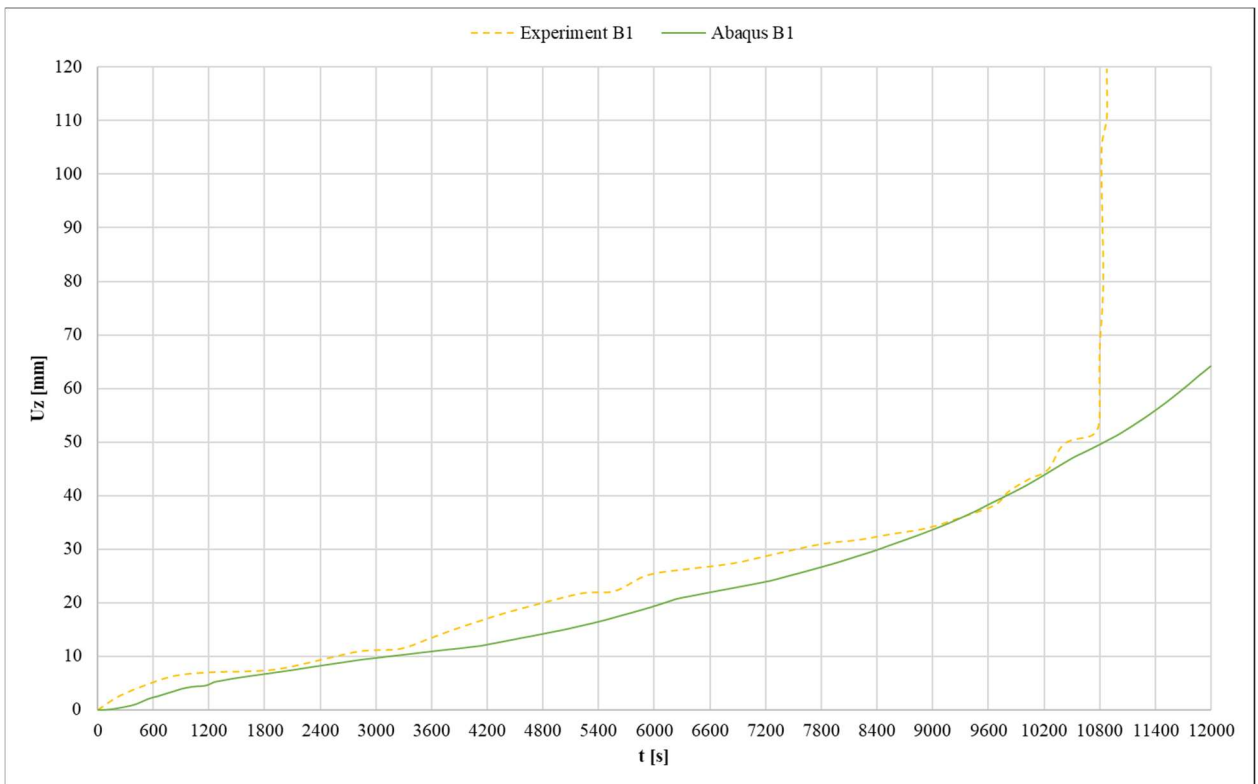Figure 35: Horizontal displacements for mechanical analysis of modelled beam B2 at t=3,000 s.

43

Figure 36: Vertical displacements for mechanical analysis of modelled beam B2 at t=10,000 s.

Figure 37: Horizontal displacements for mechanical analysis of modelled beam B2 at t=10,000 s.

Figure 38: Comparison of measured experimental values of vertical deflections of the beam B1 and the numerical results obtained with the models in Abaqus.
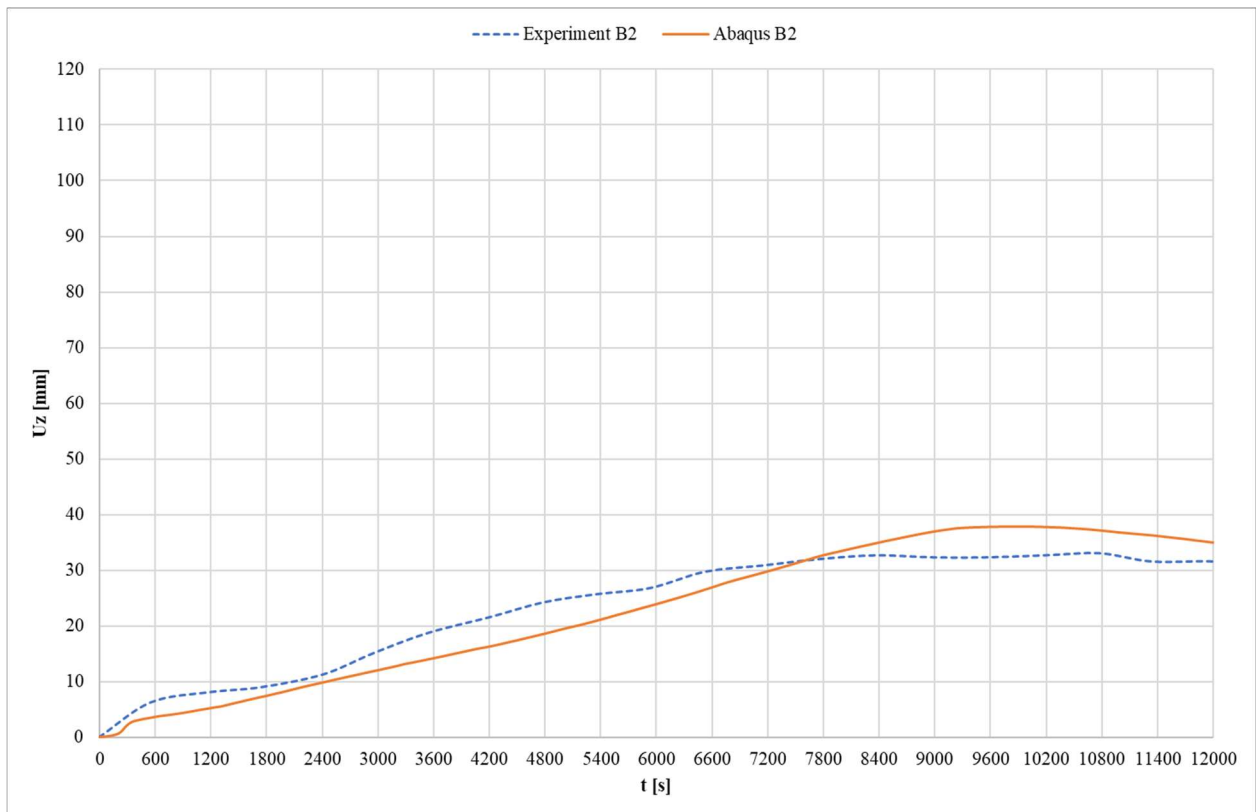
Figure 39: Comparison of measured experimental values of vertical deflections of the beam B2 and the numerical results obtained with the models in Abaqus.

As is shown in the figures above, the results obtained through the mechanical analyses models have a satisfactory correlation with the experimentally measured values. While there is a slight divergence, the difference is not significant, with a maximal difference of approx. 15% for beam B1 and a difference of approx. 20% for beam B2 for the experimental values (from the period from 3,000 to 8,000 seconds).

There are a few possibilities of why this is the case; for the model of beam B1, most likely it is inaccurate assigning of boundary conditions in the numerical model (slight deviations in temperature values, obtained experimentally and replicated numerically, see Fig. 29) or human error with processing the data.

While, for the results for the model of beam B2, in addition to the mentioned possibilities, the difference can mainly be attributed to the experimental test setup, which could not be replicated in the numerical model. A relief valve in the restraint system was put in place to reduce the axial restraint stiffness when the axial restraint force is near a value of $120kN$. This was put in action, to avoid possible damage of the test facility and loading frame.
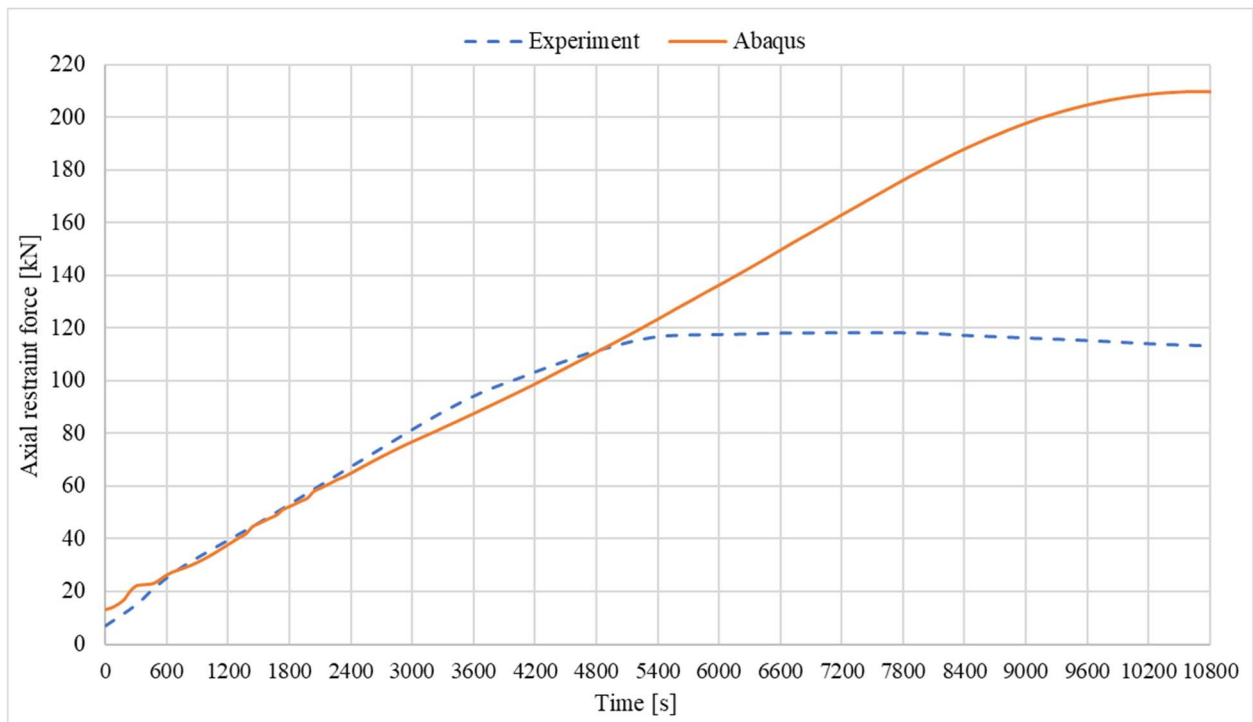
Figure 40: Comparison of measured experimental values of axial restraint force of beam B2 and the numerical results obtained with the models in Abaqus.

As shown above in the figure above, the numerical results gathered have a good corelation with the experimental values of the axial restraint force until 5,000 seconds. While a plateau of the axial restraint force can be observed for the experimental values, the values of the restraint force obtained from the numerical model does not follow the plateau and the restraint force increases over time. The difference of the axial restrain force influences the vertical displacements of the beam model (Fig. 40), before the axial restraint force reaches a value of $120kN$ (approx. at 5,000 seconds), the vertical displacement graph of the numerical analysis is slightly below the experimentally gathered one, while after reaching the said force, the vertical displacements of the numerical model increase and are slightly above the experimentally gathered one for the remaining period of the test.

Chapter 3: Case study

To answer the main questions of this master's thesis, highlighted in its introductory part (see Introduction), a set of fire analyses of a selected real RC structure will be presented in Chapter 3.

The building chosen for analysis will be the building discussed in the recent work of Maglica [4]. In terms of its characteristics, this building is similar to a building for the sales and service of cars in Jesenice (Slovenia), where a severe fire occurred at the end of 2016 (this fire was later described in [17]). The fire occurred in a part of the building's basement with a floor area of $620 m^2$, the floor plan shown in Fig. 41 below.

At the time of the fire, the northern part of this floor area was occupied with piles of approximately 3000 car tires stacked 2.2m high (the position of the piles is also marked in Fig. 41). Several cars were also parked in the southern part of the basement at this time Still, they were not damaged substantially by the fire. As assumed by the authors of [17], the fire in the building most likely occured due to the ignition of an overheated ceiling lamp where the flame was transferred to the piles of tires below the ceiling through falling of burning droplets.

The building has three floors (basement, ground floor and first floor). The floor plan of the ground floor and part of the first floor, which are located directly above the fire-affected basement area shown in Fig. 41, are generally the same as those of the basement floor, so they are not shown separately. The only difference is that here (unlike in the basement), the north, east, and south exterior walls are not RC walls but are glazed surfaces with RC beams on top of them.

Moreover, the RC wall on the west side of Fig. 41 is an inner wall with some door openings. This wall is the same as those on the two upper floors. The building continues straight from this location and to the left of it. For the structural system of this (adjacent) part of the building, we will assume that it will only have a time-independent effect on the structural fire response of the presented part of the structure which will be able to suitably compensate simply by selecting appropriate constant boundary conditions at the junction of the two parts in our model.

In the following text, more detailed information about the structure system of the building in question is summarized according to the propositions of Maglica [4]:

- The building consists of three storeys (basement + ground floor + first floor) and a flat roof (clear floor height is 2.85m)
- The load-bearing structure of the building is an RC structure (vertical structural system: a mixed system of RC frames and walls, horizontal structural system: RC plates with a thickness of 16cm)
- The cross-sections of all of the RC columns are square with a side of 40 cm, and the cross-sections of the RC beams supporting the RC plates are rectangular (b/h = 40/50 cm)
- The horizontal loads on the structure are taken over primarily by the RC walls
- The floor plans of all floors are generally the same (the exception being the execution of the external walls as already explained previously)

- The characteristic values of the assumed to be permanent and live loads are as follows:

Permanent load (including DL)	$g_k[kN/m^2]$	floors	RC plate + perm. layers	5.80
		roof	RC plate + perm. layers	
Variable load	$q_k[kN/m^2]$	floors	live load $\psi_1=0.5$	2.80
		roof	live load $\psi_1=0$	0.40
			snow $\psi_2=0$ $Y_0=0.5$	1.20

Table 13: Values of gravitational load on the structure.

- Materials: concrete class C40/50, reinforcing steel class B500
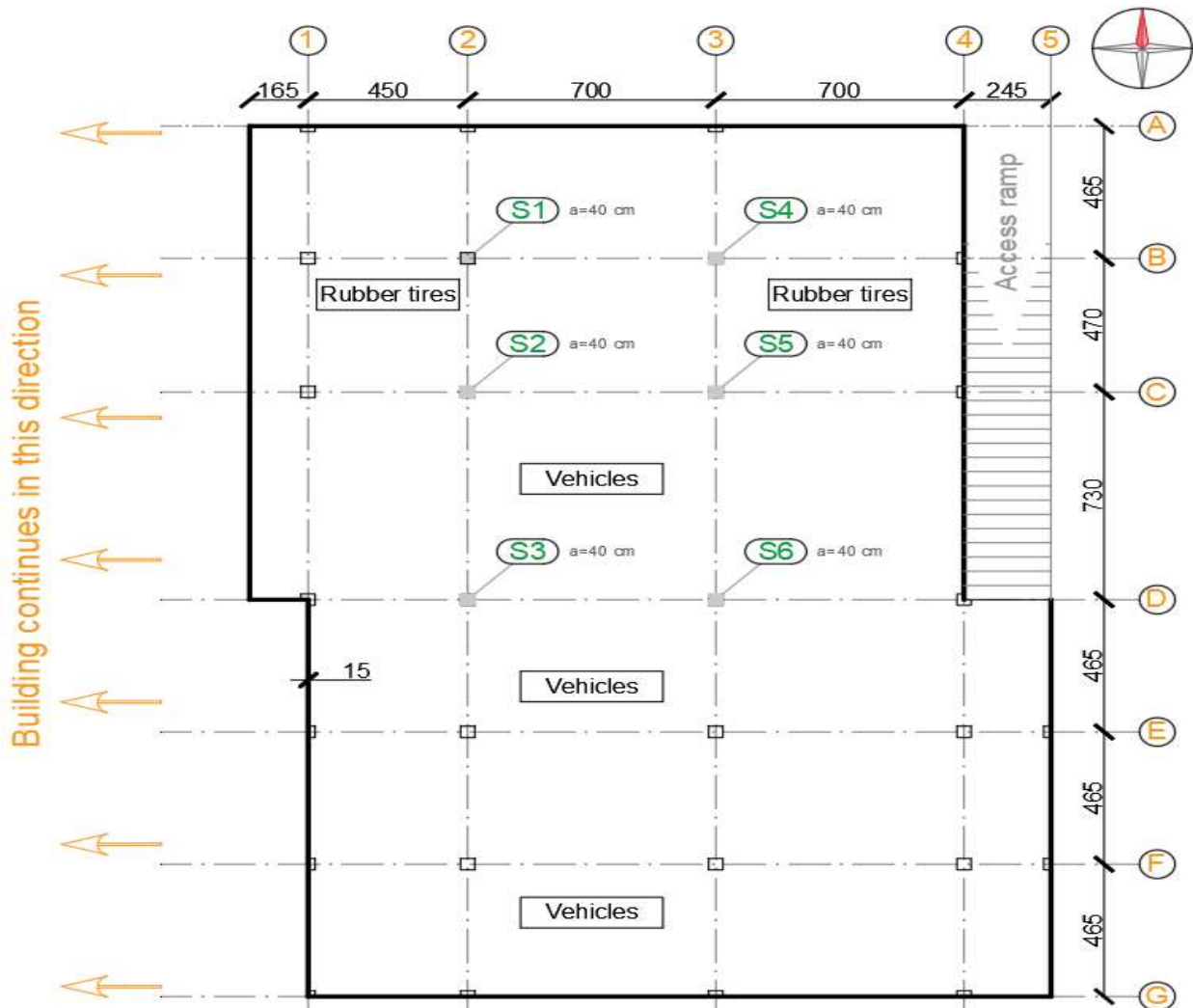
Figure 41: Floor plan of the part of the basement of the analysed building. Symbols S1-S6 label the RC columns that were exposed to the highest temperatures during the fire.

3.1. Fire analysis of column S6

The previously discussed fire in the building in Jesenice and the fire response of its supporting structure was analysed in more detail in the article [1]. The preparation of numerical models, which have been made in this master's thesis, was done following the article. In the article, alongside the models, a computer replication of the Jesenice fire, that was prepared in FDS [11] software, was also shown. With the computer replication, the authors later determined more accurrate fire curves near individual structural elements. However, since modelling of a fire in this software is not the subject of this master's thesis, we will refrain from such models here. Instead, for the analyses used, fire is defined simply by one of the nominal fire curves as proposed by EN 1991-1-2 [3], among which the *hydrocarbon*[4] fire curve was used:

$$\theta_g = 1080(1 - 0.325e^{-0.167t} - 0.675e^{-2.5t}) + 20 \qquad [°C] \qquad (24)$$

Where:
- θ_g is the gas temperature in the fire compartment [°C]
- t is the time [min]
- e is Euler's number: 2.71828...

Let us assume that we are observing for a time period of 240min of the hydrocarbon fire, and that we are interested in the fire response of the most loaded RC column in the basement, i.e. column S6 (Fig. 41). To avoid the assumption, that there is a constant axial force in the column during the fire, we shall not model the column as an isolated element, but instead, test it as a model of a larger part of the structure. Initially (Section 3.1.1.), a model of the entire structure in the affected basement part was prepared (Fig. 42) and the whole structure above this area. The assumption is that all of the columns in this part of the basement are exposed to fire, as well as the entire ceiling slab and beams from the bottom side. Later on, the model is gradually modified, as described below.

3.1.1. Thermal analysis of the structure

The thermal analysis model of the structure was prepared according to the geometrical measurements from the building's project and the found state of the building. A more detailed description of the building is given in the opening paragraphs of this chapter.

To summarize, the building consists of three stories and the basement floor; the structural system is a reinforced concrete spatial frame, with $b/h = 40/40cm$ columns, $b/h = 40/56cm$ beams and horizontally stiff plates with a thickness of $d = 16cm$.

In reality, the basement of the structure also contains walls on the outside edges of the building. However they were not included in the model. Since we are not interested in the behaviour of walls, but instead of the columns exposed to elevated temperatures.

---

[4] Based on the chemical composition of the basic raw materials from car tires, it is likely that this fire represents a kind of hydrocarbon fire.
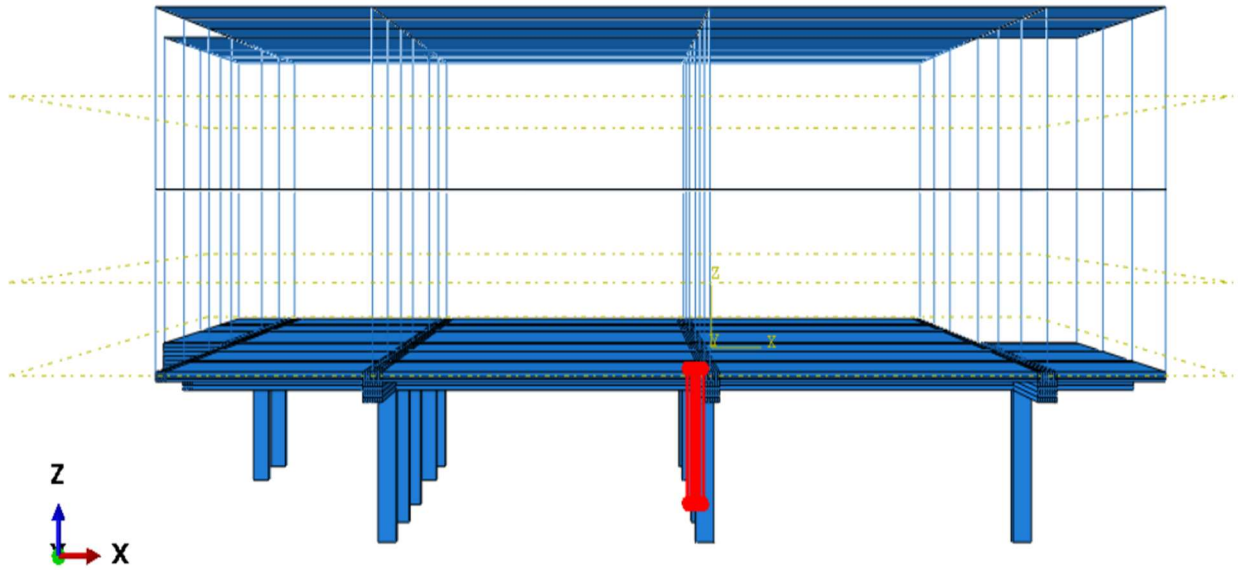
Figure 42: Display of the thermal analysis model of the building with highlighted column S6.

The structural elements in the basement (along with the base floor plate) are made of 3D quadratic quadrilateral elements. For the upper levels, in the case of beams and columns, 1D quadratic line elements were used, and as for the plates, 2D quadratic shell elements were used. The reason being, that we are not interested in the results of the upper-level elements (they have not been subjected to the fire load), so they were simplified to just transfer the loads of the upper levels to the structural elements of the basement.

In this way, also, the computing time was significantly decreased. Mesh of the model, consists of 158,650 quadratic heat transfer finite elements with more detailed characteristics shown in Tab. 14 below.

Element geometry	Structural element	Element type	Approx. element size [mm]	Number of elements	Element denotation
3D	Beams	Quadratic quadrilateral cubic elements	50/85/150	152,506	C3D20R
	Columns		50/50/150		
	Plates		150/150/40 or 150/150/80		
2D	Plates	Quadratic shell elements	40/40	4,050	S8R
1D	Beams	Quadratic line elements	850	2,094	B32
	Columns		1,500		

Table 14: Detailed heat transfer finite element characteristics of the prepared model.

All of the exposed surfaces in the basement (outside surfaces of columns, bottom side of the plate and exposed surfaces of the beams) were subjected to a transient heating regime according to the hydrocarbon temperature curve. At the same time, the rest of the model was assigned to be as ambient temperature.
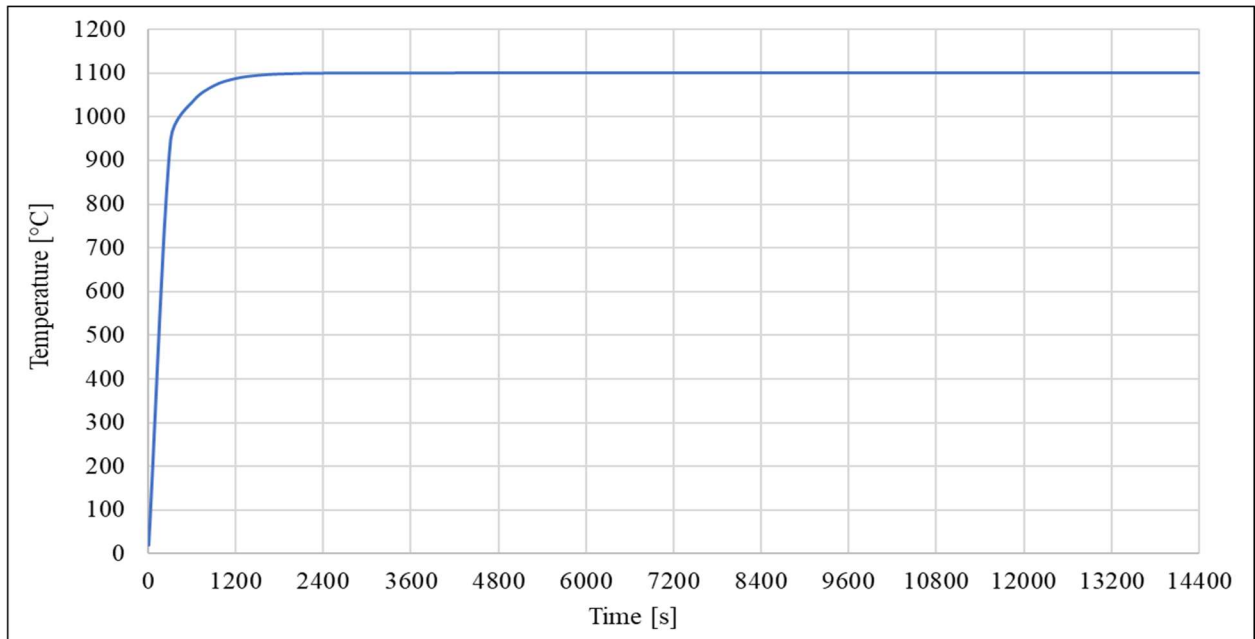
Figure 43: Hydrocarbon fire curve for a time period of t= 14,400 s.

Thermal characteristics of the material were calculated according to EN 1992-1-2 [3] (see Tab. 16). Furthermore, data for the ambient heating, convection and surface radiation, was also used as per the recommendations of EN 1992-1-2 [3] and is listed below (Tab. 15).

	Ambient	Convection	Surface radiation
Film coefficient	*9.00*	*25.00*	-
Sink temperature	*20.00*	*1.00*	*1.00*
Sink amplitude	-	*Hydrocarbon curve*	*Hydrocarbon curve*
Emissivity	-	-	*0.70*

Table 15: Ambient, convection and radiation properties assigned to the building thermal analysis model.

As is the case for all of the previously mentioned thermal analysis models, the values for thermal conductivity, specific heat, thermal expansion coefficient and the density of concrete were calculated according to EN 1992-1-3 [3]. The values for concretes thermal characteristics used in the model are listed in the table below.

Temperature	Thermal conductivity	Specific heat	Thermal elongation	Thermal expansion	Density
			Siliceous aggregate		
θ [°C]	λ_c [W/mK]	c_P (θ) [J/kg K]	α_{CL} [-]	α_{CV} [-]	γ [kg/m³]
0	1.68	900.00	1.84E-07	9.06E-06	2500.00
20	1.64	900.00	1.84E-07	9.06E-06	2500.00
30	1.62	900.00	9.06E-05	9.06E-06	2500.00
40	1.61	900.00	1.81E-04	9.07E-06	2500.00
50	1.59	900.00	2.73E-04	9.10E-06	2500.00
60	1.57	900.00	3.65E-04	9.12E-06	2500.00
70	1.55	900.00	4.58E-04	9.16E-06	2500.00
80	1.53	900.00	5.52E-04	9.20E-06	2500.00
90	1.52	900.00	6.47E-04	9.24E-06	2500.00

100	1.50	2020.00	7.43E-04	9.29E-06	2500.00
110	1.48	2020.00	8.41E-04	9.34E-06	2500.00
120	1.46	1960.00	9.40E-04	9.40E-06	2500.00
130	1.45	1840.00	1.04E-03	9.46E-06	2500.00
140	1.43	1720.00	1.14E-03	9.53E-06	2500.00
150	1.41	1600.00	1.25E-03	9.60E-06	2500.00
160	1.40	1480.00	1.35E-03	9.67E-06	2500.00
170	1.38	1360.00	1.46E-03	9.75E-06	2500.00
180	1.36	1240.00	1.57E-03	9.84E-06	2500.00
190	1.35	1120.00	1.69E-03	9.93E-06	2500.00
200	1.33	1000.00	1.80E-03	1.00E-05	2500.00
210	1.32	1005.00	1.92E-03	1.01E-05	2500.00
220	1.30	1010.00	2.04E-03	1.02E-05	2500.00
230	1.29	1015.00	2.17E-03	1.03E-05	2500.00
240	1.27	1020.00	2.30E-03	1.04E-05	2500.00
250	1.25	1025.00	2.43E-03	1.06E-05	2500.00
260	1.24	1030.00	2.56E-03	1.07E-05	2500.00
270	1.23	1035.00	2.70E-03	1.08E-05	2500.00
280	1.21	1040.00	2.84E-03	1.09E-05	2500.00
290	1.20	1045.00	2.99E-03	1.11E-05	2500.00
300	1.18	1050.00	3.14E-03	1.12E-05	2500.00
310	1.17	1055.00	3.30E-03	1.14E-05	2500.00
320	1.15	1060.00	3.45E-03	1.15E-05	2500.00
330	1.14	1065.00	3.62E-03	1.17E-05	2500.00
340	1.13	1070.00	3.78E-03	1.18E-05	2500.00
350	1.11	1075.00	3.96E-03	1.20E-05	2500.00
360	1.10	1080.00	4.13E-03	1.22E-05	2500.00
370	1.09	1085.00	4.32E-03	1.23E-05	2500.00
380	1.07	1090.00	4.50E-03	1.25E-05	2500.00
390	1.06	1095.00	4.69E-03	1.27E-05	2500.00
400	1.05	1100.00	4.89E-03	1.29E-05	2500.00
410	1.04	1100.00	5.10E-03	1.31E-05	2500.00
420	1.02	1100.00	5.30E-03	1.33E-05	2500.00
430	1.01	1100.00	5.52E-03	1.35E-05	2500.00
440	1.00	1100.00	5.74E-03	1.37E-05	2500.00
450	0.99	1100.00	5.97E-03	1.39E-05	2500.00
460	0.98	1100.00	6.20E-03	1.41E-05	2500.00
470	0.97	1100.00	6.44E-03	1.43E-05	2500.00
480	0.95	1100.00	6.68E-03	1.45E-05	2500.00
490	0.94	1100.00	6.94E-03	1.48E-05	2500.00
500	0.93	1100.00	7.20E-03	1.50E-05	2500.00
510	0.92	1100.00	7.46E-03	1.52E-05	2500.00
520	0.91	1100.00	7.73E-03	1.55E-05	2500.00
530	0.90	1100.00	8.01E-03	1.57E-05	2500.00
540	0.89	1100.00	8.30E-03	1.60E-05	2500.00
550	0.88	1100.00	8.60E-03	1.62E-05	2500.00
560	0.87	1100.00	8.90E-03	1.65E-05	2500.00
570	0.86	1100.00	9.21E-03	1.67E-05	2500.00
580	0.85	1100.00	9.53E-03	1.70E-05	2500.00
590	0.84	1100.00	9.85E-03	1.73E-05	2500.00
600	0.83	1100.00	1.02E-02	1.76E-05	2500.00
610	0.82	1100.00	1.05E-02	1.78E-05	2500.00
620	0.81	1100.00	1.09E-02	1.81E-05	2500.00

630	0.81	1100.00	1.12E-02	1.84E-05	2500.00
640	0.80	1100.00	1.16E-02	1.87E-05	2500.00
650	0.79	1100.00	1.20E-02	1.90E-05	2500.00
660	0.78	1100.00	1.24E-02	1.93E-05	2500.00
670	0.77	1100.00	1.28E-02	1.96E-05	2500.00
680	0.76	1100.00	1.32E-02	2.00E-05	2500.00
690	0.76	1100.00	1.36E-02	2.03E-05	2500.00
700	0.75	1100.00	1.40E-02	2.06E-05	2500.00
710	0.74	1100.00	1.40E-02	2.03E-05	2500.00
720	0.73	1100.00	1.40E-02	2.00E-05	2500.00
730	0.73	1100.00	1.40E-02	1.97E-05	2500.00
740	0.72	1100.00	1.40E-02	1.94E-05	2500.00
750	0.71	1100.00	1.40E-02	1.92E-05	2500.00
760	0.71	1100.00	1.40E-02	1.89E-05	2500.00
770	0.70	1100.00	1.40E-02	1.87E-05	2500.00
780	0.69	1100.00	1.40E-02	1.84E-05	2500.00
790	0.69	1100.00	1.40E-02	1.82E-05	2500.00
800	0.68	1100.00	1.40E-02	1.79E-05	2500.00
810	0.67	1100.00	1.40E-02	1.77E-05	2500.00
820	0.67	1100.00	1.40E-02	1.75E-05	2500.00
830	0.66	1100.00	1.40E-02	1.73E-05	2500.00
840	0.66	1100.00	1.40E-02	1.71E-05	2500.00
850	0.65	1100.00	1.40E-02	1.69E-05	2500.00
860	0.65	1100.00	1.40E-02	1.67E-05	2500.00
870	0.64	1100.00	1.40E-02	1.65E-05	2500.00
880	0.64	1100.00	1.40E-02	1.63E-05	2500.00
890	0.63	1100.00	1.40E-02	1.61E-05	2500.00
900	0.63	1100.00	1.40E-02	1.59E-05	2500.00
910	0.63	1100.00	1.40E-02	1.57E-05	2500.00
920	0.62	1100.00	1.40E-02	1.56E-05	2500.00
930	0.62	1100.00	1.40E-02	1.54E-05	2500.00
940	0.61	1100.00	1.40E-02	1.52E-05	2500.00
950	0.61	1100.00	1.40E-02	1.51E-05	2500.00
960	0.61	1100.00	1.40E-02	1.49E-05	2500.00
970	0.60	1100.00	1.40E-02	1.47E-05	2500.00
980	0.60	1100.00	1.40E-02	1.46E-05	2500.00
990	0.60	1100.00	1.40E-02	1.44E-05	2500.00
1000	0.59	1100.00	1.40E-02	1.43E-05	2500.00
1010	0.59	1100.00	1.40E-02	1.41E-05	2500.00
1020	0.59	1100.00	1.40E-02	1.40E-05	2500.00
1030	0.59	1100.00	1.40E-02	1.39E-05	2500.00
1040	0.59	1100.00	1.40E-02	1.37E-05	2500.00
1050	0.58	1100.00	1.40E-02	1.36E-05	2500.00
1060	0.58	1100.00	1.40E-02	1.35E-05	2500.00
1070	0.58	1100.00	1.40E-02	1.33E-05	2500.00
1080	0.58	1100.00	1.40E-02	1.32E-05	2500.00
1090	0.58	1100.00	1.40E-02	1.31E-05	2500.00
1100	0.58	1100.00	1.40E-02	1.30E-05	2500.00
1110	0.58	1100.00	1.40E-02	1.28E-05	2500.00
1120	0.57	1100.00	1.40E-02	1.27E-05	2500.00
1130	0.57	1100.00	1.40E-02	1.26E-05	2500.00
1140	0.57	1100.00	1.40E-02	1.25E-05	2500.00
1150	0.57	1100.00	1.40E-02	1.24E-05	2500.00

1160	0.57	1100.00	1.40E-02	1.23E-05	2500.00
1170	0.57	1100.00	1.40E-02	1.22E-05	2500.00
1180	0.57	1100.00	1.40E-02	1.21E-05	2500.00
1190	0.57	1100.00	1.40E-02	1.20E-05	2500.00
1200	0.57	1100.00	1.40E-02	1.19E-05	2500.00

Table 16: Calculated material properties assigned to the buildings thermal analysis model.

The analysis was carried out for a time period of 14,400 seconds with the standard calculation protocol.

3.1.2. Structural analysis of the structure

The mechanical analysis model was prepared in accordance to the thermal analyses model. Mesh of the model, consists of 158,650 quadratic stress finite elements. The mesh is compatible with the thermal analysis model mesh.

Element geometry	Structural element	Element type	Approx. element size [mm]	Number of elements	Element denotation
3D	Beams	Quadratic quadrilateral cubic elements	50/85/150	152,506	C3D20R
	Columns		50/50/150		
	Plates		150/150/40 or 150/150/80		
2D	Plates	Quadratic shell elements	40/40	4,050	S8R
1D	Beams	Quadratic line elements	850	2,094	B32
	Columns		1,500		

Table 17: Detailed stress finite element characteristics of the prepared model.
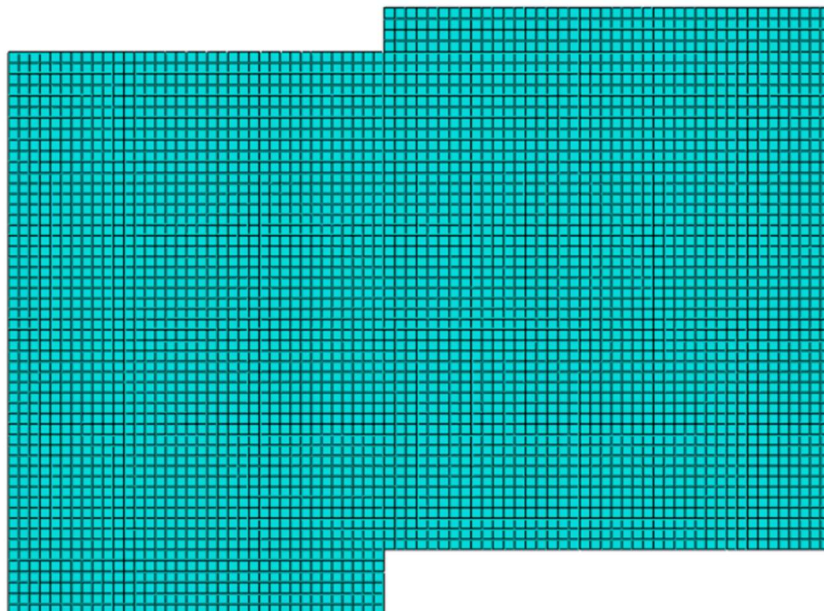
Figure 44: Display of the 2D quadratic shell element mesh for the first floor, second floor and roof plates.
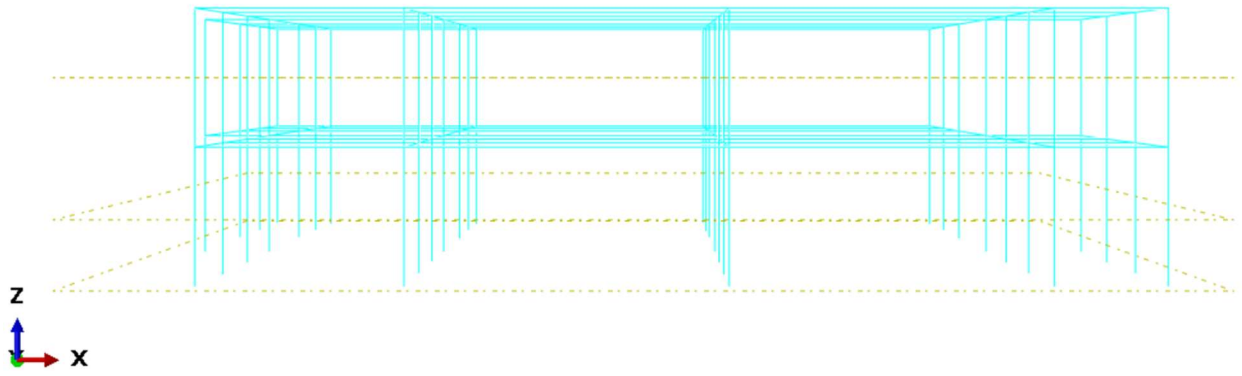
Figure 45: Display of the 1D quadratic line element mesh for the first floor, second floor and roof beams and columns.
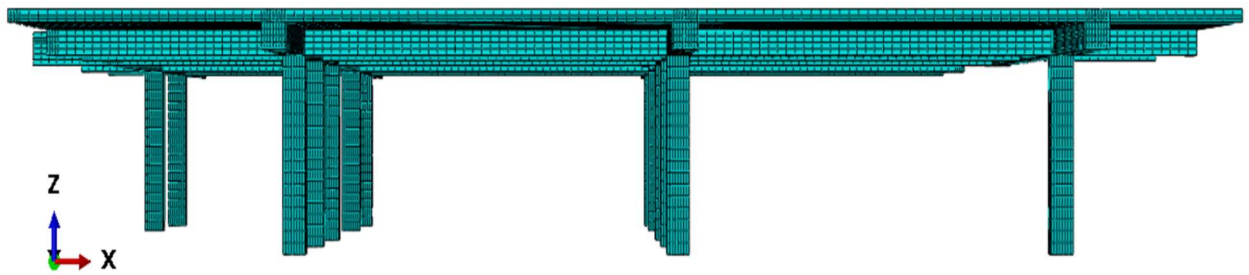
Figure 46: Display of the 3D quadratic cubic element mesh basements structural elements.
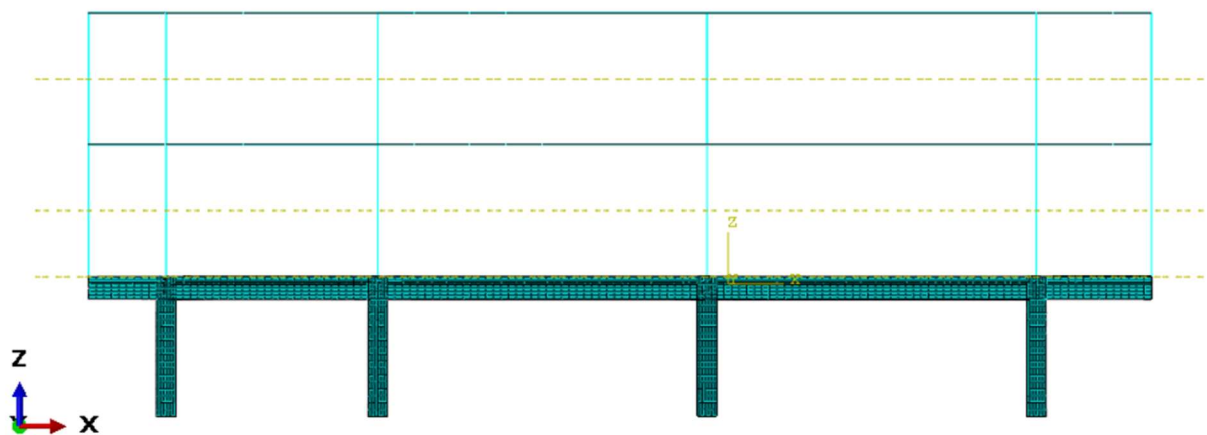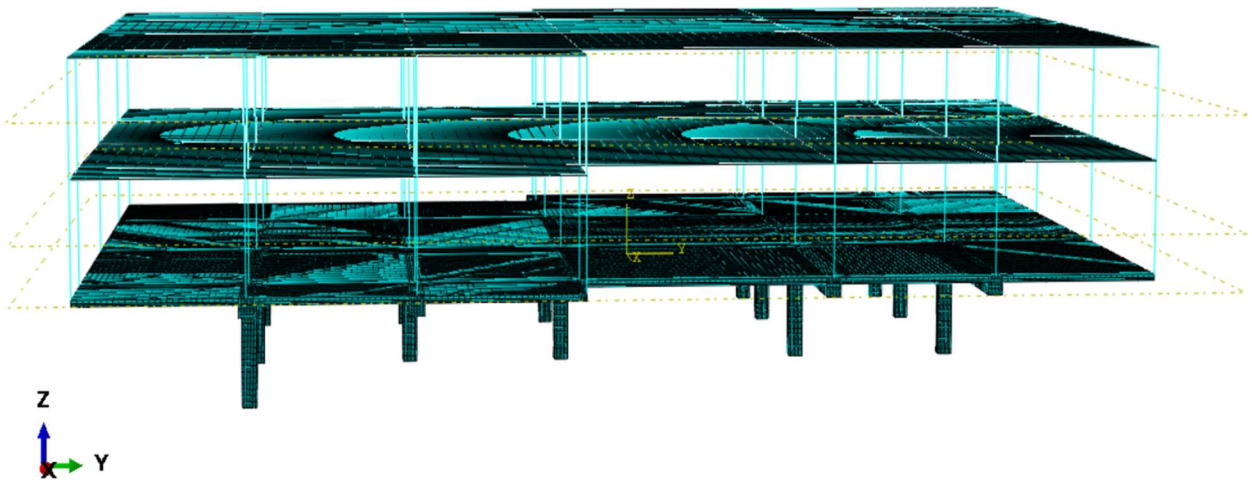
Figure 47: Perspective (*top*) and side view (*bottom*) display of the combined mesh elements.

55

For the first step of the analysis, boundary conditions were assigned to the model. The bottom of the columns in the basement were assigned as fixed supports. Outside edges of the basements ceiling slab (that are in reality supported by walls, which were disregarded in the models) were assigned a vertically restrained boundary condition ($U_3 = 0$).

As was the case for the thermal analysis, for the mechanical analysis at elevated temperatures, all material properties were calculated according to EN 1992-1-2 [3] and the experimental values that were measured. However, there are slight deviations from the norms. Additional reduction coefficients were needed for the material's elastic Young modulus and yield strength to replicate experimental results and simulate the ralistic behaviour of the structural elements.

Yield strength	Elastic modulus	Yield strain	Poisson ratio
f_{ck}	E_c	ε	ν
[MPa]	[GPa]	[-]	[-]
43.2	33.78	0.0025	0.2

Table 18: Project concrete characteristics of structural elements at ambient temperature.

For the columns, beams and plates of the base and upper levels of the building, which were not directly exposed to the thermal loading, the elastic material characteristics were not modified additionally. Instead the project material characteristics were used.

In case of the beams and plates on the basement's ceiling level were directly exposed to the thermal loading, the material characteristics were modified according to the steel elastic modulus reduction factors found in EN 1992-1-2 [3]. Additionally, similar to the mechanical properties of plates in section 2.2.2. and beams in section 2.4.2., for simulating the cracking of concrete and decline of stiffness (EI) of the cross-section under mechanical loading, the values have been further reduced according to the formula from ACI 318-08 [18] (section 10.10.4.1) for flexural members.

The formula was adjusted as a elastic modulus reduction factor. For the analysed beams, the additional stiffness reduction was used as a value of 0.35, and for the case of the analysed plates, the further reduction was used as a value of 0.25, both of which were applied as a constant reduction for all temperatures. Finally, the superposition of both reduction factors was made to replicate the realistic beahaviour as closely as possible.

Temperature	Elastic modulus	Poisson ratio
θ	$E_{c,\theta}$	ν
[°C]	[N/m2]	[-]
0	8.75E+09	0.10
20	8.75E+09	0.10
100	8.75E+09	0.10
200	7.88E+09	0.10
300	7.00E+09	0.10
400	6.13E+09	0.10
500	5.25E+09	0.10
600	2.71E+09	0.10
700	1.14E+09	0.10
800	7.88E+08	0.10
900	6.13E+08	0.10
1000	3.50E+08	0.10
1100	1.75E+08	0.10
1200	8.75E+06	0.10

Table 19: Values of the elastic material properties used for the basement's ceiling plate.

Temperature	Elastic modulus	Poisson ratio
θ	$E_{c,\theta}$	ν
[°C]	[N/m2]	[-]
0	1.23E+10	0.10
20	1.23E+10	0.10
100	1.23E+10	0.10
200	1.10E+10	0.10
300	9.80E+09	0.10
400	8.58E+09	0.10
500	7.35E+09	0.10
600	3.80E+09	0.10
700	1.59E+09	0.10
800	1.10E+09	0.10
900	8.58E+08	0.10
1000	4.90E+08	0.10
1100	2.45E+08	0.10
1200	1.23E+07	0.10

Table 20: Values of the elastic material properties used for the basement beams.

In the case of the columns, for the mechanical analysis at elevated temperatures all material properties were calculated according to EN 1992-1-2 [3] guidelines and the experimental values that were measured. Similarly to the mechanical properties of plates and beams previously listed, the material characteristics were modified according to steel's elastic modulus reduction factors. Additionally, for simulating the cracking of concrete and the decline of stiffness (EI) of the cross-section under mechanical loading, the values have been further reduced according to the formula from ACI 318-08 [18] (section 10.10.4.1) for compressive members.

Temperature	Elastic modulus	Poisson ratio
θ	$E_{c,\theta}$	ν
[°C]	[N/m2]	[-]
0	2.80E+10	0.10
20	2.80E+10	0.10
100	2.80E+10	0.10
200	2.66E+10	0.10
300	2.38E+10	0.10
400	2.10E+10	0.10
500	1.68E+10	0.10
600	1.26E+10	0.10
700	8.41E+09	0.10
800	4.20E+09	0.10
900	2.24E+09	0.10
1000	1.12E+09	0.10
1100	2.80E+08	0.10
1200	1.23E+07	0.10

Table 21: Values of the elastic material properties used for RC of the basement columns.

Temperature	Yield strength	Plastic strain
θ	$f_{c,\theta}$	$\varepsilon_{p,\theta}$
[°C]	[N/m2]	[-]
20	2.78E+07	0.0000000
	2.85E+07	0.0000817
	2.92E+07	0.0001634
	2.98E+07	0.0002451
	3.03E+07	0.0003268
	3.08E+07	0.0004085
	3.11E+07	0.0004902
	3.14E+07	0.0005719
	3.16E+07	0.0006537
	3.17E+07	0.0007354
	3.17E+07	0.0008171
	3.17E+07	0.0200000
100	2.78E+07	0.0000000
	2.85E+07	0.0001307
	2.92E+07	0.0002615
	2.98E+07	0.0003922
	3.03E+07	0.0005229
	3.08E+07	0.0006537
	3.11E+07	0.0007844
	3.14E+07	0.0009151
	3.16E+07	0.0010458
	3.17E+07	0.0011766
	3.17E+07	0.0013073

	3.17E+07	0.0225000
	2.64E+07	0.0000000
	2.71E+07	0.0001798
	2.78E+07	0.0003595
	2.83E+07	0.0005393
	2.88E+07	0.0007190
200	2.92E+07	0.0008988
	2.96E+07	0.0010785
	2.98E+07	0.0012583
	3.00E+07	0.0014380
	3.01E+07	0.0016178
	3.01E+07	0.0017975
	3.01E+07	0.0250000
	2.36E+07	0.0000000
	2.43E+07	0.0002288
	2.48E+07	0.0004576
	2.54E+07	0.0006863
	2.58E+07	0.0009151
300	2.62E+07	0.0011439
	2.64E+07	0.0013727
	2.67E+07	0.0016014
	2.68E+07	0.0018302
	2.69E+07	0.0020590
	2.69E+07	0.0022878
	2.69E+07	0.0275000
	2.08E+07	0.0000000
	2.14E+07	0.0003268
	2.19E+07	0.0006537
	2.24E+07	0.0009805
	2.28E+07	0.0013073
400	2.31E+07	0.0016341
	2.33E+07	0.0019610
	2.35E+07	0.0022878
	2.37E+07	0.0026146
	2.37E+07	0.0029414
	2.38E+07	0.0032683
	2.38E+07	0.0300000
	1.67E+07	0.0000000
	1.71E+07	0.0004902
	1.75E+07	0.0009805
	1.79E+07	0.0014707
500	1.82E+07	0.0019610
	1.85E+07	0.0024512
	1.87E+07	0.0029414
	1.88E+07	0.0034317

	1.89E+07	0.0039219
	1.90E+07	0.0044121
	1.90E+07	0.0049024
	1.90E+07	0.0325000
600	1.25E+07	0.0000000
	1.28E+07	0.0008171
	1.32E+07	0.0016341
	1.34E+07	0.0024512
	1.37E+07	0.0032683
	1.38E+07	0.0040853
	1.40E+07	0.0049024
	1.41E+07	0.0057194
	1.42E+07	0.0065365
	1.42E+07	0.0073536
	1.43E+07	0.0081706
	1.43E+07	0.0350000
700	8.33E+06	0.0000000
	8.56E+06	0.0008171
	8.77E+06	0.0016341
	8.95E+06	0.0024512
	9.10E+06	0.0032683
	9.23E+06	0.0040853
	9.33E+06	0.0049024
	9.41E+06	0.0057194
	9.47E+06	0.0065365
	9.50E+06	0.0073536
	9.51E+06	0.0081706
	9.51E+06	0.0375000
800	4.17E+06	0.0000000
	4.28E+06	0.0008171
	4.38E+06	0.0016341
	4.47E+06	0.0024512
	4.55E+06	0.0032683
	4.62E+06	0.0040853
	4.67E+06	0.0049024
	4.71E+06	0.0057194
	4.73E+06	0.0065365
	4.75E+06	0.0073536
	4.76E+06	0.0081706
	4.76E+06	0.0400000
900	2.22E+06	0.0000000
	2.28E+06	0.0008171
	2.34E+06	0.0016341
	2.39E+06	0.0024512
	2.43E+06	0.0032683

	2.46E+06	0.0040853
	2.49E+06	0.0049024
	2.51E+06	0.0057194
	2.52E+06	0.0065365
	2.53E+06	0.0073536
	2.54E+06	0.0081706
	2.54E+06	0.0425000
1000	1.11E+06	0.0000000
	1.14E+06	0.0008171
	1.17E+06	0.0016341
	1.19E+06	0.0024512
	1.21E+06	0.0032683
	1.23E+06	0.0040853
	1.24E+06	0.0049024
	1.26E+06	0.0057194
	1.26E+06	0.0065365
	1.27E+06	0.0073536
	1.27E+06	0.0081706
	1.27E+06	0.0450000
1100	2.78E+05	0.0000000
	2.85E+05	0.0008171
	2.92E+05	0.0016341
	2.98E+05	0.0024512
	3.03E+05	0.0032683
	3.08E+05	0.0040853
	3.11E+05	0.0049024
	3.14E+05	0.0057194
	3.16E+05	0.0065365
	3.17E+05	0.0073536
	3.17E+05	0.0081706
	3.17E+05	0.0475000
1200	2.78E+01	0.0000000
	2.85E+01	0.0008171
	2.92E+01	0.0016341
	2.98E+01	0.0024512
	3.03E+01	0.0032683
	3.08E+01	0.0040853
	3.11E+01	0.0049024
	3.14E+01	0.0057194
	3.16E+01	0.0065365
	3.17E+01	0.0073536
	3.17E+01	0.0081706
	3.17E+01	0.0100000

Table 22: Values of the plastic material properties used for RC of the basement columns.

The model was subjected to vertical loads (gravitational and live loads) as per Tab. 13. The loads were maintained constant throughout the analysis. The accidental combination of loads applied for the mechanical analysis is the following:

$$E_D = 1.0 * \left(SW + DL_{bf} + DL_{ff} + DL_r\right) + 0.5 * \left(LL_{bf} + LL_{ff}\right) \qquad (25)$$

Where:

E_D is the sum of combinet loads
SW is the self weight of the structure
DL_{bf} is the dead-load of the base floor
DL_{ff} is the dead-load of the first floor
DL_r is the dead-load of the roof
LL_{bf} is the live-load of the base floor
LL_{ff} is the live-load of the first floor
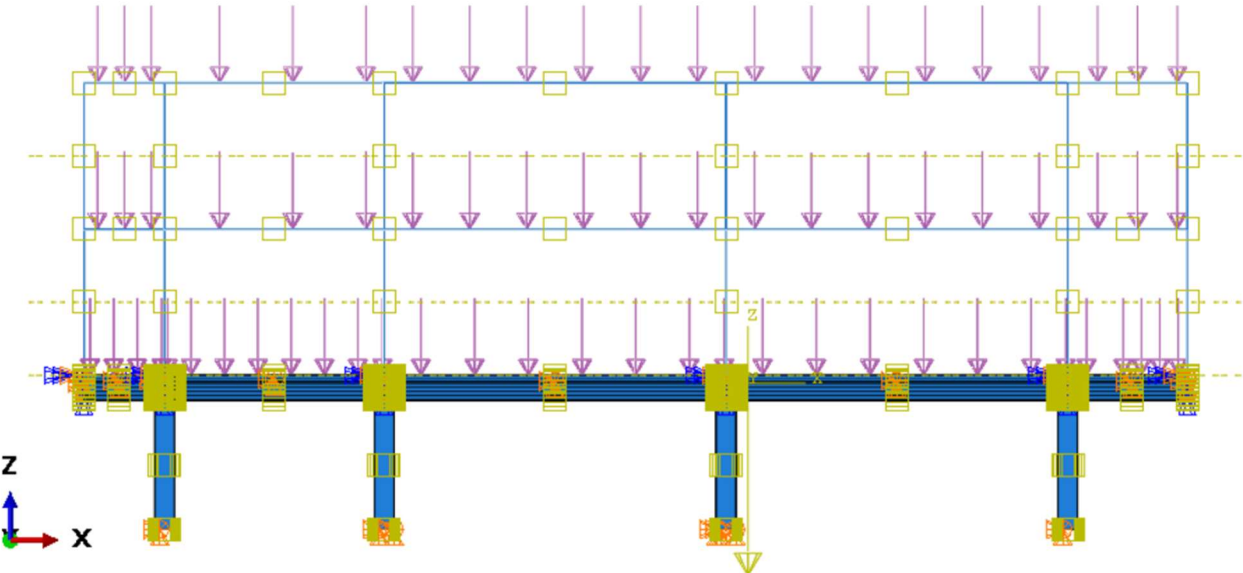
Figure 48: Gravitational load: self weight of the structure.
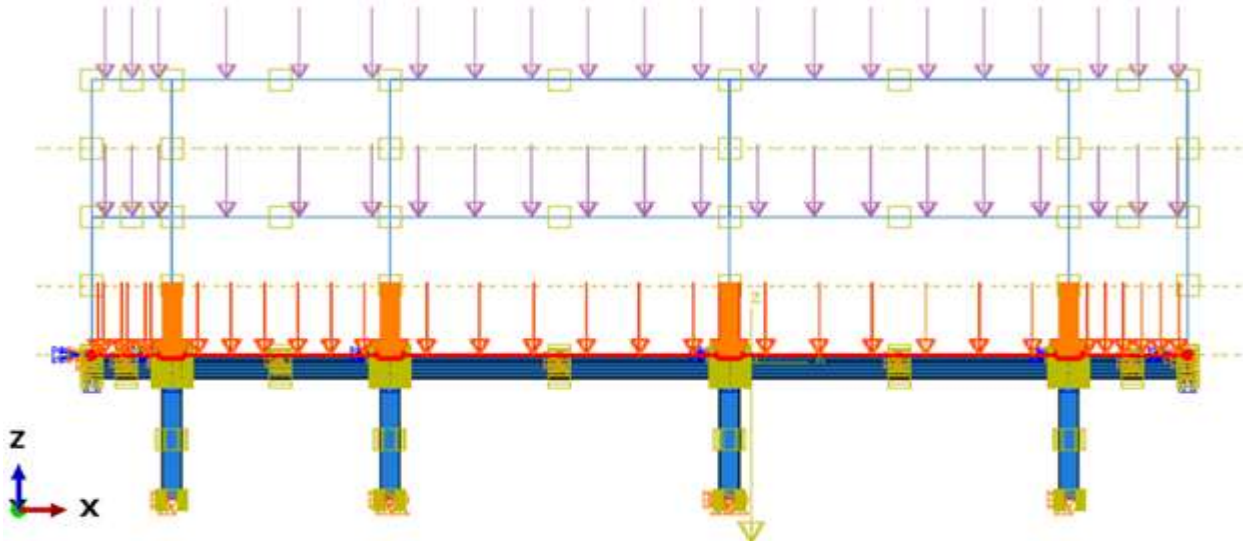
Figure 49: Gravitational load: dead-load of the base floor.
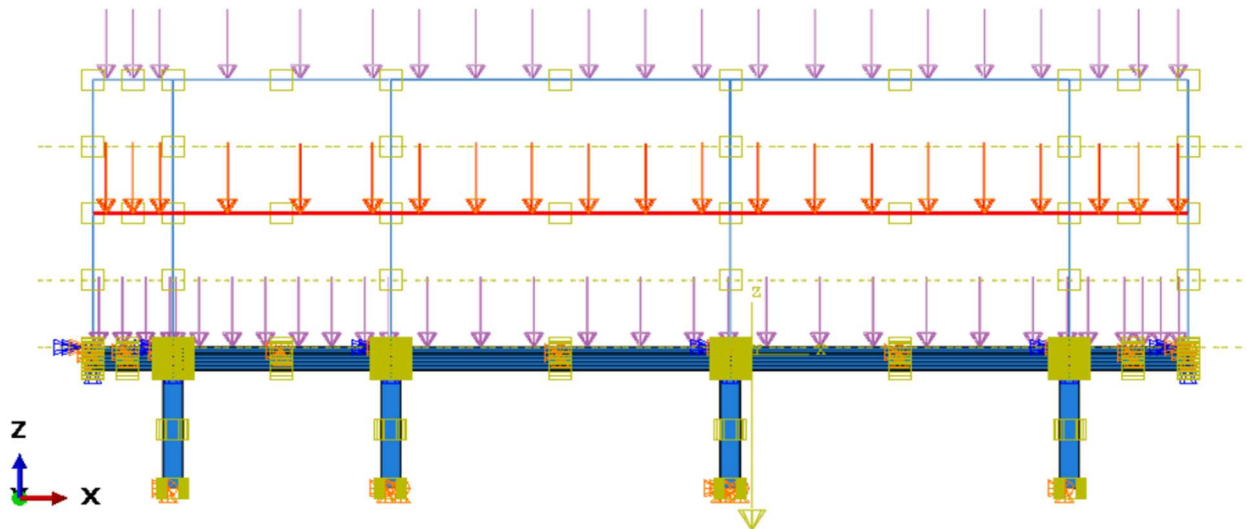
Figure 50: Gravitational load: dead-load of the first floor.
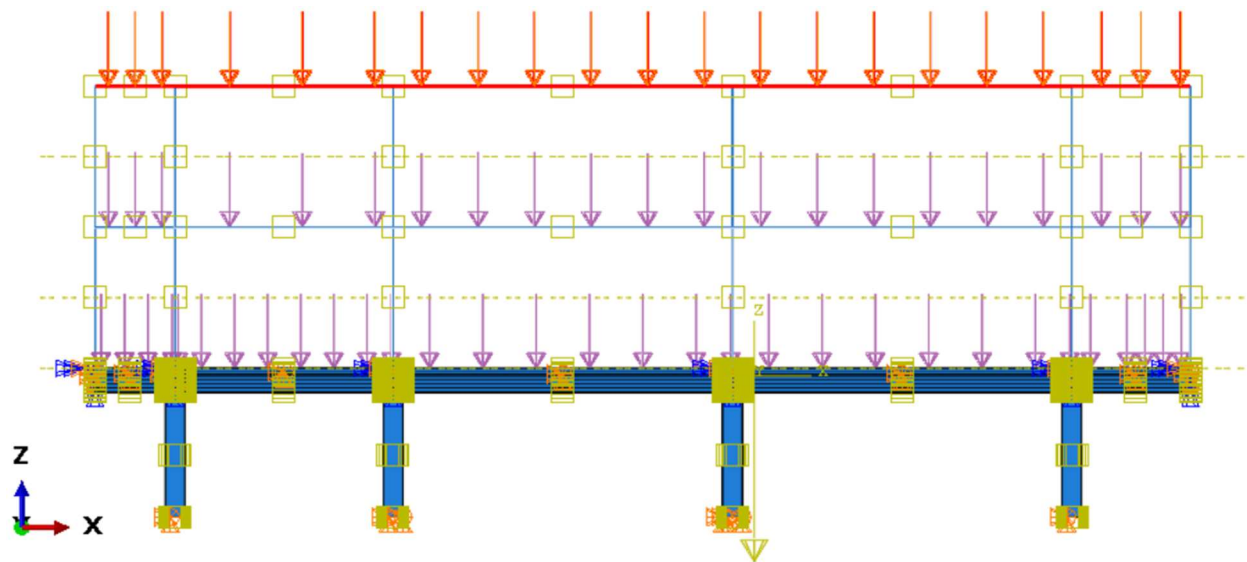
Figure 51: Gravitational load: dead-load of the roof.
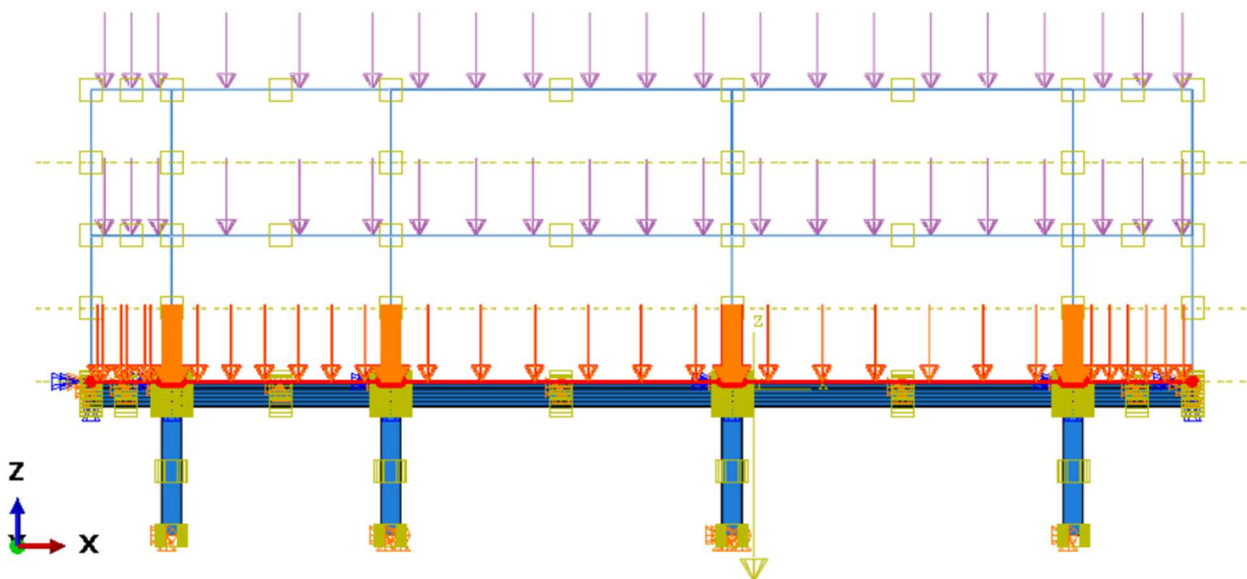
Figure 52: Vertical load: live-load of the base floor.
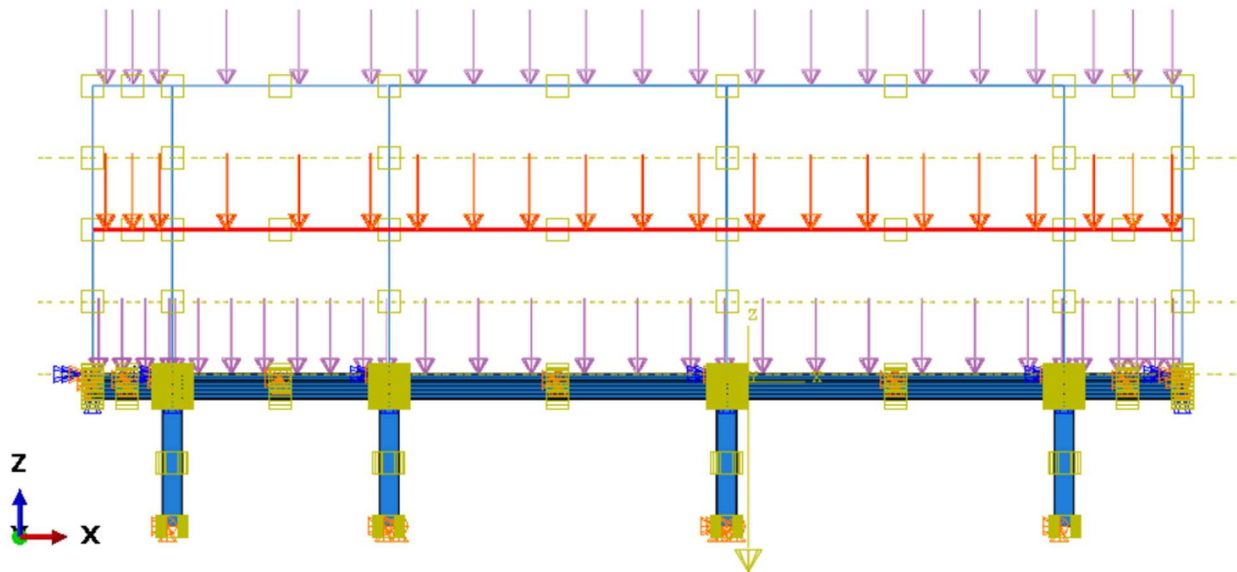
Figure 53: Vertical load: live-load of the first floor.

The analysis was carried out for a period of 14,400 seconds with the standard calculation protocol and included material and geometric non-linearity (third-order theory).
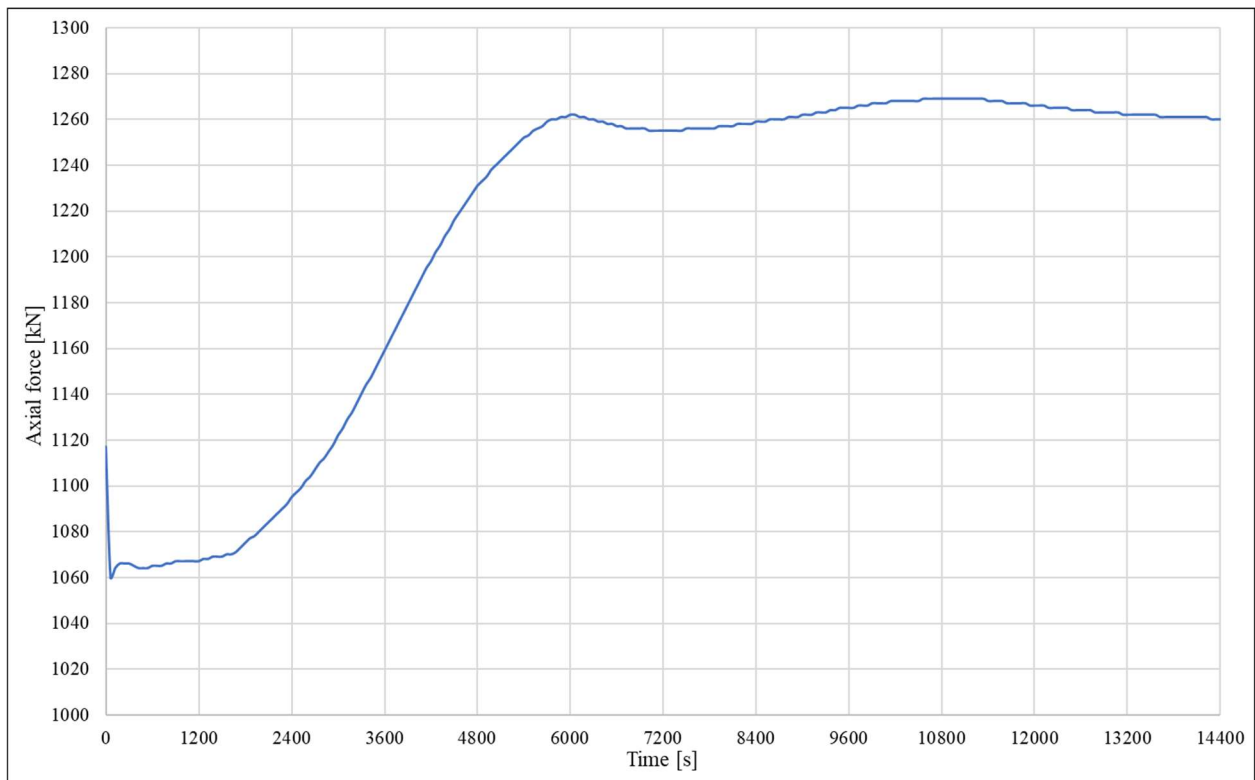
Figure 54: Axial force of column S6 obtained through the mechanical analysis of the structure.

As is shown in the numerical results gathered above, it was confirmed what was initially expected, that the axial load of the column varies over time. In the beginning, the axial force of the column declines and plateous. This is presumed to be because of the expansion of the outer surfaces of structural elements exposed to the thermal loading, which slightly 'softens' the restraint of axial deformation in the column.

After some time of exposure to the elevated temperature, the influence of heat penetrates further into the cross-section of the structural elements. This can be observed as the rise in axial force of column S6. This is because the column will tend to elongate due to the influence of high temperatures, and these elongations will be hindered by the rest of the structure (note that thermal expansion coefficient is not negligible for concrete, especially at high temperatures).

Finally, the axial force of column S6 stabilises at a value of approx. $1,260 kN$ at around $6,000 s$, after which it slightly fluctuates around the value. This is presumed to be because the temperature profile of the cross-sections in structural elements, is more uniform, which leads to an equilibrium of the stiffness affects surrounding structural members have on axial restraints of the column.

65

Conclusion

According to the present version of Eurocodes, fire analysis of RC structures can be performed in several different ways, with different levels of precision and accuracy. This usually refers to methods where, instead of a larger part of the structural system, only the observed RC column is calculated as an isolated structural element. This is only possible on the bias if the axial force in the column is considered constant during thermal loading.

This assumption was found not to be the case, as it was observed above; the affect of the stiffnesses of the surrounding structural members (i.e. beams and plates) has a direct influence on the change of axial restraints of the column, resulting in a variable axial load over time.

Considering everything written above, if we model the member as a part of a larger portion of the RC structural system, more precise and realistic values of the axial force in the RC column are obtained. However, many problems exist connected to this idea as explained previously in the Introduction. One is the complexity of such numerical models and obtaining the correct values for the material properties at elevated temperatures.

The simplified material model as proposed by J.Č.Kolšek and P. Češarek [1], with some adjustments for the stiffness of the materials, has proven quite accurate for the numerical models considered in this thesis. The numerical models yielded a good correlation with experimental test results on RC plates carried out by Bailey and Toh [16] and tests on RC beams carried out by Monther B.M. Dwaikat [19].

Results of the numerical models subjected to thermal analyses have a maximum deviation of approx. 8% and for the mechanical analyses, a maximum deviation of approx. 13% (except for the case of beam B2, with a maximum deviation of approx. 19%, due to the differences in axial restraints from the test and numerical model). Considering, that a slight element of human error while interpreting and reading the results from experimental papers was likely in play, the deviation in the results may be even smaller than the ones observed.

In conclusion, although more precise and accurate, numerical modelling of a larger section of the structural system is also highly demanding. The deviations in the value of the axial force, as observed above, are not extremely large (around 20%), which means that if assumed that there is a constant value of the axial force, we are not highly inaccurate. However, an increase of the constant axial force value of $\approx 20\%$ is recommended, in case of using simplified methods of calculations.

Literature references

[1] J.Č.Kolšek and P. Češarek, Can reinforced concrete structures designed according to established simplified Eurocode procedures and Technical guidelines for ensuring fire safety in buildings survive real fires?, Požar, 2022. (submitted, in Slovene)

[2] Abaqus, Dassault Systèmes Simulia Corp., Johnston, RI, USA

[3] Eurocode 2: Design of concrete structures - Part 1-2: General rules - Structural fire design

[4] Martin Maglica, Fire analysis of reinforced concrete structure, Master's thesis, University of Ljubljana, Faculty of Civil and Geodetic engineering, 2021. (in Slovene)

[5] Barbara Kralj, Impact of a fire in the planned steel frame extension on load-bearing capacity of an existing reinforced concrete frame structure, Master's thesis, University of Ljubljana, Faculty of Civil and geodetic engineering, 2019. (in Slovene)

[6] Eurocode 0: Basis of structural design

[7] Eurocode 1: Actions on structures - Part 1-2: General actions - Actions on structures exposed to fire

[8] Ozawa, M., Uchida, S., Kamada, T., Morimoto, H. 2012. Study of mechanisms of explosive spalling in high-strength concrete at high temperatures using acoustic emission. Construction and Building Materials, 37, 621–628

[9] Yaqub, M., Bailey, C.G., Nedwell, P., Khan, Q.U.Z., Javed, I. 2013. Strength and stiffness of post-heated columns repaired with ferrocement and fibre reinforced polymer jackets. Composites Part B: Engineering, 44, 1: 200–211

[10] Cadorin, J-F. Franssen, J-M. 2003. A tool to design steel elements submitted to compartment fires - OZone V2. Part 1: pre- and post-flashover compartment fire model. Fire Safety Journal, Vol. 38, iss. 5, pp: 395-427

[11] Kevin McGrattan, Simo Hostikka, Randall McDemott, Jason Floyd, Craig Weinschenk, Kristopher Overholt, NIST Special publication 1019, 6th edition, Fire Dynamics Simulator, User's Guide

[12] ANSYS, Inc. Workbench User's Guide. Canonsburg. Pennsylvania.

[13] Franssen, J-M. Gernay, T. 2017. Modelling structures in fire with SAFIR®: theoretical background and capabilities. Journal of Structural Fire Engineering, Vol. 8 No. 3, pp: 300-323.

[14] Srpčič, S. 2015. Trdnost I. , University of Ljubljana, Faculty of Civil and Geodetic engineering

[15] Building code requirements for structural concrete (ACI 318-08) and commentary. ACI Committee 318, American Concrete Institute ACI; 2008. h

[16] C.G. Bailey and W.S. Toh, Behaviour of concrete floor slabs at ambient and elevated temperature, ScienceDirect, Fire Safety Journal 42 (2007) 425-436, july 2007.

[17] J.Kolšek and A. Rebec, Analiza nosilne konstrukcije po požaru objekta ASP na Jesenicah, Požar, december 2017.

[18] Building Code Requirements for Structural Concrete (ACI 318-08) and Commentary, American Concrete Institute, january 2008.

[19] Flexural response of reinforced concrete beams exposed to fire, Volume I., Monther B.M. Dwaikat, Doctoral dissertaition, Michigan State University 2009. (Chapter 3. Experimental program)

Figures

Figure 1:   Total thermal elongation of concrete. Figure is taken from EN 1992-1-2 [3].

Figure 2:   Total thermal elongation of reinforcing steel. Figure is taken from EN 1992-1-2 [3].

Figure 3:   Fire-exposed RC column. Left (top and bottom): diagram of the mechanisms of explosive spalling of concrete (figure taken from source [8]), right: photo of damage to a column after a fire test (figure taken from source [9])

Figure 4:   Nominal fire curves according to EN 1991-1-2 [7].

Figure 5:   Thermal conductivity of concrete λ_c [W/mK] as a function of temperature as defined in EN 1992-1-2 [3].

Figure 6:   Specific heat c_p [kJ/kgK] as a function of temperature as defined in EN 1992-1-2 [3].

Figure 7:   Stress-strain relationships of concrete under compression at elevated temperatures according to EN 1992-1-2 [3].

Figure 8:   Stress-strain relationships of reinforcing steel at elevated temperatures according to EN 1992-1-2 [3].

Figure 9:   Material model of reinforced concrete at elevated temperatures according to [1].

Figure 10:   Setup of the elevated temperature tests (left) and general failure mode of tested slabs (right). Figures were taken from [16].

Figure 11:   Values of temperatures during test on various locations of the plate SF1. Figure was taken from [16].

Figure 12:   Comparison of temperature values on the bottom surface of the plate.

Figure 13:   Comparison of temperature values on the reinforcement of the plate.

Figure 14:   Comparison of temperature values on the top surface of the plate.

Figure 15:   Display of the meshed model with the highlighted heated bottom surface.

Figure 16:   Results of the thermal analysis model at 3,000 seconds.

Figure 17:   Results of the thermal analysis model at 10,000 seconds.

Figure 18:   Comparison of measured experimental values of temperatures in different locations of the plate ('E') and the numerical results obtained with the model in Abaqus ('A').

Figure 19:   Boundary conditions assigned to the model. Simply supported edges with vertical deflections restrained (left) and clamped corners (right).

Figure 20:   Results of vertical displacements for mechanical analysis model at 3,000 seconds.

Figure 21:   Results of vertical displacements for mechanical analysis model at 10,000 seconds.

Tables

Table 1: Mechanical characteristics of concrete with siliceous and calcareous aggregates at high temperatures (i.e. compressive strength compared to its initial value at ambient temperature, strain at peak stress, and ultimate strain at failure). The table is taken from EN 1992-1-2 [3].

Table 2: Mechanical characteristics of reinforcing steel at high temperatures compared to their initial values at ambient temperature, i.e. maximum stress level (strength of steel), proportional limit, and elastic modulus. The table is taken from EN 1992-1-2 [3].

Table 3: Details of slab tests with mild steel at elevated temperatures. The table is taken from Bailey and Toh [16].

Table 4: Ambient, convection and radiation properties assigned to the model.

Table 5: Calculated material properties assigned to the thermal analysis model.

Table 6: Concrete characteristics of the tested plate at ambient temperature.

Table 7: Values of additional reduction factor for simulating creep of reinforcement and deformation increase.

Table 8: Values of mechanical properties of concrete at elevated temperatures used for the mechanical analysis.

Table 9: Ambient, convection and radiation properties assigned to the models B1 and B2.

Table 10: Calculated material properties assigned to the thermal analysis models.

Table 11: Concrete characteristics of tested beams at ambient temperature.

Table 12: Values of mechanical properties of concrete at elevated temperatures used for the mechanical analyses.

Table 13: Values of gravitational load on the structure.

Table 14: Detailed heat transfer finite element characteristics of the prepared model.

Table 15: Ambient, convection and radiation properties assigned to the buildings thermal analysis model.

Table 16: Calculated material properties assigned to the buildings thermal analysis model.

Table 17: Detailed stress finite element characteristics of the prepared model.

Table 18: Project concrete characteristics of structural elements at ambient temperature.

Table 19: Values of the elastic material properties used for the basement's ceiling plate.

Table 20: Values of the elastic material properties used for the basement beams.

Table 21: Values of the elastic material properties used for RC of the basement columns.

Table 22: Values of the plastic material properties used for RC of the basement columns.

71